TECHNICAL REPORT 1928
August 2005

Verification and Validation Report: Microwave Office™ 2002 Modeling and Simulation for Electronic Systems

T. Q. Ho
T. J. Hilsabeck
C. A. Hewett
SSC San Diego

D. A. Zolnick
M. Kragalott
D. J. Taylor
NRL

M. C. Baugher
NSWC, Dahlgren Division

T. Itoh
UCLA

A. K. Agrawal
Johns Hopkins University APL

SSC San Diego

TECHNICAL REPORT 1928
August 2005

Verification and Validation Report: Microwave Office™ 2002 Modeling and Simulation for Electronic Systems

T. Q. Ho
T. J. Hilsabeck
C. A. Hewett
SSC San Diego

D. A. Zolnick
M. Kragalott
D. J. Taylor
NRL

M. C. Baugher
NSWC, Dahlgren Division

T. Itoh
UCLA

A. K. Agrawal
Johns Hopkins University APL

SSC San Diego
San Diego, CA 92152-5001

SSC SAN DIEGO
San Diego, California 92152-5001

T. V. Flynn, CAPT, USN
Commanding Officer

R. F. Smith
Executive Director

ADMINISTRATIVE INFORMATION

This report was prepared for the Naval Sea Systems Command PMS 500 DD(X) Program Office by the Photonics and RF Technology Branch (Code 2825), Space and Naval Warfare Systems Center San Diego; the Naval Research Laboratory; the Naval Surface Warfare Center, Dahlgren Division; and the John Hopkins University Applied Physics Laboratory.

Released by
W. Henry, Head
Photonics and RF
Technology Branch

Under authority of
D. M. Gookin, Head
Network & Information
Systems Division

SB

ACKNOWLEDGMENTS

The authors of this report gratefully acknowledge the following persons for their important contributions to the VIPER I project in general, and specifically for their efforts toward completion of the research and validation effort described in this report.

The authors first thank Dr. Raj Mittra of RMA, Inc., Mr. Will Henry and Mr. Kevin Allen of Space and Naval Warfare Systems Center San Diego (SSC San Diego), and Shawn Allen of the Naval Surface Warfare Center, Dahlgren Division, who contributed substantially to the code debugging and validation effort. We also extend our thanks to a group that provided excellent technical guidance for the entire project, including Mr. Steven Hart, formerly of SSC San Diego, Dr. William Pala of the Naval Research Laboratory, Dr. Thomas Cwik of the Jet Propulsion Laboratory, and Mr. Ray Allen of Symmetron, Inc., who also provided valuable editorial assistance with the final report.

The project could not have been accomplished without the support of Capt. Charles Goddard, Program Manager DD(X), PMS 500; the former head of PMS 500, RADM Tom Bush; and the Technical Directors associated with PMS 500, including Capt. Charles Behrle, Capt. Jim Wilkins, and Capt. Kenneth Webb, USN (ret). Finally, we recognize and acknowledge the dedicated efforts of Mr. Thomas Ready, the Program Manager for Integrated Topside Design Research and Development, who funded this project, and the PMS 500 financial support staff, Mr. Herbert Williams and Ms. Naomi Silver, who made sure the necessary resources were available when needed.

EXECUTIVE SUMMARY

To address the shortfall in adequate modeling and simulation (M&S) software that can model a wide range of electromagnetic problems, PEO-DD(X)/PMS 500 commissioned the development of a plan for delivery of a Validated, Integrated, Physics-based Electromagnetic Radiation (VIPER) tool set. Microwave Office™ was identified as one of the most promising microwave electronics simulation codes and was selected for further development and verification and validation. This report shows a wide range of EM test cases in which Microwave Office™ simulations included linear passive components, linear active components, nonlinear components, and system-level circuits.

The verification and validation (V&V) of Microwave Office™ conducted under this study was a major success. Each test case designed for this V&V effort was chosen to verify Microwave Office™ performance in a specific area of user need or to validate the underlying theoretical framework of the M&S package. Microwave Office™ demonstrated its ability to accurately predict the performance of a wide range of electromagnetic problems. Microwave Office™ was verified and validated as a capable modeling and simulation tool for electronic systems to be used on the DD(X) program.

CONTENTS

1. BACKGROUND 1
1.1 USER NEED 1
1.2 M&S DESCRIPTION 1
1.3 M&S METHODOLOGY 1

2. PERFORMANCE 3
2.1 CONCEPTUAL MODEL VALIDATION 3
2.2 FUNCTIONAL VERIFICATION 3
2.3 SYSTEM VERIFICATION 4
2.4 RESULTS VALIDATION 4

3. RESULTS 5
3.1 MICROWAVE OFFICE™ 2002 DATA INPUT AND OUTPUT METHODS 5
3.2 LINEAR PASSIVE COMPONENT ANALYSIS 6
3.2.1 Microstrip Discontinuities 6
3.2.2 Very High Frequency Bandpass Filter 11
3.2.3 Parallel-Coupled Line Filter 13
3.2.4 8:1 Power Combiner/Splitter 14
3.3 LINEAR ACTIVE COMPONENT ANALYSIS 18
3.3.1 Transistor Circuit Model 18
3.3.2 FET Circuit Model 21
3.3.3 UHF Bipolar Transistor Amplifier 23
3.3.4 Microwave FET Amplifier 25
3.3.5 Feedback Amplifier Using FET Device 27
3.3.6 Balanced Amplifier Using FET Feedback Concept 29
3.3.7 Low-Noise Amplifier Using FET Device 31
3.3.8 Distributed Amplifier Using FET Device 33
3.4 NONLINEAR COMPONENT ANALYSIS 35
3.4.1 X-Band Amplifier Block Using MESFET 35
3.4.2 Large-Signal-Band Power Amplifier 39
3.4.3 Active Mixer Using an FET Device 45
3.4.4 Microwave FET Oscillator 48
3.5 SYSTEM-LEVEL ANALYSIS 49
3.5.1 System LNA (Five-Tone) 50
3.5.1.1 Introduction 50
3.5.1.2 Experimental Setup 50
3.5.1.3 System Model Parameters 53
3.5.1.4 Results 55
3.5.2 System Cascade 57
3.5.2.1 Introduction 57
3.5.2.2 Experimental Setup 58
3.5.2.3 System Model Parameters 59
3.5.2.4 Results 62
3.5.3 System Power Amplifier (Three-Tone) 65
3.5.3.1 Introduction 65
3.5.3.2 Experimental Setup 66
3.5.3.3 System Model Parameters 68
3.5.3.4 Results 70

3.5.4 System Mixer (Three-Tone) 72
3.5.4.1 Introduction 72
3.5.4.2 Experimental Setup 73
3.5.4.3 System Model Parameters 75
3.5.4.4 Results 76
3.5.5 System Super High Frequency (SHF) Amplifier (Three-Tone) 77
3.5.5.1 Introduction 77
3.5.5.2 Experimental Setup 77
3.5.5.3 System Model Parameters 80
3.5.5.4 Results 82
3.6 COMPUTER RUNTIME 83

4. CONCLUSIONS 85

5. REFERENCE 87

Figures

1. Microstrip junctions 7
2. Microstrip step schematic 7
3. Microstrip step results 9
4. Microstrip cross schematic 9
5. Microstrip cross results 10
6. Full-wave EM simulation 10
7. Microstrip tee schematic 11
8. Microstrip tee results 12
9. VHF filter schematic 12
10. VHF filter response 13
11. Parallel-coupled line filter schematic 14
12. Parallel-coupled line filter response 14
13. 8:1 power combiner circuit schematic 15
14. 8:1 power combiner splitter physical layout 16
15. 8:1 combiner isolation 17
16. 8:1 combiner transmission 17
17. Transistor circuit schematic 19
18. Transistor model S-parameter magnitudes 20
19. Transistor model S-parameter phases 20
20. FET model schematic 21
21. FET model S-parameter magnitudes 22
22. FET model S-parameter phases 22
23. UHF amplifier schematic 23
24. UHF amplifer S-parameter magnitudes 24
25. UHF amplifier S-parameter phases 24
26. TLIN FET amplifier schematic 25
27. TLIN FET amplifier S-parameter magnitudes 26
28. TLIN FET amplifier S-parameter phases 26
29. Feedback amplifier schematic 27
30. Feedback amplifier S-parameter magnitudes 28
31. Feedback amplifier S-parameter phases 29
32. Balanced amplifier schematic 30

33. Balanced amplifier S-parameter magnitudes 30
34. Balanced amplifier S-parameter phases 31
35. LNA schematic 32
36. LNA S-parameters 32
37. LNA noise figures 33
38. Distributed amplifier using MGF1801B 34
39. Distributed amplifier S-parameter data 34
40. Two-stage X-band amplifier schematic 36
41. Two-stage amplifier S-parameters 37
42. Two-stage amplifier noise figures 37
43. Two-stage amplifier gain curves 38
44. Two-stage amplifier I-V curves 39
45. Large-signal band power amplifier using lumped elements 40
46. Power amplifier small-signal gain (S_{21}) 41
47. Power amplifier small-signal, S_{11} and S_{22}, plotted on a Smith chart. 41
48. Power amplifier I-V curves 42
49. Power amplifier large-signal gain and distortion conversion 43
50. Power amplifier power-added efficiency 44
51. Power amplifier single-tone power spectrum 45
52. Active mixer schematic 46
53. Active mixer IF power versus RF frequency 47
54. Active mixer output power spectrum 47
55. Tunable FET oscillator schematic 48
56. LTCC oscillator output spectrum 49
57. System five-tone LNA schematic 51
58. System five-tone LNA experiment 52
59. Power sweep data 54
60. LNA output spectrum low drive 55
61. LNA output spectrum middle drive 56
62. LNA output spectrum high drive 56
63. UHF system cascade schematic 58
64. UHF system cascade experiment 59
65. Functional Block I: low-pass filter 60
66. Functional Block II: LNA/attenuator 61
67. Functional Block III: Power amplifier/attenuator 61
68. UHF system input return loss magnitude comparison 62
69. UHF system gain magnitude comparison 63
70. UHF system output return loss magnitude comparison 63
71. UHF system input return loss phase comparison 64
72. UHF system gain phase comparison 64
73. UHF system output return loss phase comparison 65
74. System power amplifier schematic 66
75. System power amplifier experiment 67
76. Mini-Circuits® power amplifier 68
77. Power amplifier gain curves 69
78. Power amplifier output spectrum low drive 71
79. Power amplifier output spectrum middle drive 71
80. Power amplifier output spectrum high drive 72
81. System mixer schematic 73

82. System mixer experiment 74
83. HP 10514A mixer device 75
84. Mixer output spectrum IF range 77
85. System SHF amplifier schematic 78
86. System SHF amplifier experiment 79
87. MITEQ® SHF amplifier and Omni-Spectra power combiner 80
88. SHF amplifier gain curves 81
89. SHF output spectrum low drive 82
90. SHF output spectrum high drive 82

Tables

1. System LNA equipment list 52
2. LNA measured system parameters 55
3. UHF system cascade equipment list 58
4. System Power amplifier equipment list 67
5. Measured system parameters for power amplifier 69
6. System mixer equipment list 74
7. Measured system parameters for mixer 76
8. System SHF amplifier equipment list 78
9. Measured system parameters for SHF amplifier 81
10. Computing runtime 83

1. BACKGROUND

1.1 USER NEED

DD(X) design teams were tasked to develop low-observable, high-bandwidth radio-frequency (RF) apertures. Technology that meets design requirements of phased array antennas and design and analysis of the electronic networks suitable for phased array excitation are of primary concern to system designers. Electronic networks, which require nonlinear microwave circuit components, must combine and separate multiple carrier frequency signals. Design engineers will need to accurately predict the performance of such systems by using numerical circuit simulation software tools. Modeling and simulation (M&S) software must accurately predict the performance of general multiport (N-port) circuits, including active and passive components, nonlinear phenomena, and system analysis. The software package must include a complete library of commercial off-the-shelf (COTS) microwave circuit devices and provide a method to specify circuit parameters for prototype components. It must also provide a method to specify circuit parameters to design new components for prototype development. Data outputs in the M&S software must include all relevant parameters that the design teams need. Furthermore, the M&S software user interface must be user-friendly to promote rapid development. The design teams can use M&S software for tuning, schematic layout, and performance analysis.

To address the shortfalls in existing M&S software in this area, the DD(X) Program Manager (PMS 500) created a development plan to deliver a Validated, Integrated, Physics-based Electromagnetic Radiation (VIPER) Tool Set that is responsive to DD(X) near-term prototype design needs. An independent panel of technical experts was established to identify, evaluate, and prioritize all relevant electromagnetic (EM) software tools that could be applied to Navy requirements. The panel initially met to determine the set of integrated top-side design (ITD) problems that the VIPER Tool Set should address and met later to evaluate existing software packages to solve ITD problems. At the conclusion of the VIPER panel's review, Microwave Office™, and the Advanced Development System (ADS®), which is also known as Series IV, were identified as the most promising microwave electronics simulation codes for the Navy's electronics need. Microwave Office™ was selected as the most promising code for satisfying DD(X) requirements. The validation and verification (V&V) effort is an enhancement to Microwave Office™ that commenced once the VIPER panel's independent review was completed.

1.2 M&S DESCRIPTION

Microwave Office™ 2002 (hereafter called Microwave Office™ M&S) combines linear and nonlinear circuit simulation with EM analysis and layout to provide a powerful design solution for RF and microwave engineering. Microwave Office™ M&S includes an extensive collection of component models that support RF subsystem analysis by using the well-known linear equivalent circuit treatment and the harmonic-balance methodology for treating nonlinear circuits. Microwave Office™ M&S is a COTS product developed by Applied Wave Research, Inc. (AWR). As part of its enhancement effort for the Navy, AWR also developed a phased array add-on package.

1.3 M&S METHODOLOGY

Microwave Office™ M&S offers a solution to the user needs mentioned in Section 1.1. A fully functional system installation requires a desktop computer running a Microsoft Windows® operating system, the commercial AWR Microwave Office™ M&S package, the phased array add-on package developed for the Navy, and examples and operational notes developed during this V&V effort.

The hardware and software requirements to run Microwave Office™ are as follows:

- Pentium PC, 200 MHz or higher
- 64-MB RAM minimum
- 200-MB available disk space, minimum
- Microsoft Windows® 2000, NT®4, ME, or 98
- Microsoft® Internet Explorer Version 5.0 or later

Technical support is also available from the M&S developer and the V&V agent. The M&S developer provided instruction manuals, including tutorials and example simulations on current commercial microwave electronics research. The test cases used to verify and validate the M&S will also be available to M&S users, including documentation and source files. These test cases were chosen to include standard problems from microwave circuit theory and simulations of physical systems under development that are compatible with the DD(X) design concept.

2. PERFORMANCE

2.1 CONCEPTUAL MODEL VALIDATION

The Microwave Office™ M&S provides microwave circuitry analysis that relies on the well-known linear equivalent circuit treatment and the harmonic-balance methodology for treating nonlinear circuits. Numerical analysis of linear circuits is a straightforward and universally accepted practice. However, Microwave Office™ M&S users will also require the accurate modeling of nonlinear circuits. Validation of the conceptual model for the nonlinear circuit analysis consists of verifying the accuracy of the harmonic-balance technique as applied to system and component nonlinear circuits. Furthermore, the scope of nonlinear phenomenon that this technique covers must encompass the intended needs of the M&S users.

Harmonic-balance analysis splits the circuit into linear and nonlinear subcircuits. Input and output ports connect the subcircuits together. The harmonic-balance simulator solves the circuit equations iteratively to find the voltages at these ports, which are variables. The port currents satisfying Kirchoff's current law at every harmonic are used to determine correct solutions. Harmonic-balance analysis is applied to strongly nonlinear circuits with large-signal, single-tone excitation.

The V&V agent identified three commercial software packages for comparison: ADS®,[1] Series IV,[2] and Touchstone®.[3] Measured data from actual circuits were also used for result comparison. The assumptions and data approximations made in the theoretical developments of the M&S computational engine were also examined for technical justification. The problem domain covered by these analyses was categorized and falls within the scope of M&S user needs. This report provides the evidence needed to assess the functional adequacy of the M&S software. The information gathered concerning the applicability and expected variance of each functional element of the M&S code was matched with the specific user requirements that it addressed.

2.2 FUNCTIONAL VERIFICATION

The functional implementation of the Microwave Office™ M&S conceptual model consists of an integrated design environment that allows the user to easily enter schematic diagrams or layout planar, physical structures for full-wave EM analysis in a standard Microsoft Windows® graphical user interface (GUI). It automatically determines which type of analysis to perform by reviewing the circuit components and output data selected. Circuit parameters can be manually tuned and automatically optimized to achieve desired system performance.

Verification of functionality consisted of identifying shortfalls in the available tools needed in the accurate analysis for a given circuit simulation within the M&S software. Specific categories of microwave circuit analysis defined in the conceptual model were verified by separate test cases. These circuits represented a cross section of the devices and systems handled by the M&S computational engine. Individual test cases provided a check on the validity of each element in its functional implementation. Test cases, which included all relevant categories of circuit analysis, were analyzed to determine the effectiveness with which the M&S functions are used across a broad range of problems. For example, complex circuits or systems that require ordinary linear and harmonic balance analysis were modeled and simulated. The range of output data options were also investigated to determine whether the needs of the M&S user will be completely satisfied. A list of available validated device models and components was assembled and analyzed for applicability,

[1] ADS® version 2002, Agilent EEsof, Inc..
[2] Series IV® version 6.6, Agilent EEsof, Inc.
[3] Touchstone® version 3.0. 1991. EEsof, Inc.

including system architecture and N-port devices that are critical to DD(X) designers. Output data visualization functions were assessed for accuracy and compatibility with other software featuring visualization functions. Available options for plots, tables, and output file formats were evaluated for comprehensiveness and portability.

2.3 SYSTEM VERIFICATION

System verification was performed at the University of California, Los Angeles (UCLA) and SPAWAR Systems Center San Diego (SSC San Diego). Both teams performed basic checks on the algorithms used in the M&S software. Test results confirmed the proper functional implementation of the conceptual models. During the test case evaluation, the Microwave Office™ M&S software was compared against similar commercial software. Input and output data formats were tested for compatibility with the M&S software under test. The M&S software's GUI is highly efficient and user-friendly. The GUI closely resembles the process used in experimental procedures. M&S software documentation is informative and provides tutorials of simple design problems; however, the user must be adequately trained in microwave engineering. The computational engine and GUI input modules were stable and no major problems were detected.

2.4 RESULTS VALIDATION

The V&V teams constructed test models within Microwave Office™ and generated data against performance metrics relevant to the circuits and systems under investigation to validate the M&S software. Test case simulation results were compared to experimental measurements taken on actual systems and numerical data were obtained from widely used microwave circuit simulators. Some test cases were chosen to verify the M&S software performance in a specific area of user need. In other cases, the underlying theoretical framework of the M&S software was validated. In all cases described in Section 3, the comparisons were favorable.

3. RESULTS

3.1 MICROWAVE OFFICE™ 2002 DATA INPUT AND OUTPUT METHODS

Microwave Office™ M&S is a powerfully integrated design and analysis tool for RF, microwave, and millimeter wave circuits and systems. Software users can design complex circuits composed of linear and nonlinear components and EM structures and generate physical layouts of these designs. They can also perform fast and accurate design analysis by using linear, nonlinear harmonic balance, EM simulation engines, and real-time tuning and optimizing tools.

The design environment in Microwave Office™ M&S allows projects to manage and link related designs in a directory tree. Projects can encompass any desired set of designs and can include one or more linear schematics, nonlinear schematics, and/or EM structures. Projects can also include anything associated with the designs, such as imported files, layout views, or plots.

Users can design a system within Microwave Office™ in two ways. When starting a new project, the user can use the element catalog to assemble a schematic. The element catalog has a comprehensive database of electrical component groups such as lumped elements or microstrips that can be selected and included in the desired schematic. Users can drag and drop these elements in any configuration by connecting the elements together, using connection wires to define a circuit. They can then edit element parameters, i.e., resistance, capacitance, etc., to define each element in the schematic.

Another way to design a system in Microwave Office™ M&S is to import data files. Imported data files can be raw data, Touchstone® data files, or DC-IV data files. The DC-IV data file format is a Microwave Office™-specific format reserved for reading in DC-IV curves for comparison. They are typically S-parameter files or some other type that contain frequency-domain N-port parameters. These imported data files will define a subcircuit within the project and can be dragged and dropped into the schematic like any other subcircuit.

Once the circuit has been designed in Microwave Office M&S, the user must specify the desired output format for the results before the simulation can run. Microwave Office™ M&S allows users to choose from a wide variety of plots or tables to display the results. As an alternative to displaying simulation results on graphs, users can also export the results to data files for Touchstone®, SPICE,[4] AM to AM, AM to PM, or spectrum data file format.

Microwave Office™ M&S features extensive post-processing capabilities that allow display of computed data on rectangular graphs, polar grids, Smith charts, histograms, and antenna pattern plots. Microwave Office™ M&S can display any port parameter (such as S, Y, Z, H, G, or ABCD), voltage standing-wave ratio (VSWR), maximum gain, and stability plots. It can display the magnitude, angle, real, or imaginary component of any measurement that uses a decibel or linear scale. It can also display port impedances and propagation constants. Users can also change the position and size of graphs and legends by using click-and-drag mouse editing and can zoom and pan to see small details. All these post-processing capabilities allow the user to rapidly design a circuit and see its predicted results in any effective format. The GUI allows the user to easily adjust the desired output parameters and facilitates quick turnaround and fine-tuning schematics.

[4] SPICE, University of California, Berkeley, CA. http://bwrc.eecs.berkeley.edu/Classes/IcBook/SPICE/

3.2 LINEAR PASSIVE COMPONENT ANALYSIS

Purpose

In the following four test cases, we investigated the M&S software's proficiency in analyzing various linear passive microwave circuits. These examples included lumped and distributed elements. The successful simulation of linear passive components is a prerequisite for any microwave M&S software because they are used in virtually all RF applications.

Assumptions

Empirical formulas used to represent these devices are only valid within certain operating regimes (usually below a certain frequency). For example, lumped elements such as resistors, capacitors, and inductors behave as classical devices only in the limit where the wavelength is long compared to the physical dimensions of the circuit. Distributed elements such as microstrip components are treated as quasi-transverse electromagnetic, non-radiating structures. At higher microwave frequencies, these assumptions are not valid. We remain within the established limits for the components and specify failure conditions where possible.

Procedures

In general, the technique used to validate these linear passive components is to construct the following circuits in several different M&S packages and compare their respective results. For linear passive components, only reflected and transmitted power magnitudes and phases for one propagation direction are compared because the devices respond symmetrically (i.e., $S_{11} = S_{22}$ and $S_{12} = S_{21}$ for a two-port linear passive reciprocal device). Different software packages will not always use the same models (especially for distributed elements), and the source of any discrepancies is identified. The M&S results may then be verified by using the more rigorous electromagnetic analysis.

S-parameter data, or the scattering matrix, which represents device performance, were generated from each M&S software used. The scattering matrix provides a complete description of the network as seen at its N ports. It relates the power waves incident on the ports to those reflected from the ports. In these examples, four S-parameters are of interest. S_{11}, S_{21}, S_{22}, and S_{12}. S_{11} represent the input return loss, or impedance mismatch, at the input. S_{11} can also be described as the reflection coefficient seen at port 1 when port 2 is terminated with a load. S_{21} represents the insertion loss at the input. It can also be described as the transmission coefficient from port 1 to port 2.

3.2.1 Microstrip Discontinuities

Simulation of microstrip junction components is an essential element in any microwave circuit analysis because virtually all distributed microwave components contain these components. During this study, simulations were performed for microstrip step, cross, and tee empirical models (Figure 1). We constructed and analyzed simple passive circuits that use these devices. The simulation frequency range is 1 to 14 GHz. The M&S software uses empirical models to represent the microstrip junctions in the circuit analysis. In general, these models are valid only in a limited parameter regime because they do not account for radiation or propagation of higher order modes. Test case results identified general conditions under which the models were valid.

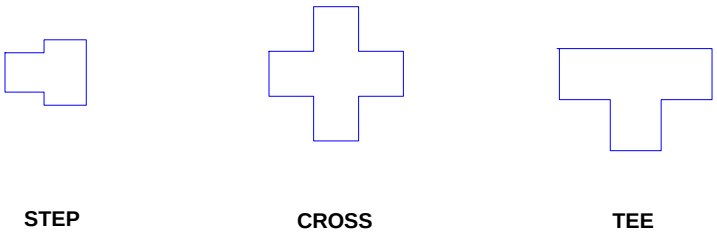

Figure 1. Microstrip junctions.

All three microstrip junction components are generally used in similar applications. They are individual elements of an integrated circuit that can be designed for different applications. Some element applications are in impedance-matching networks, filters, and power-splitting circuits. At low frequencies, the responses of these elements are easy to model. As the frequency increases, parasitic effects at the discontinuities make these elements much more difficult to model accurately. For the M&S software to accurately predict the performance of circuits that use these elements at high frequencies, the software must account for these parasitic effects.

In the first example, we simulated a microstrip step device in Microwave Office™ M&S and a comparison code, Advanced Design System (ADS®), and compared the outputs from each code. This device connected microstrip lines of differing widths and is commonly used for impedance transformation and half-wave filters. The junction of two lines with different widths, w1 and w2 (i.e., different impedances, Z1 and Z2), forms an impedance step. This impedance mismatch causes a transmission line discontinuity. At lower frequencies, the losses associated with this discontinuity may not be significant enough to warrant characterization; however, at higher frequencies, the losses will become significant enough to warrant characterization. In this model, the thickness, h, and relative dielectric constant of the substrate were kept constants for either line. Figure 2 shows the configuration used in this example.

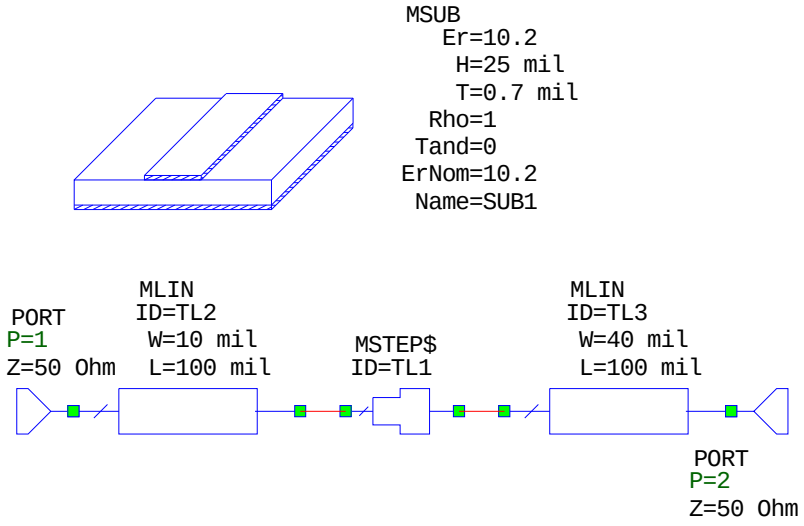

Figure 2. Microstrip step schematic.

ADS® is a powerful electronic design simulation package that Hewlett-Packard® (now part of Agilent Technologies Inc.) originally developed. It offers a complete design integration software package to designers of products such as pagers, wireless networks, cellular and portable phones, and radar and satellite communications systems. ADS® is one of many M&S software packages used in the RF design community for modeling and simulation of radio-frequency integrated circuit (RFIC) and RF/microwave monolithic integrated circuit (MMIC)/microwave circuits.

As Figure 3 shows, the prediction results from MWO and ADS® for the microstrip step example are virtually identical. The plot shows that at lower frequencies below 3 GHz, the input return loss is very small; thus, almost all energy is transmitted. At higher frequencies above 9 GHz, the input return loss increases to about –5 dB as more energy is reflected as the signal encounters the step. This increase in input return loss corresponds to an increase in the insertion loss to about –2 dB. At higher frequencies, less energy is transmitted than at lower frequencies for the microstrip step element, which agrees with the prevailing theory. MWO and ADS® predictions agree almost exactly for the entire 1- to 14-GHz frequency range.

The second microstrip discontinuity example was a cross element. A microstrip cross element is needed for impedance-matching networks in which the simple impedance transformation does not suffice. Cross elements can also frequently be found in filters and power-division applications. The cross element simulated in this example operates as a bandpass filter. A cross element has four ports that, depending on the application, are terminated differently. In an impedance-matching or filter application, only two ports are terminated, with the other two ports left open. In a power-division application, all four ports are terminated. For the cross element in this example, ports 1 and 2 are the input and output ports respectively, while ports 3 and 4 are terminated reactively. Figure 4 shows the configuration used for this example. The simulation was performed in MWO and ADS® for comparison.

Figure 5 shows MWO and ADS® microstrip cross simulation results. Data from the two codes agree reasonably well over the simulated frequency band. An observable shift in the center frequency exists between the two codes. The center frequency in the MWO simulation was 10 GHz, while the ADS® center frequency was 11 GHz, a 10% shift. MWO's improved ability to account for the parasitic effects at higher frequencies causes this discrepancy. Figure 6 compares MWO circuit analysis, MWO full-wave EM analysis, and Conformal Finite Difference Time Domain (CFDTD). The data show excellent agreement across the spectrum and a 10-GHz center frequency. This result shows that compensating for parasitic effects is more accurate in the Microwave Office™ simulation than in the ADS® simulation.

The S-parameter data in Figure 5 describe the input return loss, S_{11}, and the insertion loss, S_{21}, performance of the microstrip cross element. The microstrip cross element in this example behaves as a bandpass filter, as designed. In this particular example, the bandpass region is approximately 8 to 12 GHz. This region has the lowest insertion loss and lowest input return loss.

A tee element was the final microstrip discontinuity example. A microstrip tee element is also needed for impedance-matching networks in which the simple impedance transformation does not suffice. Like cross elements, tee elements can frequently be found in filter and power-splitting/ power-combining applications. In this example, a tee element was used in the bandpass filter design. A tee element has three ports that can be terminated differently, depending on the application. In a filter or impedance-matching application, only two ports would be terminated. In a power-dividing application, all three ports would be terminated. The tee element in this example has ports 1 and 2 as the input and output ports respectively, while port 3 is terminated reactively. Figure 7 shows the configuration used for this example. The filter was simulated in MWO and ADS® for comparison.

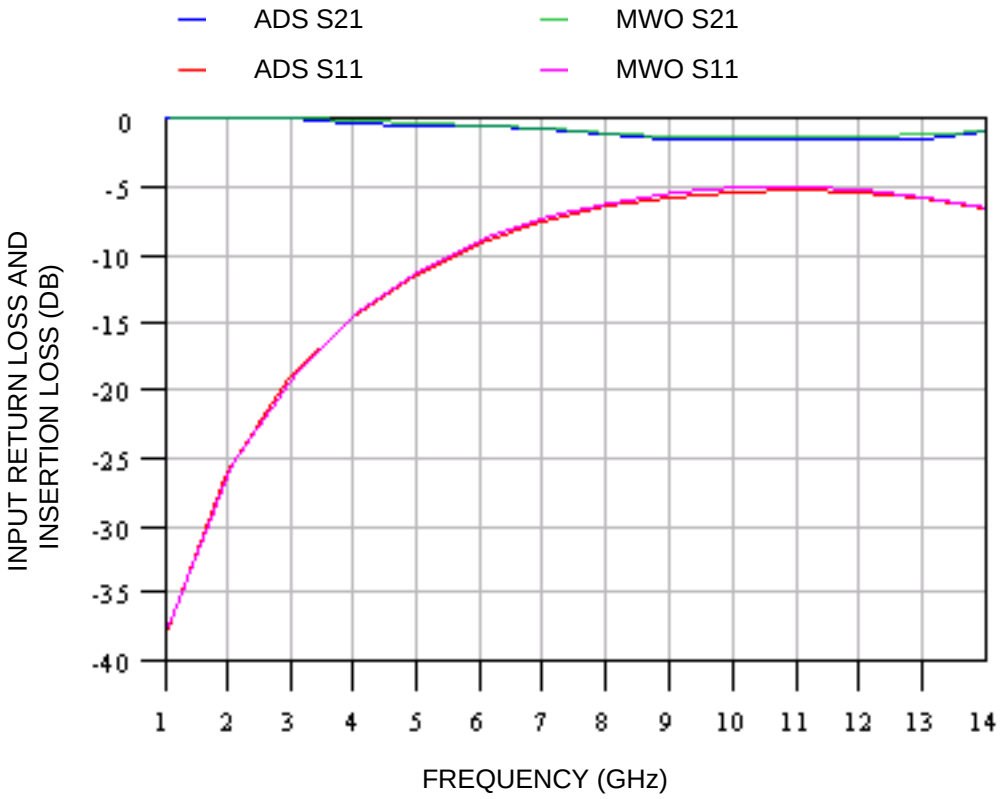

Figure 3. Microstrip step results.

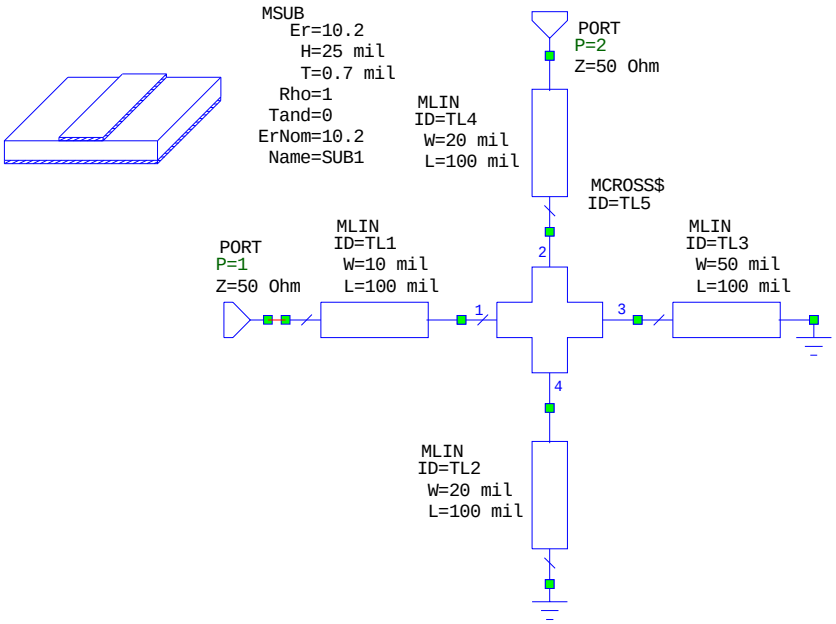

Figure 4. Microstrip cross schematic.

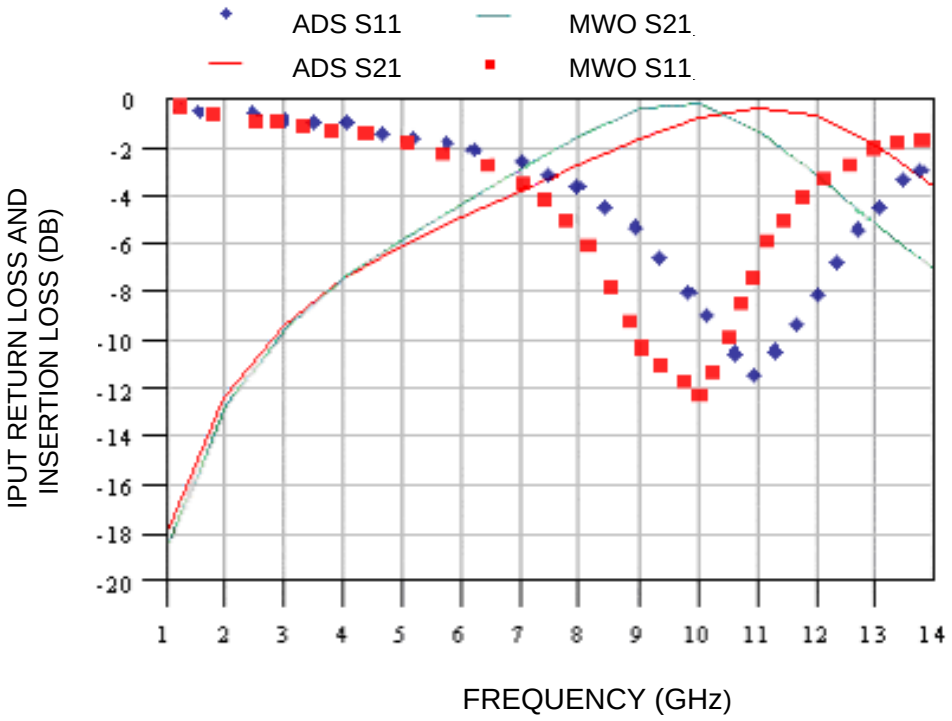

Figure 5. Microstrip cross results.

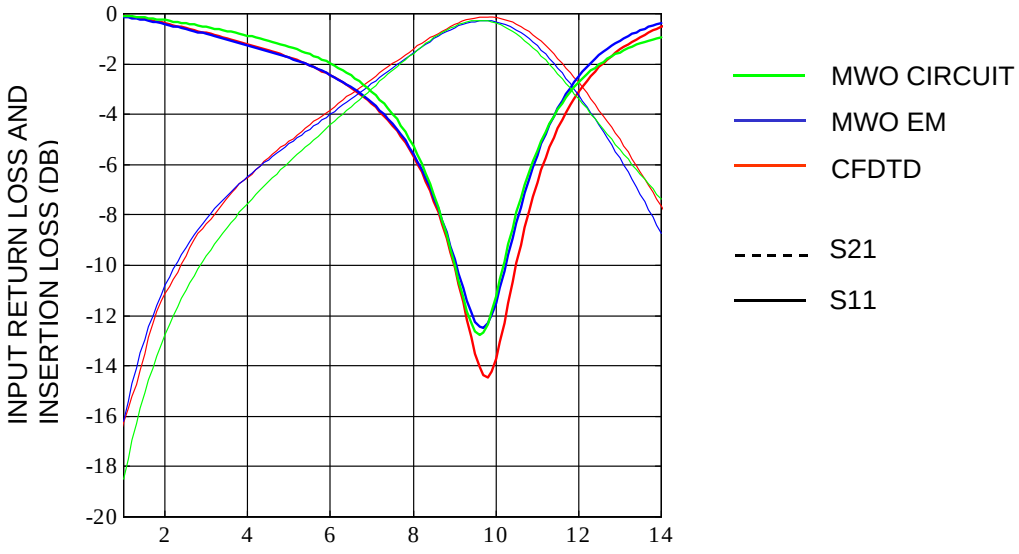

Figure 6. Full-wave EM simulation.

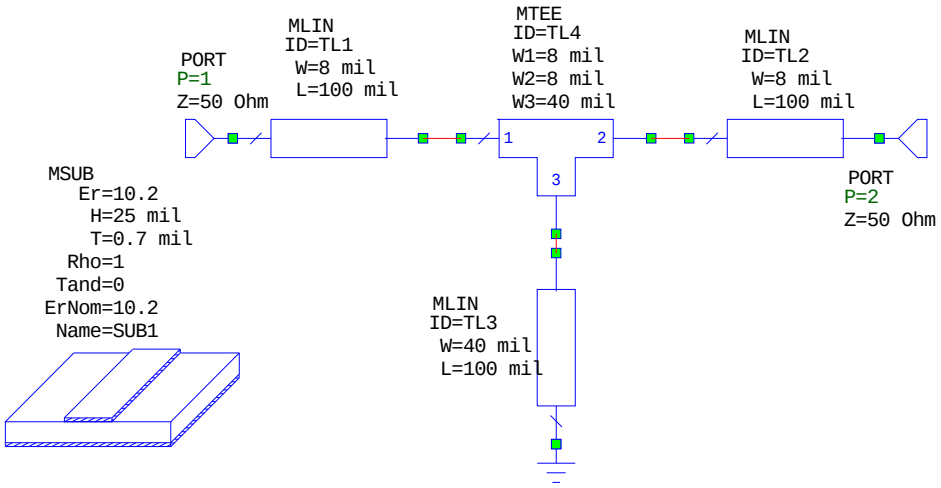

Figure 7. Microstrip tee schematic.

Figure 8 shows the MWO and ADS® microstrip tee simulation results. The two codes agree reasonably well, as the curve profiles nearly match. The center frequency of the bandpass region from codes is about 11 GHz. The curves have the same profile over the entire frequency band, with just a slight frequency shift.

S-parameter data in Figure 8 describe the input return loss, S_{11}, and the insertion loss, S_{21}, performance of the microstrip tee element. This microstrip tee element behaves as a bandpass filter. In this particular example, the bandpass region is approximately 10.5 to 11.5 GHz. The input impedance is matched in this region, and as a result, the insertion loss is low. The spectral response shown here is typical for a microstrip tee element.

3.2.2 Very High Frequency Bandpass Filter

The very high frequency (VHF) bandpass filter test case analyzed the electrical performance of a lumped-element bandpass filter. This case was simulated at low frequencies, so lumped elements were appropriate to use because they are essentially lossless and can be realized at low frequencies. This circuit consists of fixed value and variable capacitors and inductors. Variable components allow tuning the filter to achieve the appropriate center frequency and desired bandwidth. The simulation operates in the 200- to 300-MHz frequency range, and the filter passes signals from 230 to 270 MHz. Figure 9 shows the schematic used for this simulation. The filter in the example consists of many resonators, each consisting of a capacitor, inductor pair. A capacitor between each resonator couples each resonator together. By using the superposition principle, many resonators are coupled together this way so that the resulting circuit acts as a filter in the desired frequency range. We compared simulation data in Microwave Office™ and Touchstone®.

Touchstone® is a computer-aided-engineering M&S software program for RF/microwave design and was originally a product of EES Incorporated and is now with Agilent Technologies Inc. With Touchstone®, users can perform linear analysis, interactive tuning, optimizing, and Monte Carlo yield prediction of virtually all RF/microwave circuits. Touchstone® is a generally accepted M&S software package for designing RF/microwave circuits. Touchstone® was used here for comparison with MWO's ability to simulate RF/microwave circuits accurately.

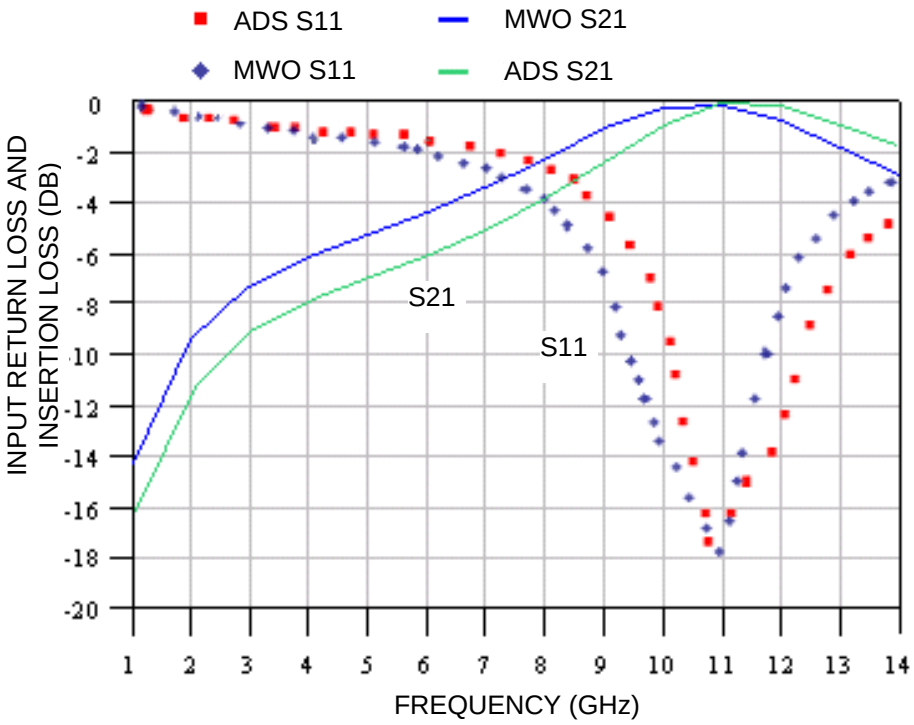

Figure 8. Microstrip tee results.

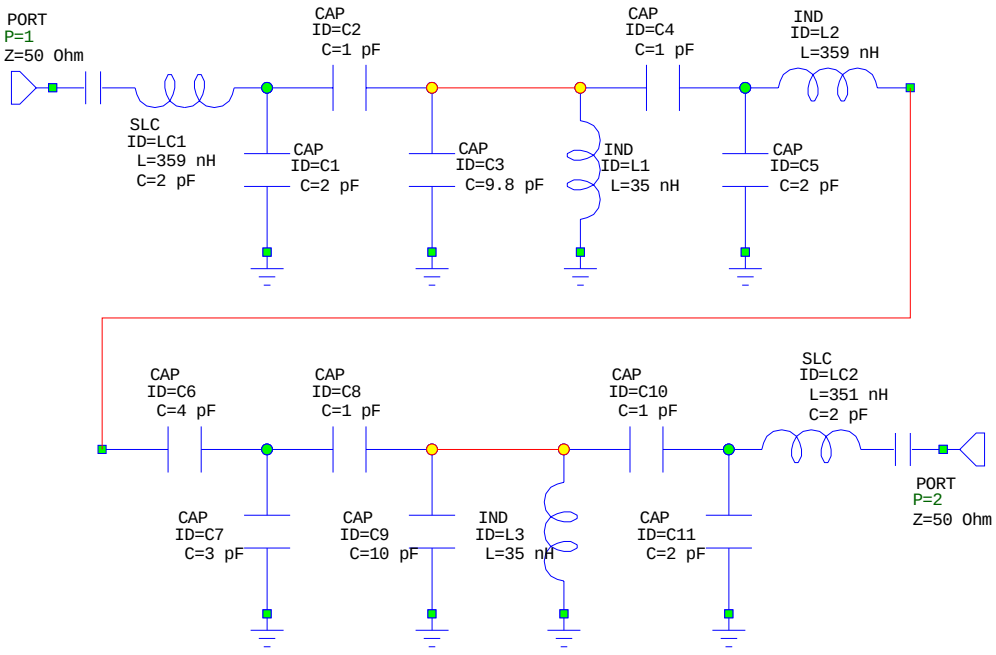

Figure 9. VHF filter schematic.

Figure 10 shows results from Microwave Office™ and Touchstone®. The circuit in the problem was not optimized; it only compared the codes. The amplitude response of the filter shows that the bandpass region of this filter is from approximately 230 MHz to 270 MHz, exactly the bandpass range for which the circuit was designed. In this region, the input return loss and insertion loss are at their lowest. Some losses exist at around 250 MHz, which is a degradation of about 5 dB in insertion loss and a corresponding rise in the input return loss to about –1.8 dB. These losses occur because the circuit was not optimized for this bandpass range. The response magnitude and phase are plotted for both codes. Results agree exactly between the two codes over the 200- to 300-MHz operating region.

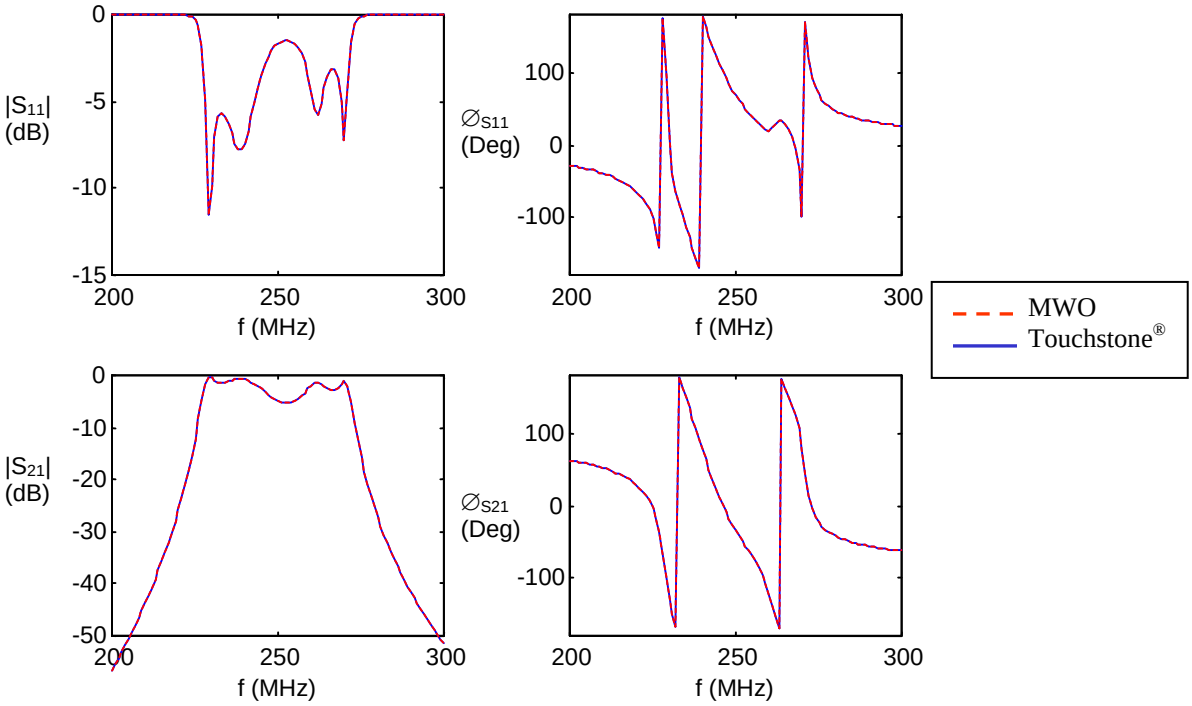

Figure 10. VHF filter response.

3.2.3 Parallel-Coupled Line Filter

In this test case, we used the parallel-coupled line concept to analyze the frequency response of a microwave filter. The filter consists of four microstrip resonator sections on a quartz substrate. Microstrip line spacing determines the coupling factor. Resonator length determines the resonant frequency of this filter type. Physical parameters specify design details. This filter type is used at high frequencies in microwave printed circuit elements. Lumped elements cannot be used in this type of circuit because lumped elements such as inductors and capacitors are generally available only for a limited range of values and are difficult to realize at microwave frequencies. At microwave frequencies, the dimensions are also not negligible for the operating wavelength. We used Microwave Office™ to simulate the filter frequency response at between 9 and 14 GHz and compared the results with Touchstone® numerical data. Touchstone® is a valid simulation program for this type of problem. Figure 11 shows the distributive circuit configuration used for this simulation.

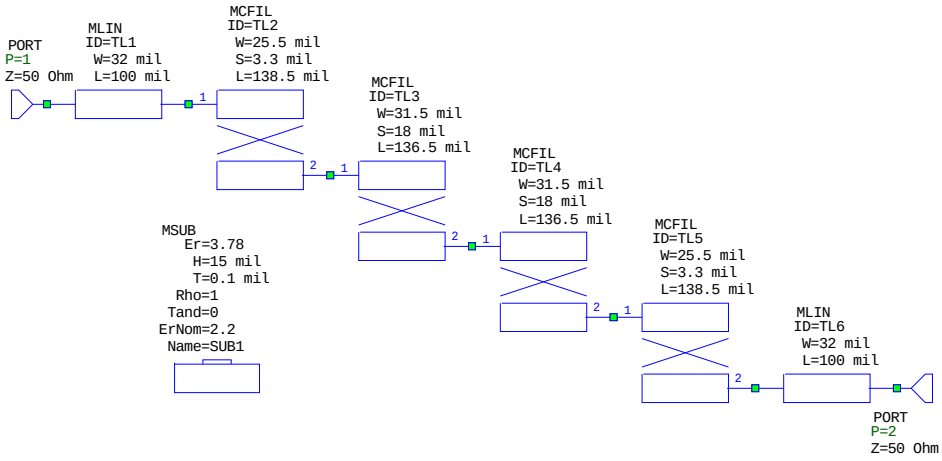

Figure 11. Parallel-coupled line filter schematic.

Figure 12 shows S-parameter data simulated from each code. Data compared from each code closely agree. The S_{21} parameter shows the bandpass region for this filter as approximately 11.5 to 12.5 GHz. The S_{11} parameter shows that the input return loss over the bandpass region is below –13 dB and is about 0 dB at the low and high ends. Coupled-microstrip elements modeled between the two codes are almost identical in the operating frequency. The magnitudes of the S-parameters differ by a fraction of a decibel in the bandpass region. The bandpass region frequencies are nearly the same in the two analyses.

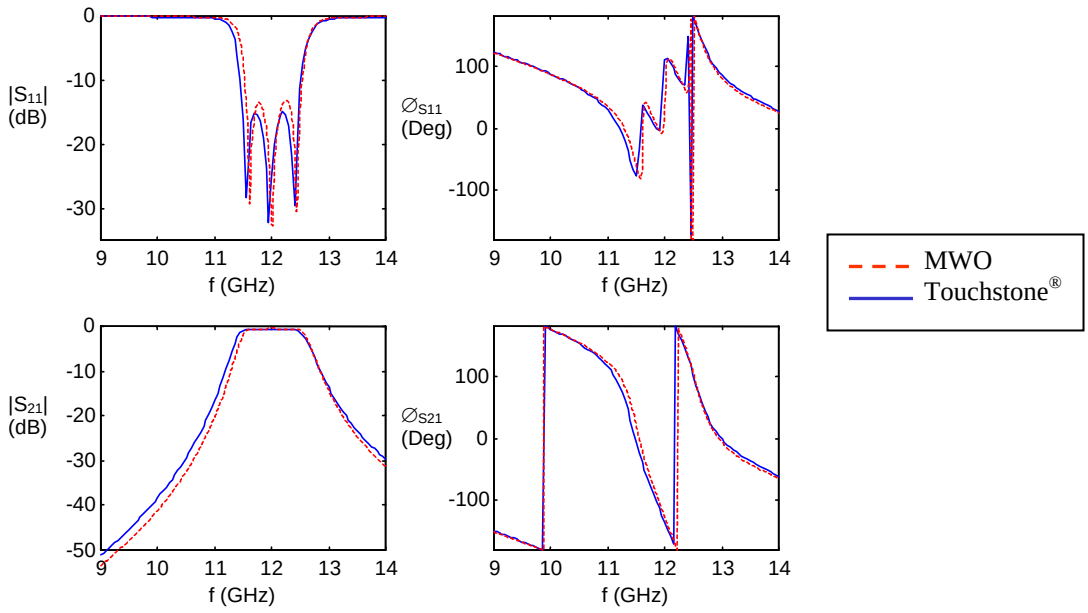

Figure 12. Parallel-coupled line filter response.

3.2.4 8:1 Power Combiner/Splitter

This example simulated the multiport S-parameters of an 8:1 corporate-feed network for an antenna array. This type of feed network can be used to combine/split power or as a feed network

to antennas. When combining or splitting power, this type of network can be designed to split the power equally or disproportionably, depending on the application.

We used a transmission line model circuit and electromagnetic models of the circuit discontinuities to perform analyses. The intention was to use the design to achieve constant amplitude and proper phase response over the operating bandwidth. The phase shift along each path must be the same, which required that the physical length of each path be the same. We also needed to characterize isolation between different input/output ports. The circuit layout (Figure 13) was simulated over the 1- to 10-GHz frequency range. A microstrip transmission line design was used with resistors for added isolation. To incorporate the 50-ohm resistors into the simulation, the passive microstrip circuits were first physically laid out so they could be represented by multiport S-parameters. To simulate the whole circuit, we connected the resistors to their respective ports on the schematic layout.

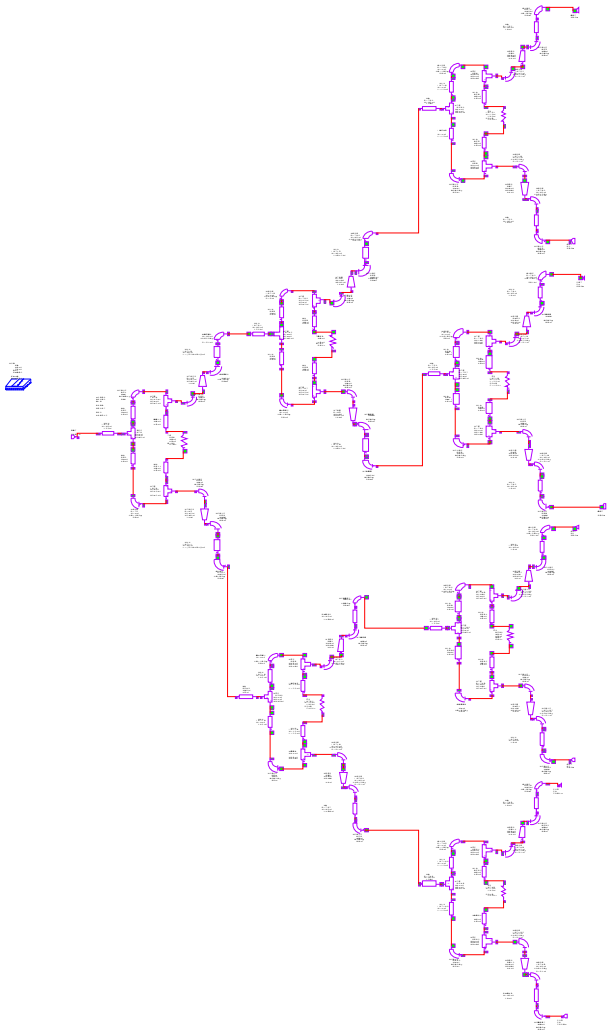

Figure 13. 8:1 power combiner circuit schematic.

Besides schematic design and analysis, the MWO software contains physical layout capabilities. For example, the MWO software can convert the schematic in Figure 13 into a physical layout with

all the physical dimensions of the designed structure (Figure 14). The physical layout is exportable in several file formats that are required for automated etching and fabrication.

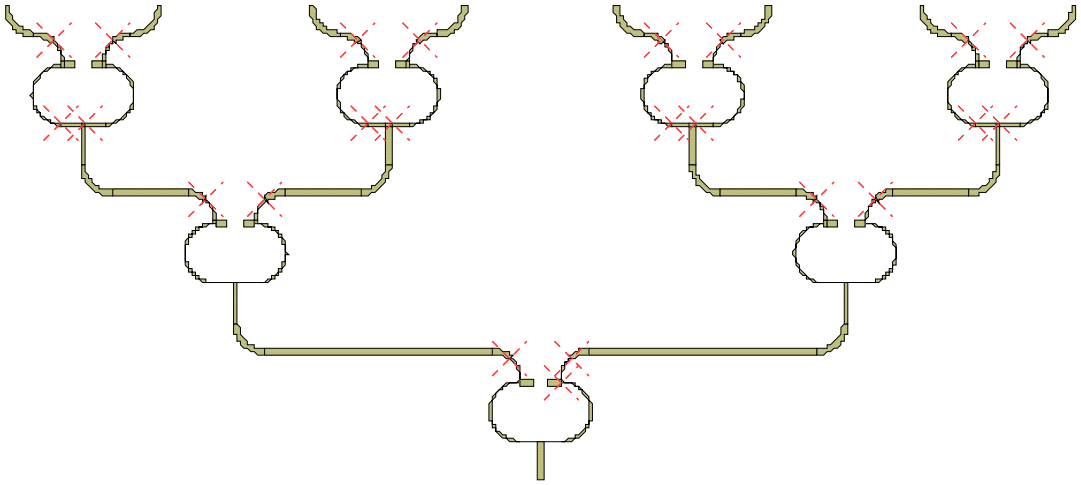

Figure 14. 8:1 power combiner splitter physical layout.

This example was simulated in Microwave Office™ and ADS® and we compared their respective multiport S-parameters. Figure 15 shows the combiner isolation among three sets of ports over the entire frequency range. Isolation curves are shown between ports 2 and 3 (S_{23}), ports 3 and 4 (S_{34}), and ports 5 and 6 (S_{56}). These sets of curves were selected because of the layout symmetry. These isolation calculations represent the typical isolation calculations of concern. Combiner isolation varies with frequency. Isolation is optimized between 5 and 7 GHz. Results from each code correlated very well because the profiles of each curve are similar over the entire frequency range. Differences between 5 and 7 GHz in high isolation beyond –20 dB values are insignificant. Because these isolation maxima occur in the passband between 5 and 7 GHz, this slight difference can be attributed to Microwave Office's ability to account for the parasitic effects at points of discontinuity.

Figure 16 shows the combiner transmission curves over the entire frequency band. Combiner transmission is below –9.2 dB over the entire frequency band. In theory, there should be a 3-dB loss through each split. Since the signal is split three times between the input and output ports, 3 dB per split should add up to 9 dB. Thus, the simulation agrees with theory. However, transmission loss goes down to –10.2 dB with ADS® and –10.8 dB with MWO at about 8.5 GHz. The codes correlate very well over the entire frequency band. About a 0.2-dB difference exists between the two codes; however, this difference is less than 2% and is insignificant. Example results demonstrate the multiport S-parameter simulation capability of MWO.

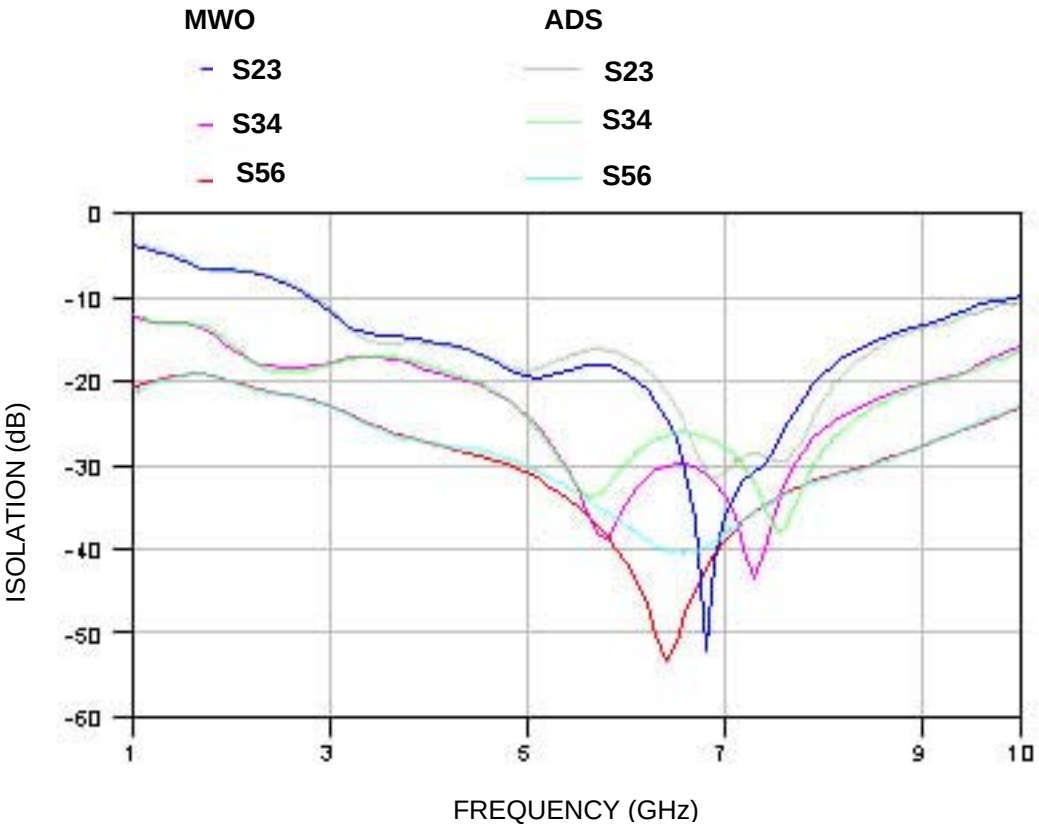

Figure 15. 8:1 combiner isolation.

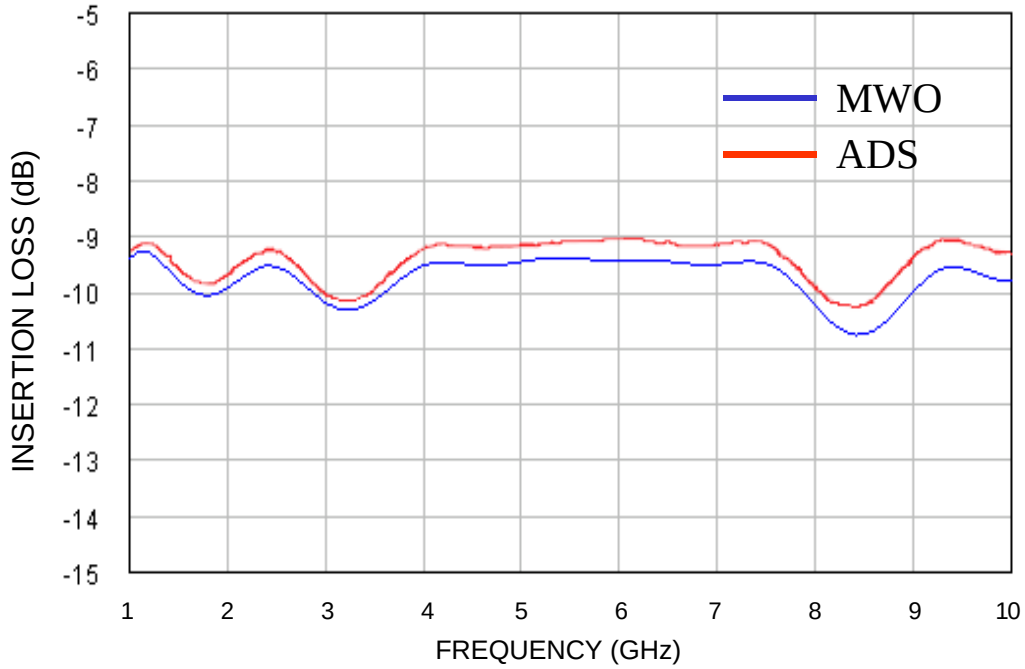

Figure 16. 8:1 combiner transmission.

3.3 LINEAR ACTIVE COMPONENT ANALYSIS

Purpose

The next eight validation cases are examples of linear components that use active devices. All these cases use transistor devices. In some cases, S-parameters obtained from measurements of devices operating in the linear regime characterize the device. Other cases use equivalent circuit models containing lumped elements and ideal sources to represent the transistor behavior.

Assumptions

Linear active circuits used in these test cases contain many of the same structures examined in the preceding passive examples. A major difference is that the circuit is now non-reciprocal. Accordingly, the assumption on the validity of the passive models is extended to cover the linear active test cases. The linear models used to represent the active transistor elements must also be valid over the operating regime of the simulation. A complete set of complex S-parameters must characterize linear active elements because energy propagation generally has a preferred direction. In these linear test cases, it was assumed that the devices were operating well within the linear regime and that nonlinear effects such as gain compression and harmonic generation were negligible.

Procedures

In general, the technique used to validate these linear active components is to model the following circuits and compare their results with either alternate simulation software or experimentally measured data. Typical circuits contain active elements (transistor) and impedance-matching networks. Low-frequency examples contain lumped element matching networks, but higher frequencies need distributed networks that can be specified by electrical or physical parameters. In the amplifier cases, the active element performance may be specified in a standard format of S-parameter data over a frequency range by an analytic expression derived from an equivalent circuit model. In either case, the performance metrics used in the validation were complex S-parameters measured over a specified frequency range.

3.3.1 Transistor Circuit Model

Transistors are active elements typically used in amplifier and oscillator applications. Field-effect transistors (FETs) are generally used, depending on the application, to produce higher gain, higher output power, or lower noise figures in amplifiers. One type of FET that is commonly used is the metal-oxide semiconductor field-effect transistor or MOSFET. These types of transistors are also used in low-frequency linear circuits. Advantages of these devices include high gain, relative immunity from thermal runaway, and the ability to withstand severely mismatched loads without suffering damage.

In this example, we examined an equivalent circuit model MOSFET and used a transistor element available in the M&S software's device library instead of an equivalent lumped-element circuit to model the transistor. Figure 17 shows the circuit configuration used for this test case. To use this transistor element, the user must define the Longitudinal Redundancy Check (LRC) components that define the transistor characteristics (i.e., components RI, CDG, etc.) within the FET. This transistor device is commercially available from Motorola® (MRF134). The equivalent circuit contains 11 LRC elements and an idealized voltage-controlled current source. The intrinsic device is characterized by various characteristic components (Computer Ground Station [CGS], Ground Guidance Station [GGS], RI, CDG, CDC, CDS, RDS, RS). The inductors and resistors (RL1, RL2) represent the input and output lead characteristics. This circuit is intended for VHF operation.

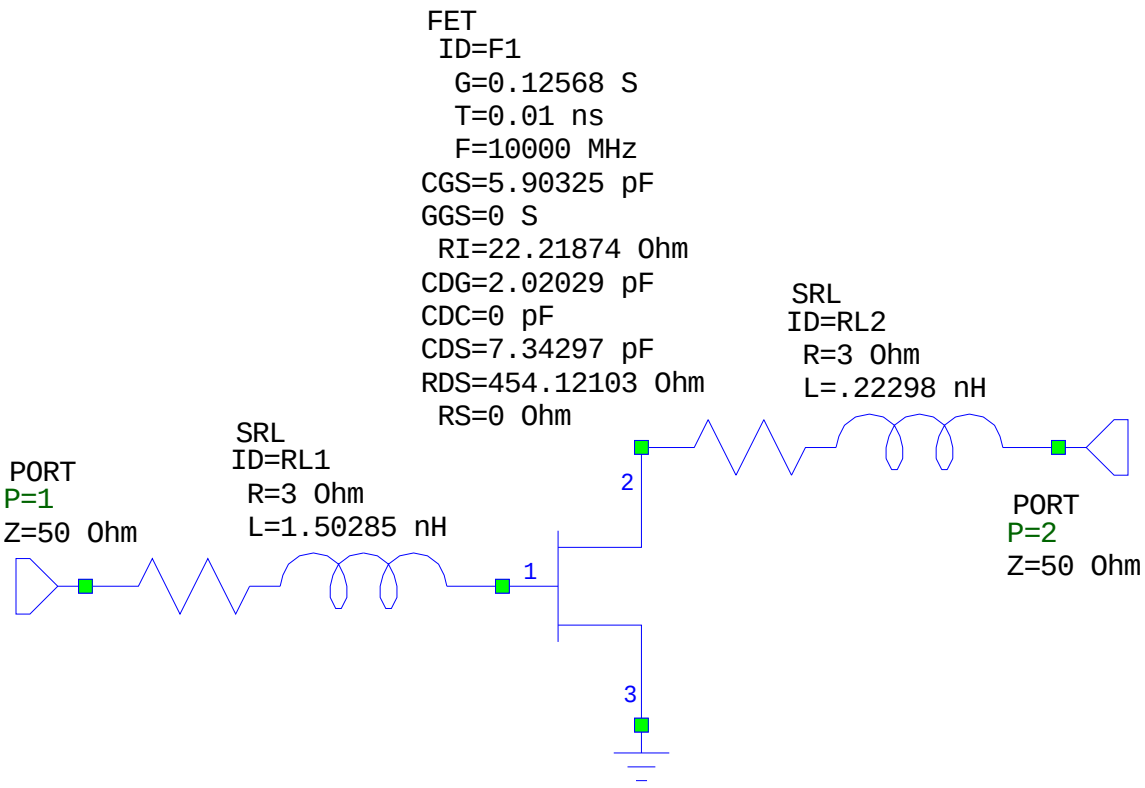

Figure 17. Transistor circuit schematic.

Figures 18 and 19 show the predictions from Microwave Office™ and Touchstone® for the S-parameter magnitudes and phases. The gain achieved, S_{21}, starts at about 21 dB at 1 MHz and decreases as frequency increases. This measurement is consistent with MOSFET theoretical operation. Input return loss starts from 0 dB at 1 MHz and gracefully degrades to –6.4 dB at 300 MHz, while the output return loss starts from about –1.9 dB at 1 MHz, degrading to about –4.8 dB at 300 MHz. These values will improve through matching networks. Isolation between the input and output ports, S_{12}, is greater than –40 dB at 1 MHz and increases to about –19 dB at 200 MHz. Isolation of –20 to –40 dB is typically considered adequate for this type of transistor. Predictions from Microwave Office™ and Touchstone® agree exactly for magnitude and phase over the entire band.

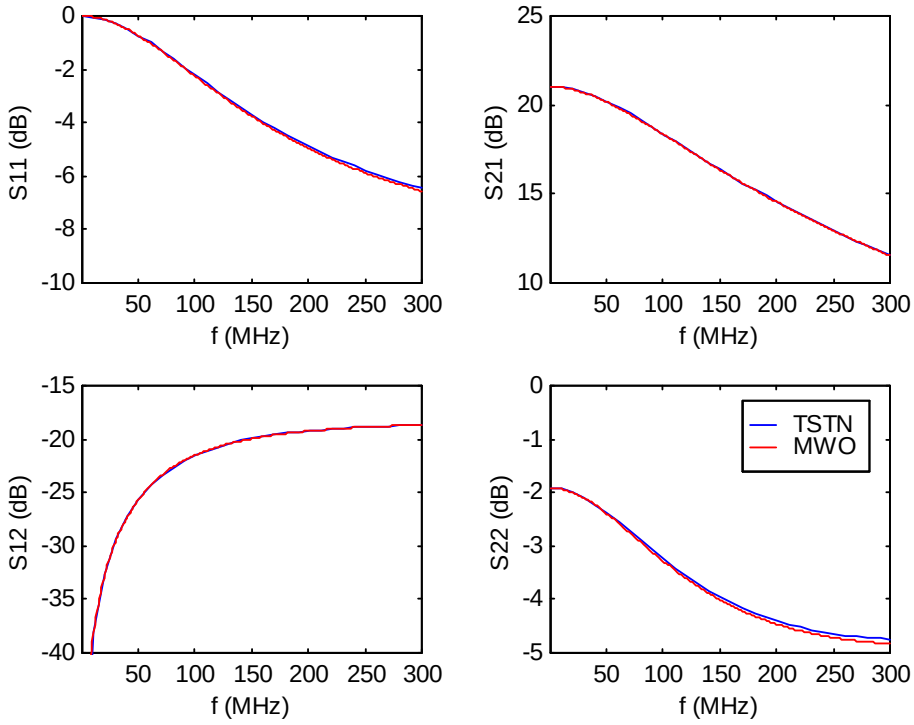

Figure 18. Transistor model S-parameter magnitudes.

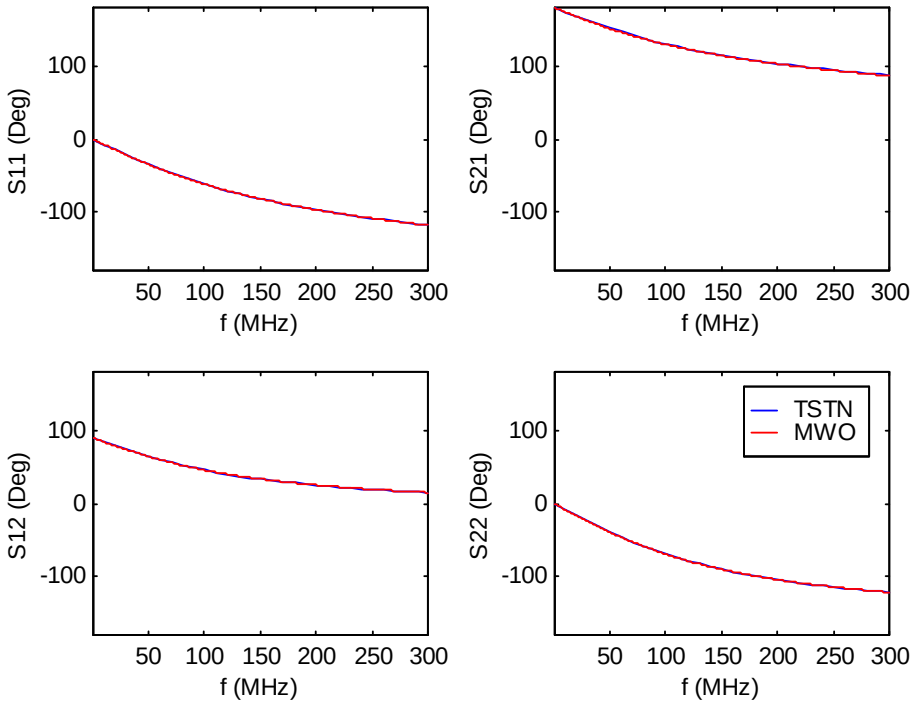

Figure 19. Transistor model S-parameter phases.

3.3.2 FET Circuit Model

As noted previously, transistors are commonly used elements in amplifier and oscillator applications. However, above 2 GHz, microwave integrated circuit designs more typically use FETs because of their intrinsic characteristics. FETs can produce higher amplifier gain, higher output power, or lower noise figures. Manufacturers sometimes do not give enough information on their FETs for the microwave design engineer to accurately model its performance in circuit designs. To use FETs to model a circuit, they must first create and simulate the FET's equivalent circuit to characterize the intrinsic device. The M&S software must accurately describe the performance of the FET equivalent circuit.

This test case verified an equivalent FET circuit model. The transistor is represented as a circuit of lumped elements. Figure 20 shows the circuit configuration. The commercial transistor (NEC70000) is available from NEC Electronics. The equivalent circuit contains 12 LRC elements and an idealized voltage-controlled current source. The various characteristic components (C2, R1, C1, C3, C4, U1) represent intrinsic device behavior. The inductors and resistors (RL1, RL2, and RL3) represent the input, output, and ground leads. This model is intended for high-frequency applications.

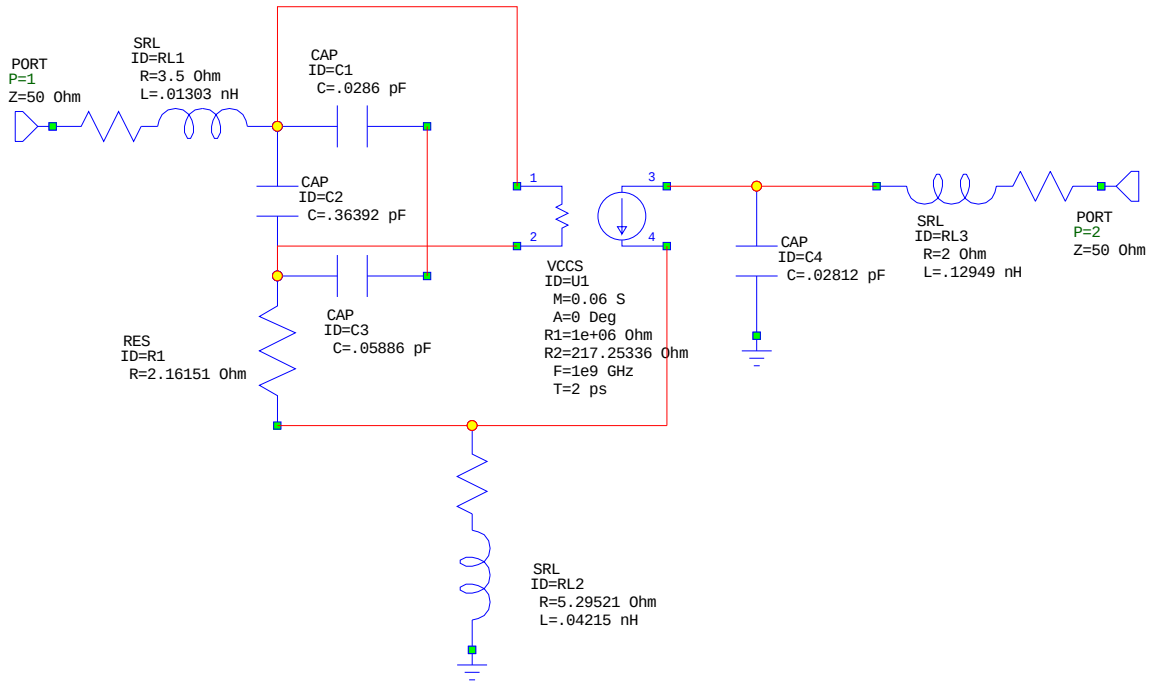

Figure 20. FET model schematic.

Figures 21 and 22 show the predictions from Microwave Office™ and Touchstone® for the S-parameter magnitudes and phases. Results correlate reasonably well between the two M&S codes. All the S-parameter curves have very similar spectral profiles. The gain achieved, S_{21}, starts at about 12 dB at 1 GHz and decreases as frequency increases. This increase is typical behavior of the intrinsic device of FETs. As the gain decreases to 2.5 dB, the cutoff frequency is a typical parameter defining the transistor characteristics. Transistor input return loss (S_{11}) and output return loss (S_{22}) are high. Input return loss goes from 0 dB at 1 GHz down to about –4 dB at 25 GHz, while the output return loss reaches about –7 dB at the edge of the band. Input and output return losses show a considerable impedance mismatch at both ports. In practice, impedance-matching networks are often used to minimize these losses to maximize the transmission efficiency. Isolation between the input

and output ports, S_{12}, is very good. Isolation is around –35 dB at 1 GHz and increases to about –17 dB at 25 GHz. These are typical values for isolation for this type of device. Results show that Touchstone® and MWO differ by about 1.5 dB over the entire band for isolation.

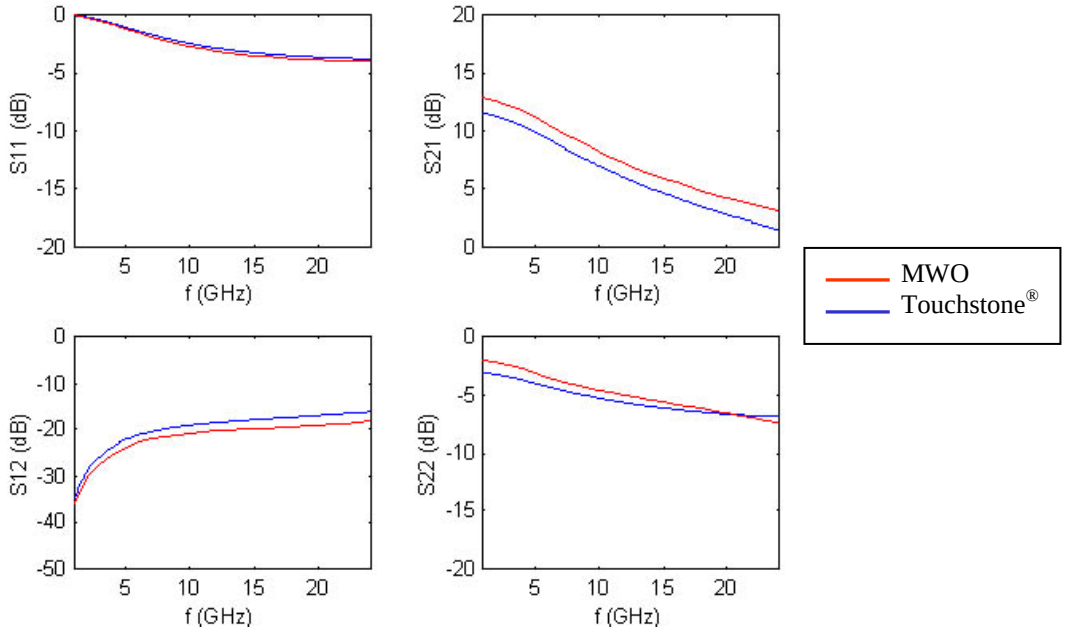

Figure 21. FET model S-parameter magnitudes.

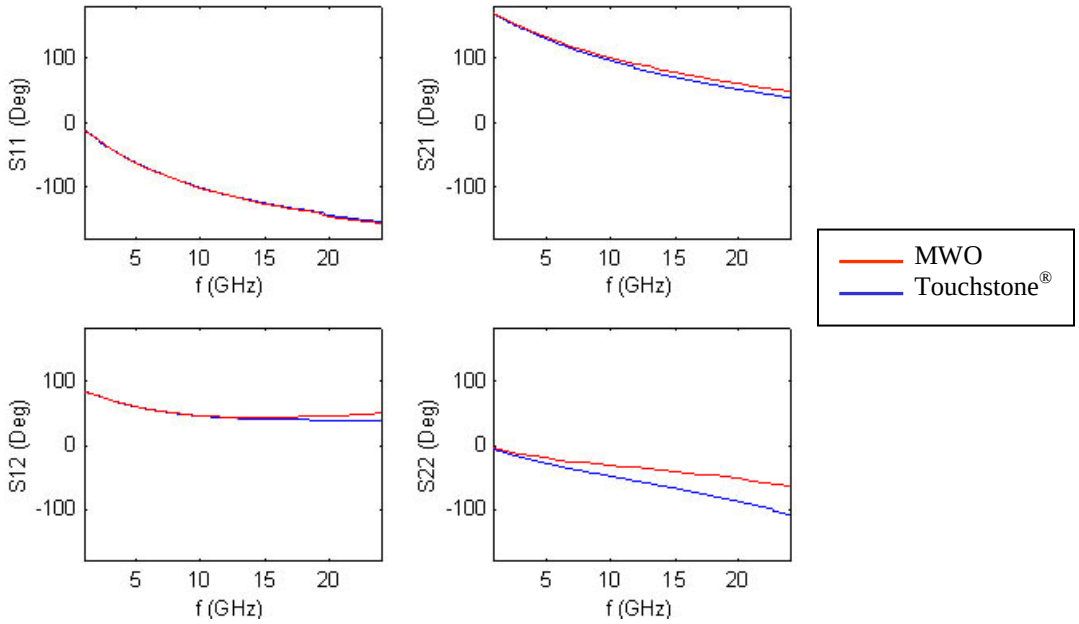

Figure 22. FET model S-parameter phases.

3.3.3 UHF Bipolar Transistor Amplifier

This test case addressed another type of transistor, the bipolar transistor. Bipolar transistors differ from FETs in their construction and the way they control the current through the device. FETs use a single pole and field effects to control the current while bipolar transistors use two poles, one positive and one negative.

We used a bipolar transistor device to analyze the performance of a UHF amplifier. This circuit consists of a commercial NEC transistor (NEC645) and a network of lumped elements that provide feedback and matching functions. Matching networks optimize the gain parameter and circuit stability. Feedback networks provide circuit gain stability. A transistor's electrical parameters specify the LRC elements in the matching network. The simulation covers the 500- to 1500-MHz frequency range. Figure 23 shows the circuit configuration for this test case.

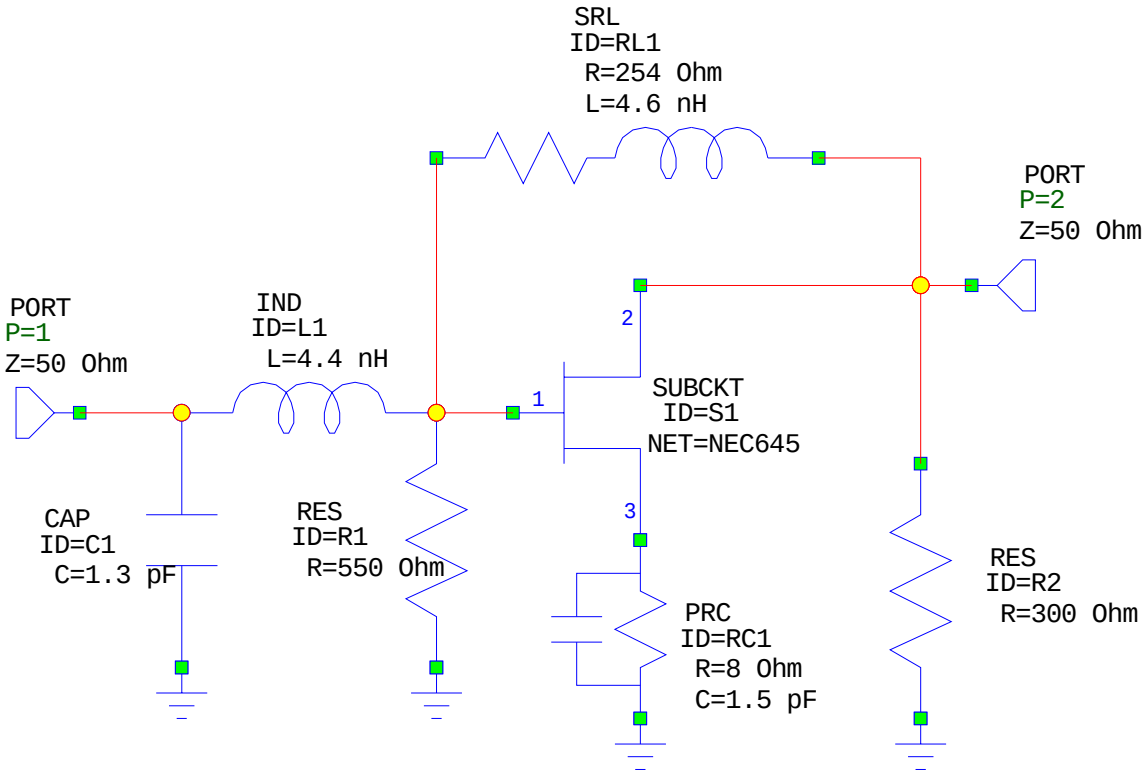

Figure 23. UHF amplifier schematic.

Simulations were performed on MWO and Touchstone® for comparison. Figures 24 and 25 show the results from each simulator. Data from the two codes correlate reasonably well. The spectral profiles of the curves are very similar for all the S-parameters. Input return loss, S_{11}, from each code is about –20 dB. Touchstone® shows an input return loss within about 2 dB of MWO data over the 0.5- to 1.5-GHz frequency band. This difference is insignificant because it represents only a small fraction of the actual input return loss at this level. The impedance matching at the input is generally acceptable because a –20-dB mismatch is only about 0.043 dB in the insertion loss. Gain, S_{21}, of this circuit is 10 dB over the entire frequency range. Both codes agree to within 0.1 dB over the entire frequency range. Output return loss, S_{22}, shows losses of about –26.1 dB at 0.5 GHz, with Touchstone® increasing linearly to –22 dB at 1.5 GHz. MWO shows output return losses of –27 dB at 0.5 GHz increasing linearly to –24.8 dB at 1.5 GHz. The difference between the two codes can be insignificant because a few decibels of difference well below –20 dB represent an insignificant

amount of energy. The impedance matching at the output is adequate because a –24.8-dB mismatch only amounts to about a 0.013-dB loss caused by the reflection.

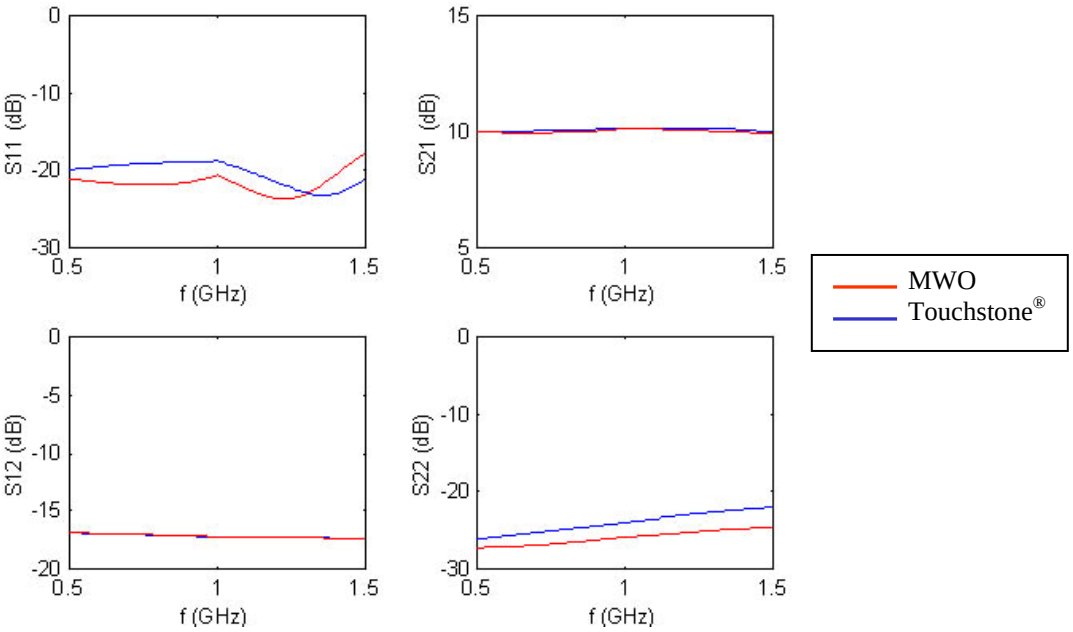

Figure 24. UHF amplifier S-parameter magnitudes.

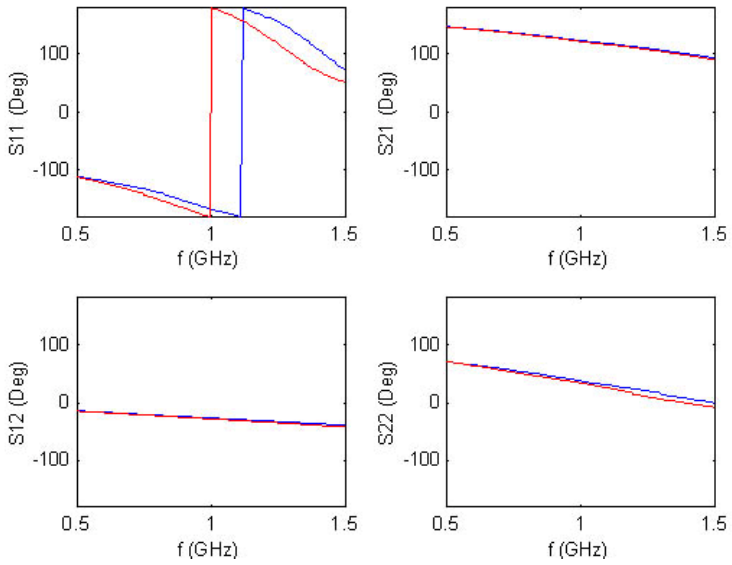

Figure 25. UHF amplifier S-parameter phases.

3.3.4 Microwave FET Amplifier

The microwave FET amplifier simulated in this case is used in amplification applications where gain with maximum efficiency is important. This circuit uses a FET transistor with an impedance-matching network. The output should show good gain over the frequency band, with low input and output return losses.

This test case simulated the performance of a microwave amplifier. The circuit consists of an NEC Electronics® FET (NEC70000) and distributed matching networks composed of transmission line (TLIN) elements. Matching networks optimize the gain parameter and minimize the input and output return losses. Distributed elements in the matching network are specified by their electrical characteristics. We performed the simulations over the 4- to 20-GHz frequency range and compared the obtained data to Touchstone® numerical data. Figure 26 shows the circuit configuration for this example.

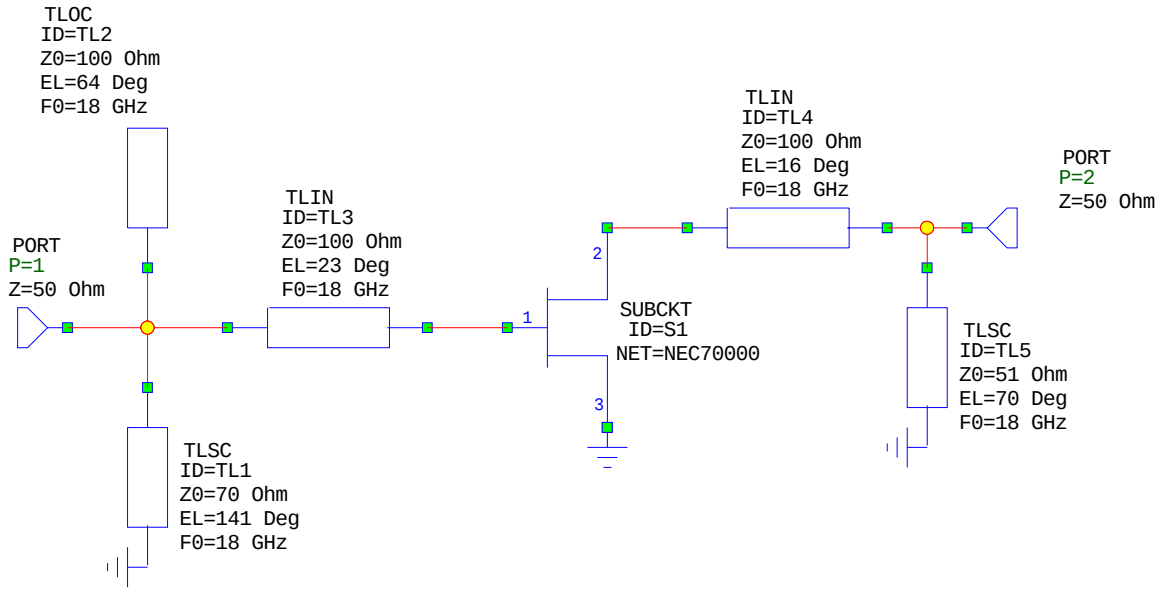

Figure 26. TLIN FET amplifier schematic.

Magnitude and phase of the four S-parameters were calculated and compared to the Touchstone® results (Figures 27 and 28). In this example, the two codes produced identical results for magnitude and phase. Results show the input return loss, S_{11}, of this circuit as 0 dB at 4 GHz, decreasing as the frequency increases and spiking to –21 dB at 18 GHz. This result shows excellent input impedance matching across 18 GHz. Gain, S_{21}, of this circuit is 7.8 dB from 7 to 18 GHz, rolling off below 7 GHz and above 18 GHz. Output return loss, S_{22}, starts at 0 dB at 4 GHz, decreasing steadily to a dip of –15 dB at 14 GHz and then increasing back to –6.2 dB at 20 GHz, which shows that the impedance matching at the output is relatively good at about 14 GHz. These results agree with what was expected for this circuit across the band. The transistor was represented by an S-parameter file in the Touchstone® file format. The same file was used in each simulator. The performance of the S-parameter import function, open-circuit, and short-circuit TLIN elements are identical between the two codes.

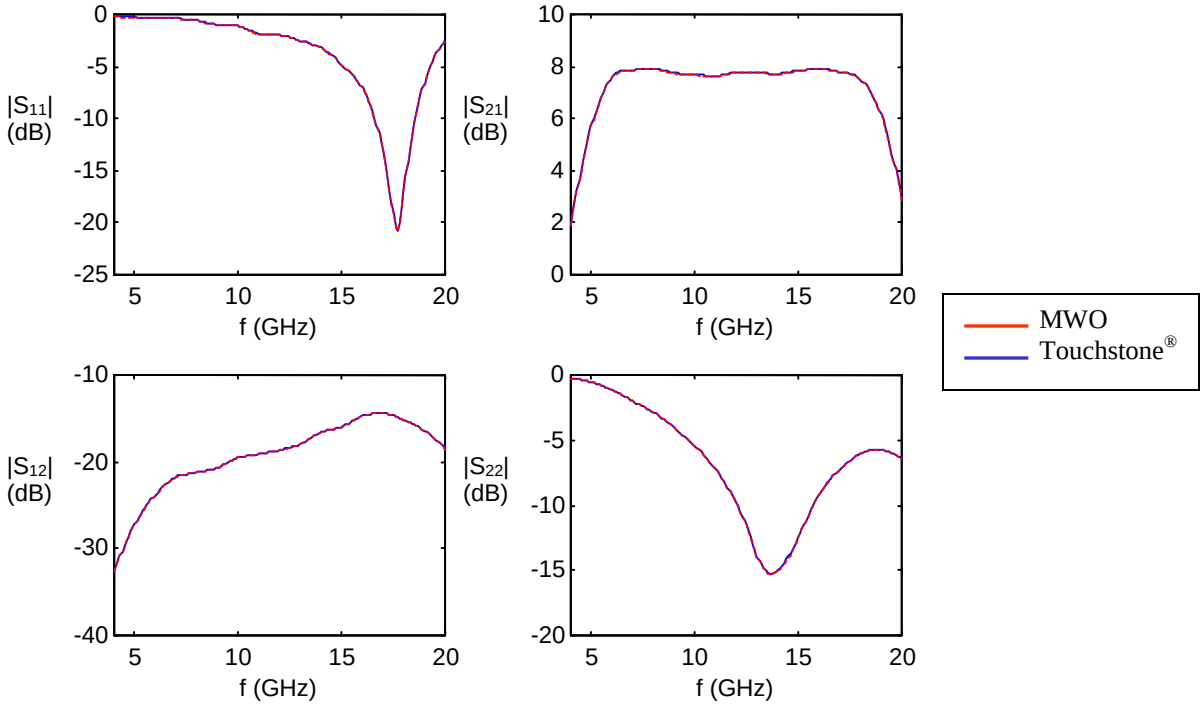

Figure 27. TLIN FET amplifier S-parameter magnitudes.

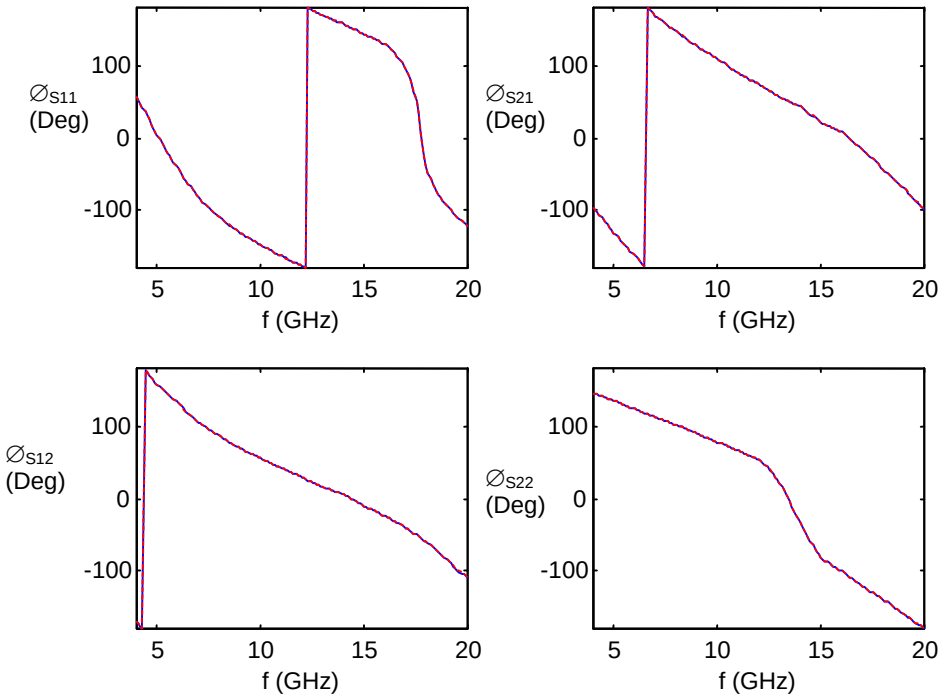

Figure 28. TLIN FET amplifier S-parameter phases.

3.3.5 Feedback Amplifier Using FET Device

We used the feedback concept to analyze wideband amplifier performance. A sample of the output signal was fed back into the input signal. Feedback amplifiers are useful because they provide great stability of output signals and allow broadband amplification. They are generally noisier and provide relatively lower gain than reactively matched amplifiers.

The feedback amplifier circuit includes a combination of distributed and lumped elements for the feedback and matching networks (Figure 29). The active device is a commercial FET (MIT1801). The matching network optimizes the gain parameter and stabilizes the performance over a wide bandwidth. Matching networks minimize the input and output return losses. Lumped elements contribute to the performance at low frequencies while the distributed elements are used for the higher end of the spectrum. Distributed elements in the matching network are specified by their electrical parameters. The simulation operates in the 0.1- to 6.0-GHz frequency range.

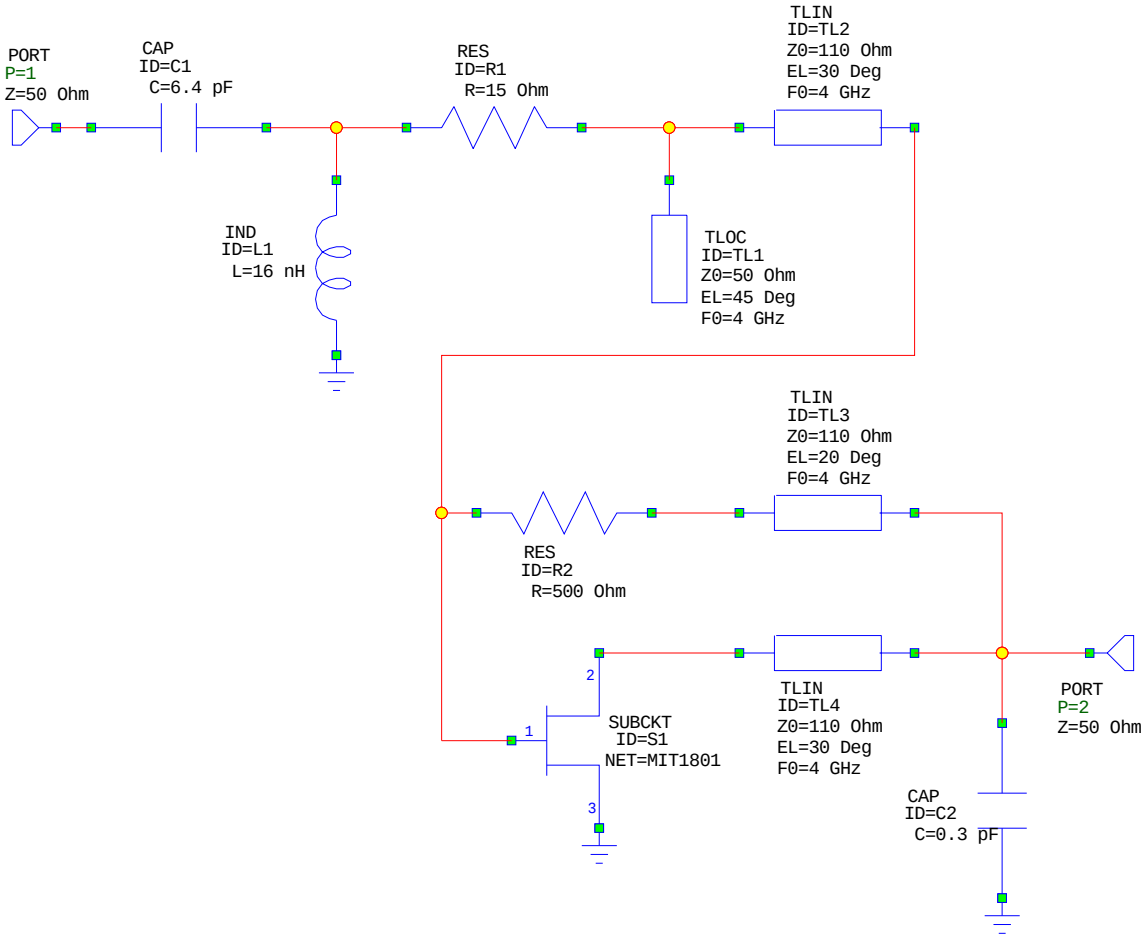

Figure 29. Feedback amplifier schematic.

Figures 30 and 31 show the magnitude and phase S-parameter results. Touchstone® (blue) and Microwave Office™ (dashed red) results are identical in this example. The results show good stability in gain and reasonable return losses. Input return loss, S_{11}, starts at 0 dB at 0.1 GHz and quickly spikes down to –14 dB. The input return loss is 13.5 dB at 4.0 GHz. This stability shows that the impedance matching at the input is relatively good because a –10 dB mismatch is only a small percentage of the input signal strength. Gain, S_{21}, is about 11 dB over the designated bandwidth. The isolation between the ports, S_{12}, is typically better than –16.8 dB over the entire band. The output return loss, S_{22}, is low over most of the band. It is –10 dB at 0.1 GHz, and spikes down to –34 dB at 900 MHZ. Above 1 GHz, it slowly increases over the rest of the band to about –7.1 dB at 6 GHz. The impedance matching at the output is reasonably good over the design frequencies because a –10 dB mismatch is only a small percentage of the output signal strength. These results extend the equivalency between the two codes to include the lumped elements: capacitor, resistor, and inductor.

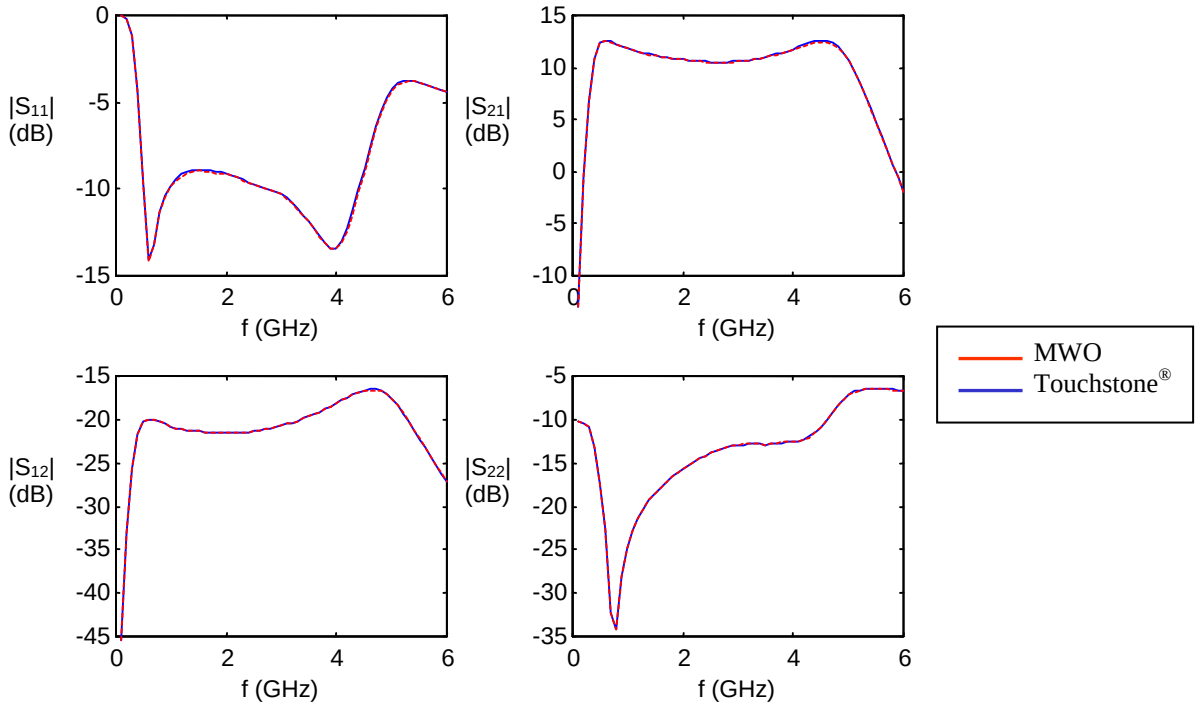

Figure 30. Feedback amplifier S-parameter magnitudes.

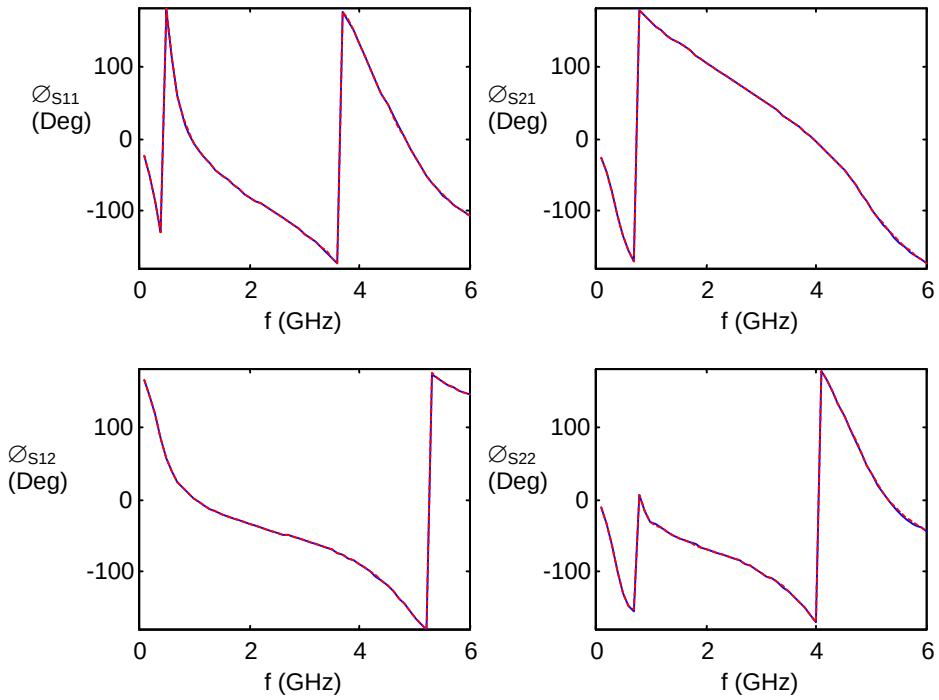

Figure 31. Feedback amplifier S-parameter phases.

3.3.6 Balanced Amplifier Using FET Feedback Concept

This test case simulated the performance of a balanced amplifier constructed from four feedback amplifiers outlined in the previous test case. Balanced amplifiers are used for high-power applications. When a single amplifier cannot generate the required output power, other amplifiers are added to the circuit until adequate output power is achieved. The combiner/ isolator (CLIN) at the output of the amplifiers provides output impedance matching that would otherwise be lacking.

This balanced amplifier configuration (Figure 32) provides power capabilities above the power of the individual devices. Two FET feedback amplifiers are cascaded to provide up to a 30-dB gain. Two cascaded circuits are also coupled together by using hybrid couplers. Couplers provide isolation between the amplifier and the external circuits in an attempt to lessen the losses generated by the interaction. The simulation operates in the 0.1- to 6.0-GHz frequency range.

Figures 33 and 34 show the magnitude and phase S-Parameter results from this test case. Comparison with Touchstone® shows an exact correspondence between the two codes and extends the verified element models to include the coupled TLINs. The results agree with the theory for this circuit. The gain, S_{21}, has approximately doubled over 20 dB for most of the band. It decreases dramatically above 5 GHz. The input and output return losses, S_{11} and S_{22}, respectively, are very low. Both return losses are below –20 dB over most of the frequency band, only going above –20 dB below 0.7 GHz and above 4.6 GHz. This stability shows that the impedance matching at the input and output is reasonably good. The isolation, S_{12}, also shows good characteristics and is below –32 dB over the entire band.

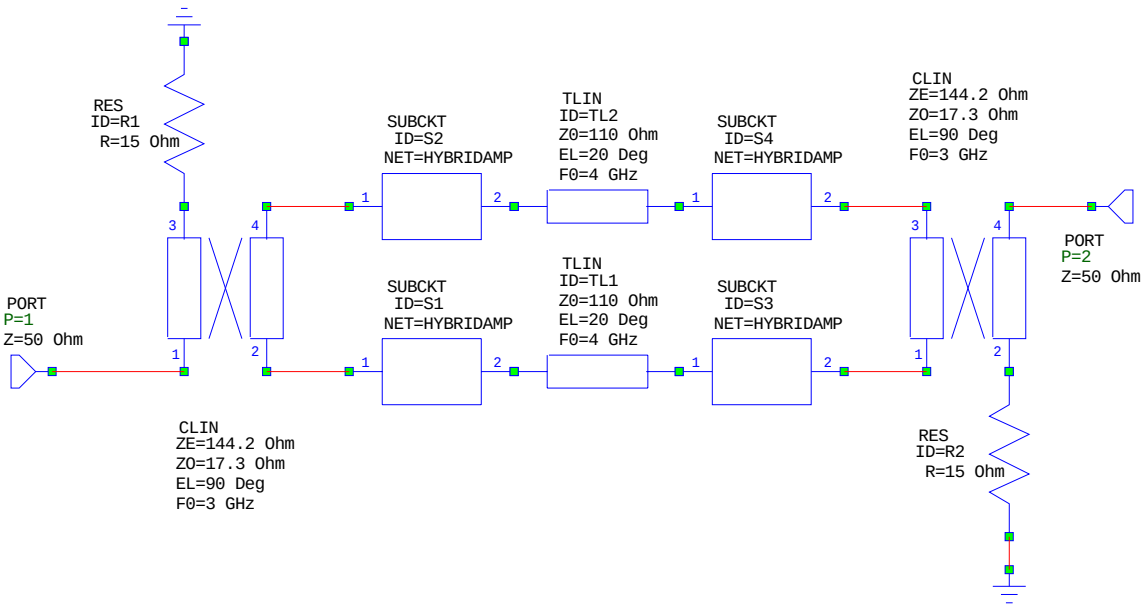

Figure 32. Balanced amplifier schematic.

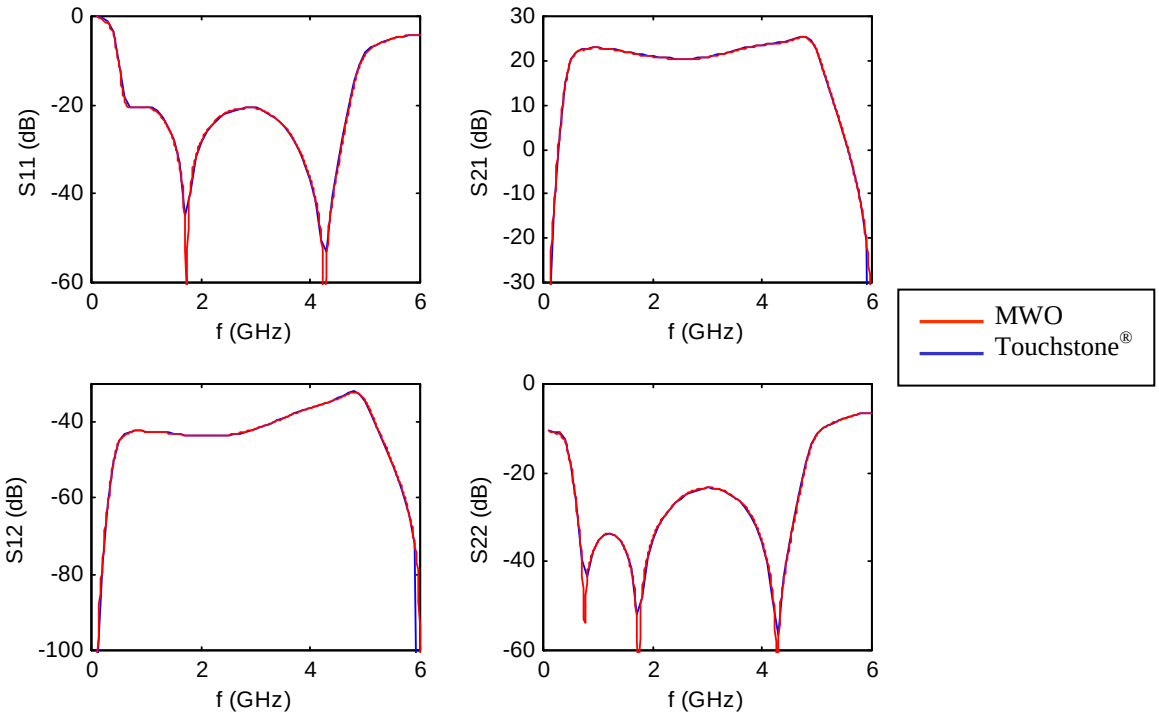

Figure 33. Balanced amplifier S-parameter magnitudes.

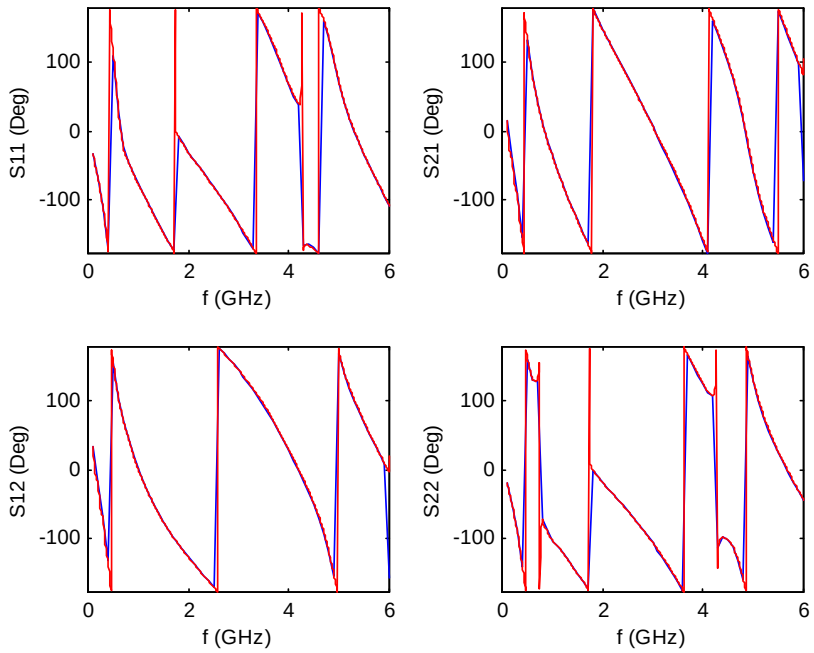

Figure 34. Balanced amplifier S-parameter phases.

3.3.7 Low-Noise Amplifier Using FET Device

Low-noise amplification is important in a receiving application. Receivers require a low-noise figure so they cannot be desensitized. Low-noise-amplifier (LNA) performance dictates receiver sensitivity because the LNA is among the first components a signal detects as it enters the receiver. An LNA uses constant gain circles and circles of constant noise figure to select a usable tradeoff between noise figure and gain. Generally, the goal is to obtain minimum noise figure and maximum gain for an amplifier. If input impedance is mismatched, an additional isolator must be added to minimize the interaction loss.

We designed a LNA based on a Metal Semiconductor Field-Effect Transistor (MESFET) device (NE76038A). Figure 35 shows the circuit layout. In the simulation, the linear device model (S-parameter model) is used. Bias circuits and matching circuits are designed and optimized to have the best noise performance at 11 GHz. All network parts are designed with microstrip lines and a dielectric constant of 10.2. Matching networks are composed of distributed elements that are specified by their electrical parameters. This simulation was performed in MWO and in ADS® for comparison.

Figure 36 shows the simulation results in the 8- to 14-GHz frequency range when using MWO and ADS®. The gain over the designated band is about 7 dB, as expected. The calculations agree well with similar frequency response over the designed operating range. The maximum gain predicted by MWO is at about 11 GHz, while in ADS®, it is at about 11.5 GHz. This discrepancy may be caused by the modeling difference of the matching circuits where tee components are extensively used. These results also show adequate impedance matching at the input port. Input return loss shows a dip of better than 15 dB at the center frequency.

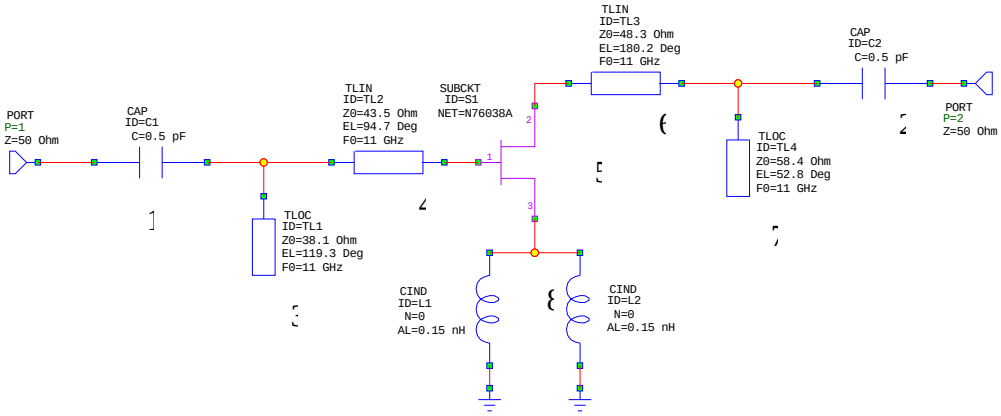

Figure 35. LNA schematic.

Based on the above simulations, a circuit was fabricated and the S-parameters were measured with a Hewlett Packard® (HP) 8510 network analyzer and compared to the numerical data. The measured data are superimposed on the numerical data for comparison. These data show that the curves of gain and reflection coefficient of MWO simulation coincide with measured results much better than ADS®. However, both simulators failed to predict a second dip in the measured reflection coefficients. The test setup, which was not considered in the calculations, may have caused this failure.

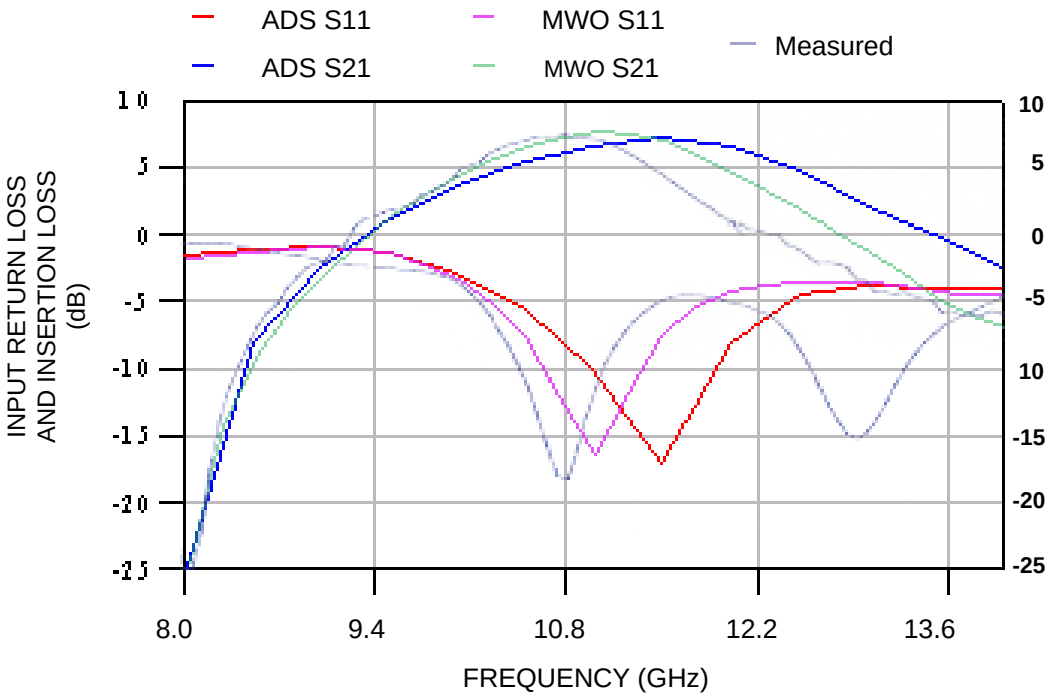

Figure 36. LNA S-parameters.

The noise figure of a LNA is an important parameter to measure. Thus, the noise figure of this circuit was simulated. Figure 37 shows the results. At low frequencies below 10 GHz, the noise is actually quite high. At the center frequency of about 11 GHz, the noise is 2.2 dB, which is expected from a LNA. The predicted noise figure data agreement is fairly good over the considered frequency range.

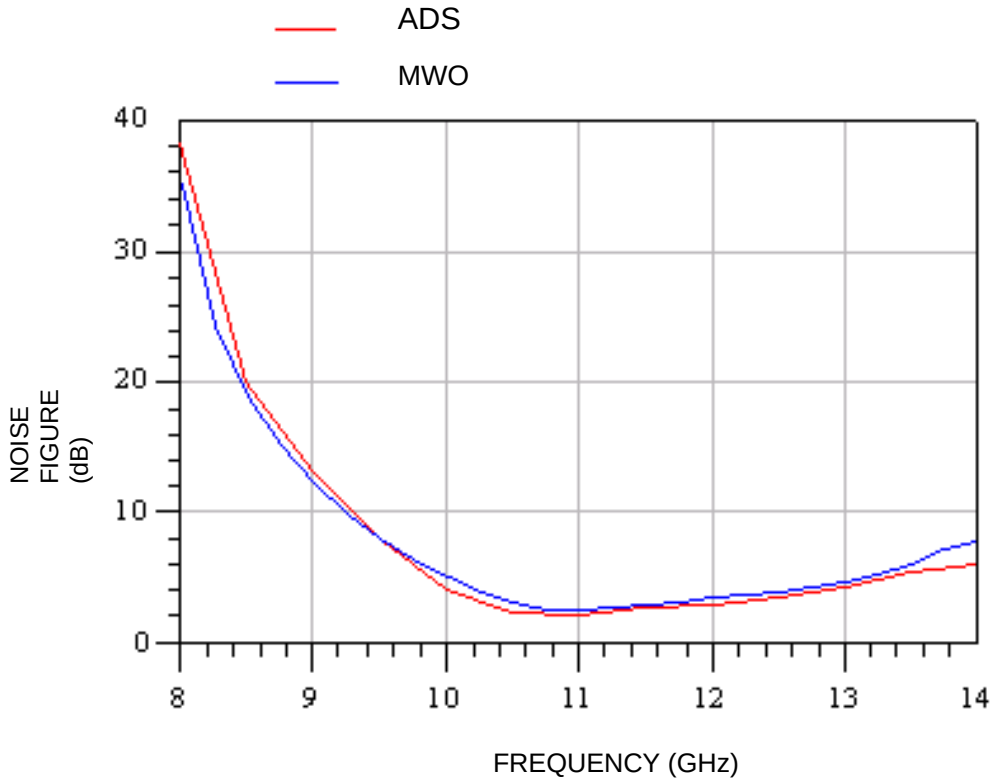

Figure 37. LNA noise figures.

3.3.8 Distributed Amplifier Using FET Device

With a traditional amplifier, any attempt to increase the gain by increasing the FET's transconductance usually increases input capacitance as well. The distributed amplifier offers a way to combine the transconductance of several FETs without combining their input capacitances. Distributed amplifiers are used primarily to provide wideband amplification.

In this example, we simulated wideband amplifier performance based on the concept of traveling wave power combining. Gate and drain transmission lines are modeled as inductors. This simulation can be realized in practice by using short sections of high-impedance Coplanar Waveguide (CPW) lines. The active device used here was a commercial-chip FET (MGF1801B). Inductance values for the gate and drain lines were tuned to equalize the phase velocity of traveling waves on these lines. The next step in the design was to provide termination resistance to produce acceptable input and output return losses. This simulation operates in the 1- to 30-GHz frequency range. The intention of the design was to achieve a 10-dB gain over the operating bandwidth. Figure 38 shows the schematic used in the test case.

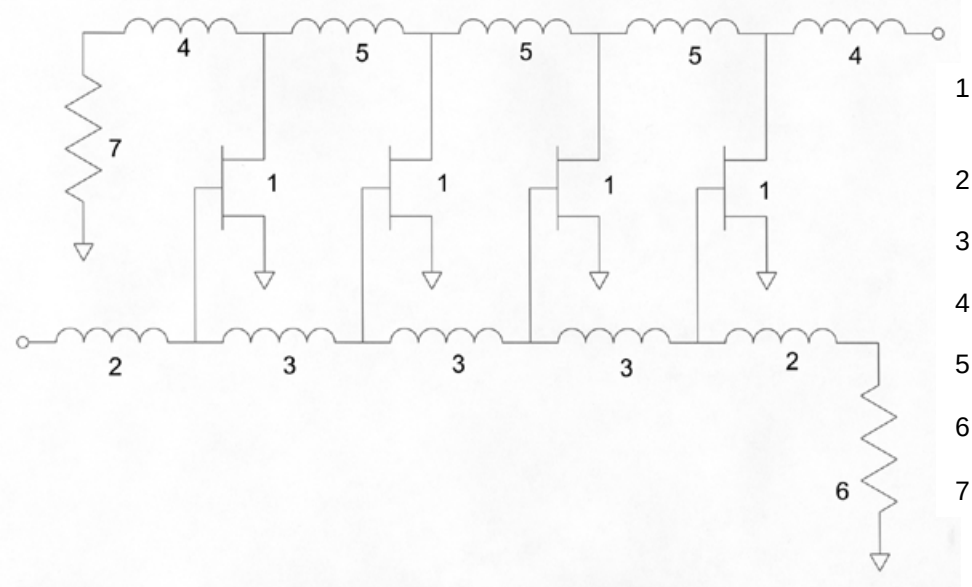

1 - MGF1801B transistor

2 - 0.66-nH inductor

3 - 1.32-nH inductor

4 - 1.34-nH inductor

5 - 2.68-nH inductor

6 - 23.7-Ω termination

7 - 65-Ω termination

Figure 38. Distributed amplifier using MGF1801B.

The results from MWO and ADS® show exact agreement (Figure 39). The input return loss is below –10 dB up to 14 GHz, which shows good impedance matching. The gain is 10 dB until 15 GHz, and drops off sharply to –50 dB at 28 GHz. The output return loss shows very similar results as the input return loss. It is better than –10 dB up to 13 GHz and approaches 0 dB beyond 25 GHz, which shows adequate impedance matching below 13 GHz because a –10 dB mismatch is only a small percentage of the output signal. The operating range of this distributed amplifier is from 1 to about 13 GHz.

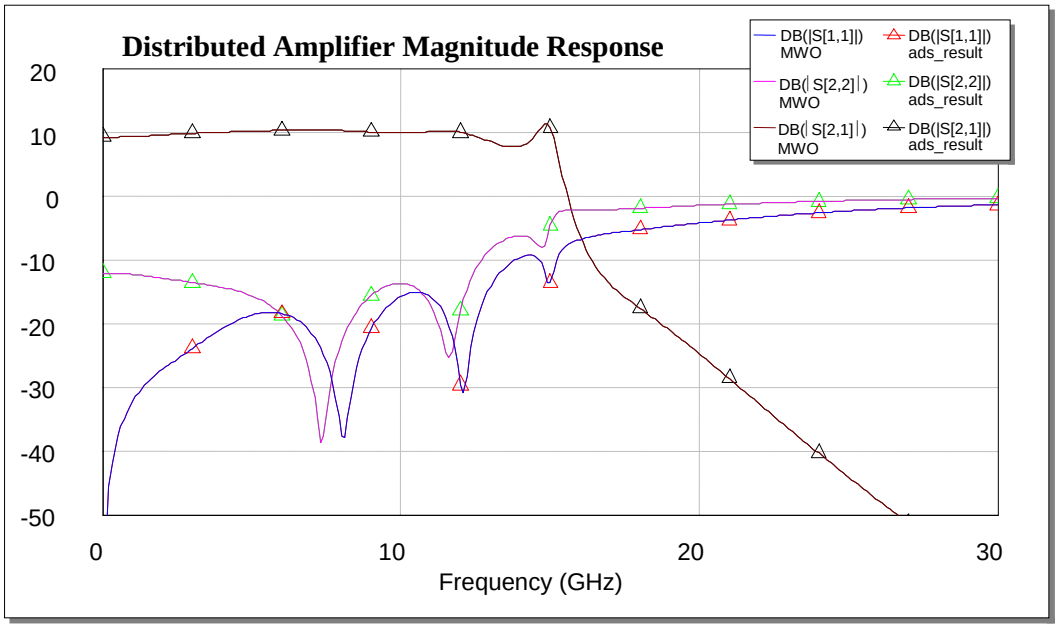

Figure 39. Distributed amplifier S-parameter data.

3.4 NONLINEAR COMPONENT ANALYSIS

Purpose

The next four test cases examine the M&S analysis capabilities for nonlinear components. Besides the gain, input/output return loss, and isolation parameters available for linear components, nonlinear effects such as gain compression, harmonic generation, and intermodulation distortion are also examined. Test cases contain two examples of amplifiers designed for linear operation that were pushed into saturation. We also examined two examples of devices designed to take advantage of nonlinear effects.

Assumptions

The following set of circuits contain linear passive elements. It is assumed that circuits are operating in a frequency regime where the models for these devices are valid. Nonlinear active elements used in these simulations are represented by an extended set of circuit models. Besides frequency-dependence, the response of these elements is also a function of the circuit power. In the harmonic-balance method, linear and nonlinear multiport devices represent the circuit, and a self-consistent solution at the fundamental and harmonic frequencies is found iteratively. No small signal assumptions are necessary in harmonic-balance analysis.

Procedures

Circuit characteristics of these elements depend on power that generates additional signals that are products and harmonics of the fundamental excitation frequencies. For these reasons, the analysis of nonlinear components requires a power sweep across the spectrum and comparison of spectral data. I-V curves for the nonlinear element models from alternate M&S software are also compared with curves in the M&S software under test. Furthermore, modulation conversion, small-signal gain, and power-added efficiency performance analysis is also evaluated.

3.4.1 X-Band Amplifier Block Using MESFET

An amplifier block usually consists of several amplifier stages in cascade. Input and intermediate amplifier stages typically operate in a small-signal mode. Their function is to amplify the small input excitation to a value large enough to drive the final power amplification stage. This output stage may be a transmitter that requires high power from the final amplification stage so the signal can be transmitted an appreciable distance via an antenna system.

In the first test case, we investigated a high-frequency power amplifier. This power amplifier uses a MESFET as its active component and its performance can be characterized as nonlinear. As the input voltages increase, the device approaches saturation, which in turn leads to a “clipping” of the output power signal. “Clipping” increases input power, which no longer results in a linear relationship by 1 dB or more of the expected output power. The resulting output power begins to level off at this saturation or compression point. Above this compression point is the nonlinear region of the device. It is important that the M&S software properly characterizes this region.

This test case simulated a two-stage amplifier. As a high-frequency amplifier, this circuit uses distributed transmission lines to match the transistors stages (Figure 40). The active device is a low-noise L to Ku-band GaAs NE76038A MESFET, and its nonlinear model is based on the Series 4 Libra TOM model. The matching network optimizes the gain (>20 dB) while satisfying the conditions in noise figure (<2 dB) and VSWR (<2:1). Figure 40 summarizes the requirements and circuit components for this amplifier. This circuit operates at 9 GHz.

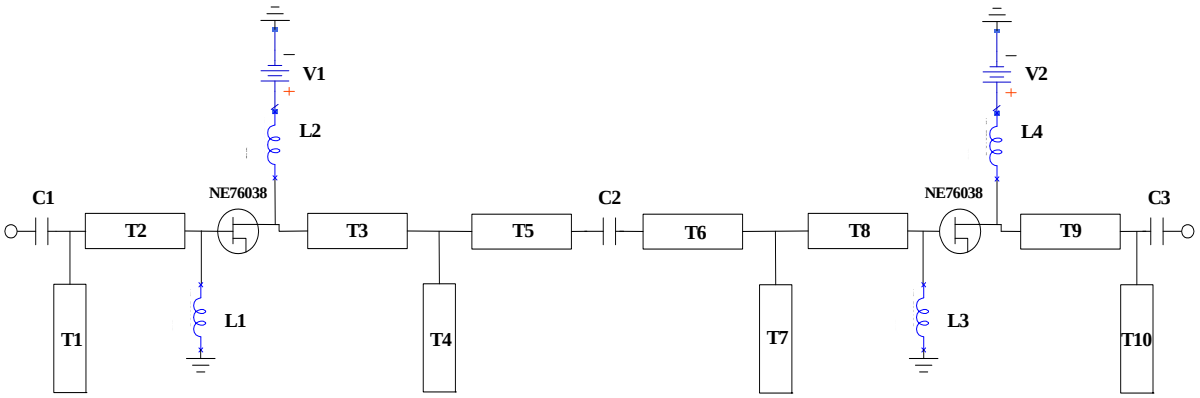

Figure 40. Two-stage X-band amplifier schematic.

Legend: Circuit Components

1. Devices: NE76038A low-noise L to Ku-Band GaAs MESFET
2. Lumped Elements: C1, C2, and C3: 5-pF capacitor
   L1 and L3: 1,000-nH inductor
   L2 and L4: 1,000-μH inductor
3. Bias Condition: V1 and V3 (Vds): 3 volts
4. Matching Circuits: 50-Ω Ideal Transmission Lines at 9 GHz
   Electrical phase length for each distributed element:
   T1: 50.25°, T2: 33.1°, T3: 63°, T4: 46°
   T5: 42.14°, T6: 84.28°, T7: 53.4°, T8: 40.88°
   T9: 63.4°, T10: 44.4°

For the simulation in the linear region of the transistor devices, the predicted S-parameters and noise figures are in excellent agreement. Figures 41 and 42 show the ADS® and MWO results. The graphs show that the circuit center frequency is about 9 GHz, as designed. The gain is about 20 dB at this frequency, as designed. The gain starts dropping off above 10 GHz, which is typical behavior for these transistors. Input return loss is at about –14.9 dB around the operating frequency, which shows low input return loss and good impedance matching around the center frequency. The corresponding output return loss is about –18.2 dB, which also indicates low output return loss over the same region. The noise figures are better than 4 dB from 6 GHz to 10 GHz. Above 10 GHz, the noise figure begins to deteriorate. The noise figure at 9 GHz is about 1.8 dB, which is where this device is designed to operate.

We increased the input power to drive this amplifier into the nonlinear region and used MWO and ADS® for simulation. We represented the transistors with nonlinear device models to find the behavior of this two-stage amplifier. Lumped element bias circuits for the devices were added in the simulation circuits. In MWO simulations, a general behavioral nonlinear model, TOM (Hallgren and Litzenberg, 1999) for MESFET device NE76038A, was used. However, the same implementation of the TOM model in ADS® failed and gave non-convergent results in a nonlinear simulation. Therefore, a packaged MESFET model of NE76038A provided in ADS® was used for reference simulation in the ADS® environment.

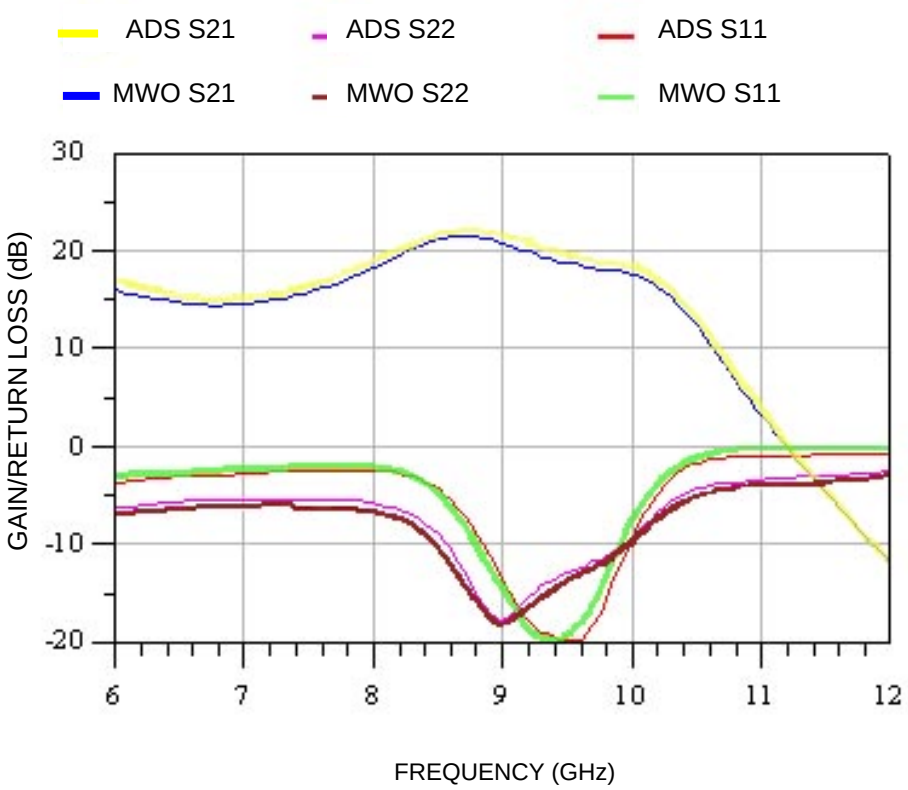

Figure 41. Two-stage amplifier S-parameters.

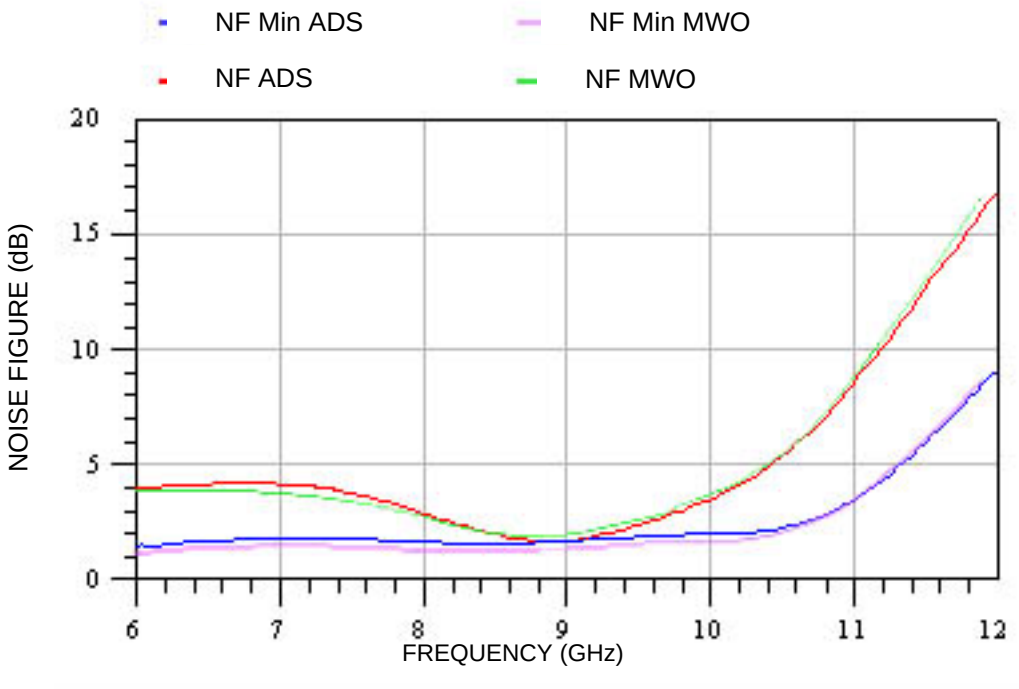

Figure 42. Two-stage amplifier noise figures.

Gain compression and output power versus input power curves were simulated (Figure 43). Each curve from the two codes has the same spectral profile and thus can be considered to have reasonable agreement; however, a slight shift in gain occurs between the two codes as they enter the compression region. MWO results show that the device enters the compression region when the input power is –5 dBm. With ADS®, it enters the compression region at –2 dBm.

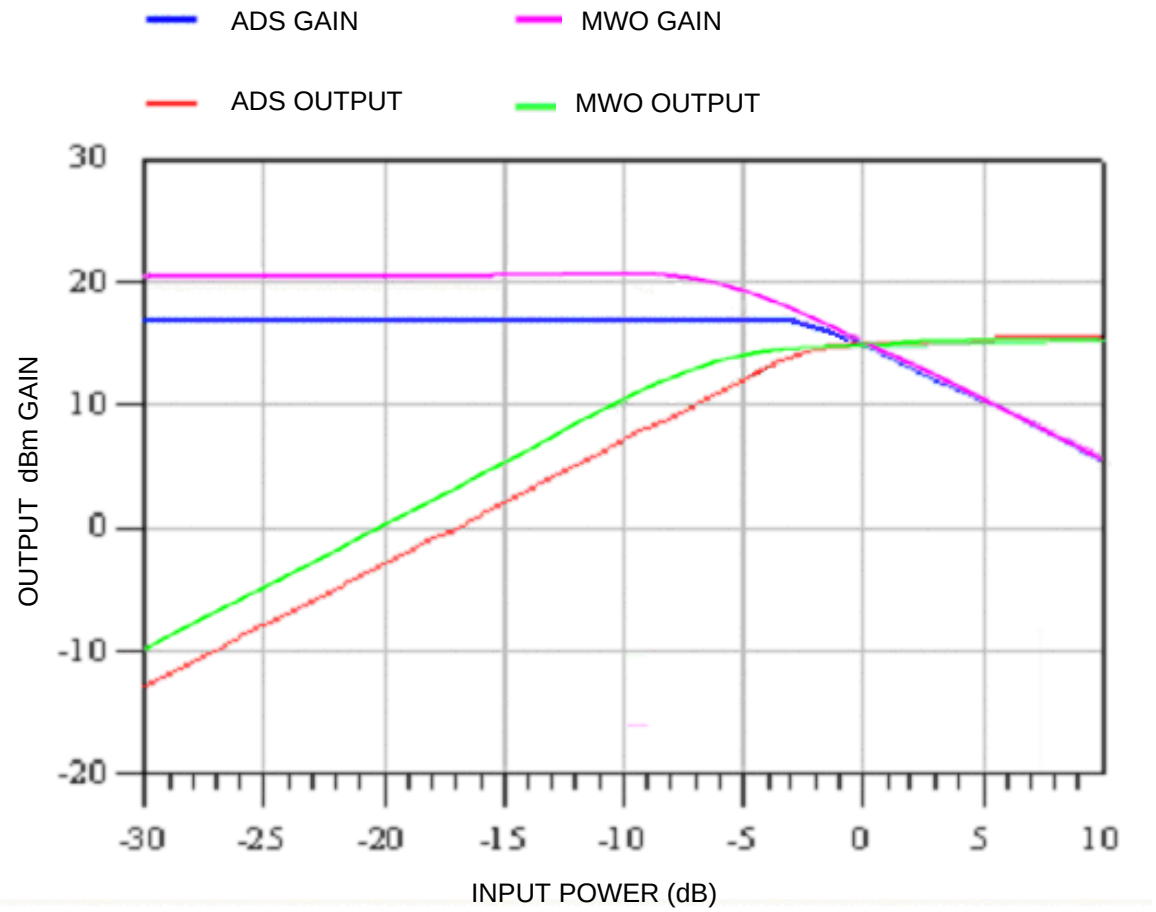

Figure 43. Two-stage amplifier gain curves.

I-V curves for the device models were simulated and were in reasonable agreement (Figure 44). This graph shows the intrinsic properties of the transistor, not amplifier performance properties. It shows the relationship between the gate-source voltage, drain-source current, and drain-source voltage. Typically, it is best to operate the transistor in the region that displays the most linearity, above 0.5 volts for this device. This graph gives the design engineer enough data to achieve the optimal drain-source current to maintain performance along a single gate-source voltage curve. The results from the two codes agree reasonably well because each individual curve has the same profile and is only off by a few milliamps.

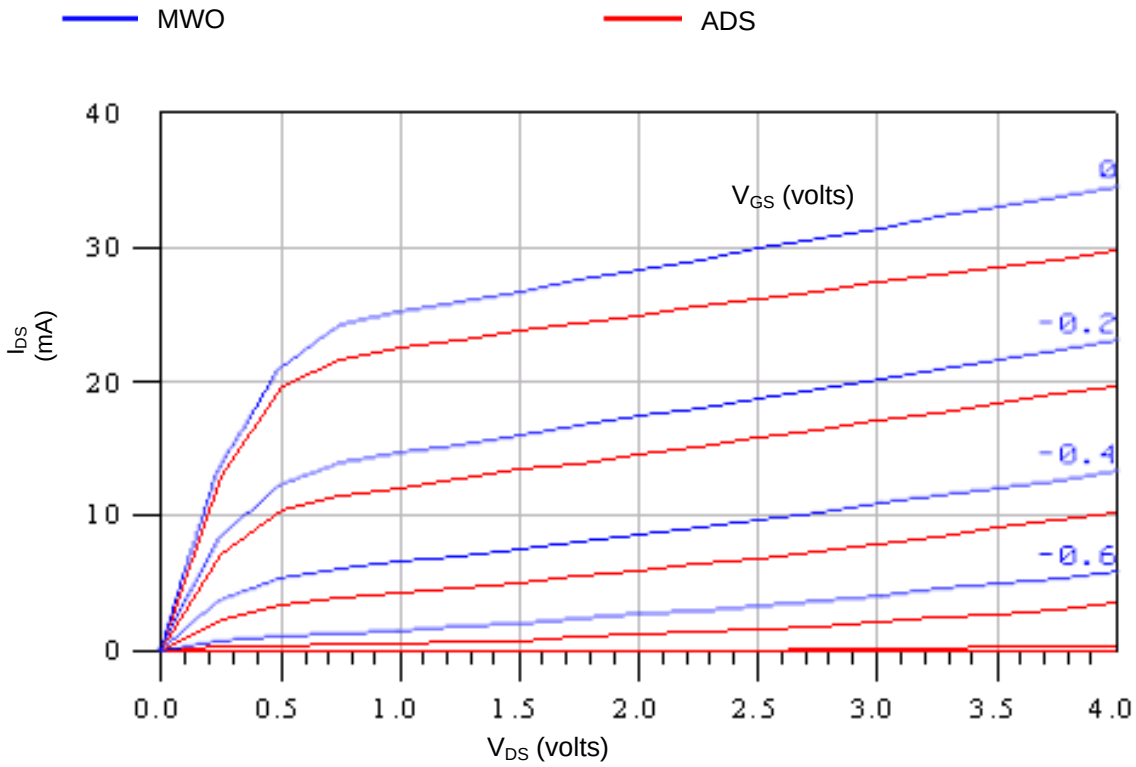

Figure 44. Two-stage amplifier I-V curves.

3.4.2 Large-Signal-Band Power Amplifier

This test case was of a large-signal amplifier that supplies power to a load with minimal distortion. Since the output voltage and current swings are so large, a linear model cannot represent the amplifier. A new type of distortion, caused by device non-linearity, manifests itself by introducing frequency components into the output that are not present in the input signal.

This simulation is similar to the previous test case except it operates at a lower frequency. The large-signal performance of this power amplifier is based on a 0.4-watt GaAs HJ-FET NE651R479A. Only lumped components are used for the matching circuit because this amplifier is operating at low frequencies. Figure 45 shows the circuit used for this test case. The matching circuit is optimized to provide the highest 1-dB compression power from 1.9 to 2 GHz. TOM nonlinear models are used for the device in MWO and Series IV. Series IV was substituted for ADS® for comparison because we constantly found instability in the TOM nonlinear model implemented in ADS®.

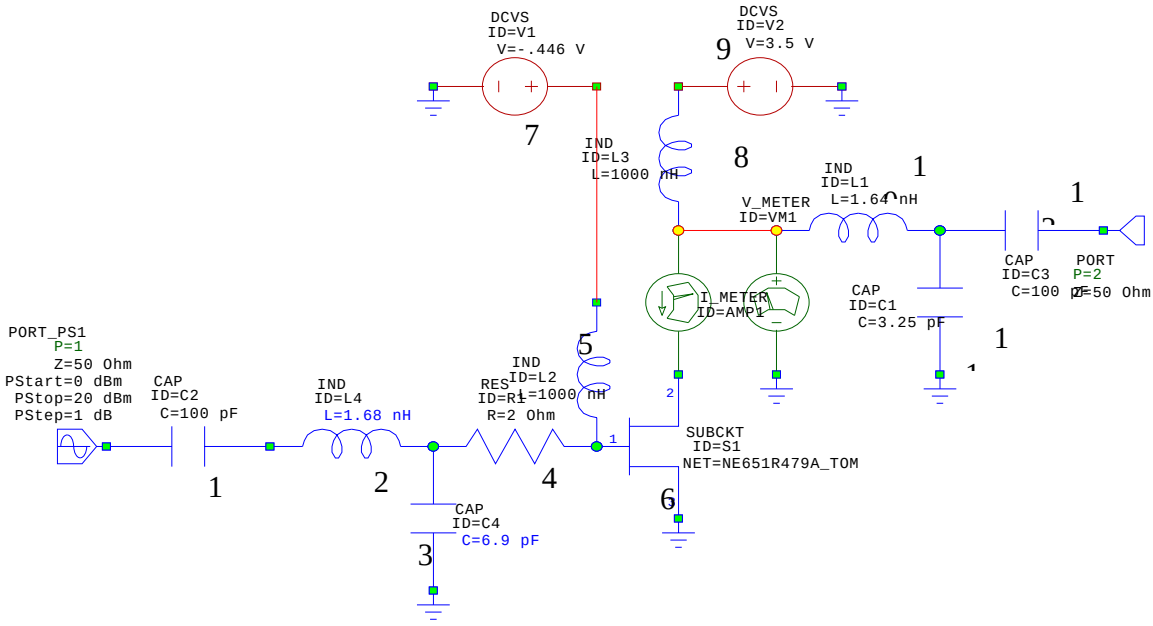

Capacitor: 100 pF
Inductor: 1.68 nH
Capacitor: C = 6.9 pF
Resistor: 2.
Inductor: 1000 nH
NEC Power: HJ-FET NE651R479A

DC Voltage: –0.446V
Inductor: 1000 nH
DC Voltage: 3.5 V
Inductor: 1.64 nH
Capacitor: 3.25 pF
Capacitor: 100 pF

Figure 45. Large-signal-band power amplifier using lumped elements.

Small-signal S-parameters were simulated first and were exactly the same between MWO and Series IV. Figures 46 and 47 show the results. Figure 46 shows that the gain parameter, S_{21}, starts high at 14.3 dB at 1.9 GHz and decreases to 12.9 dB at 2.00 GHz. The typical performance of transistor gain performance starts higher at lower frequencies and decreases as the frequency increases. Figure 47 shows the predicted input and output return losses between the codes. Input return loss curves revolve around the center of the Smith Chart, which demonstrates good impedance matching at the input. Output return loss shows marginally acceptable matching at the output. The predictions from MWO and Series IV agree almost exactly.

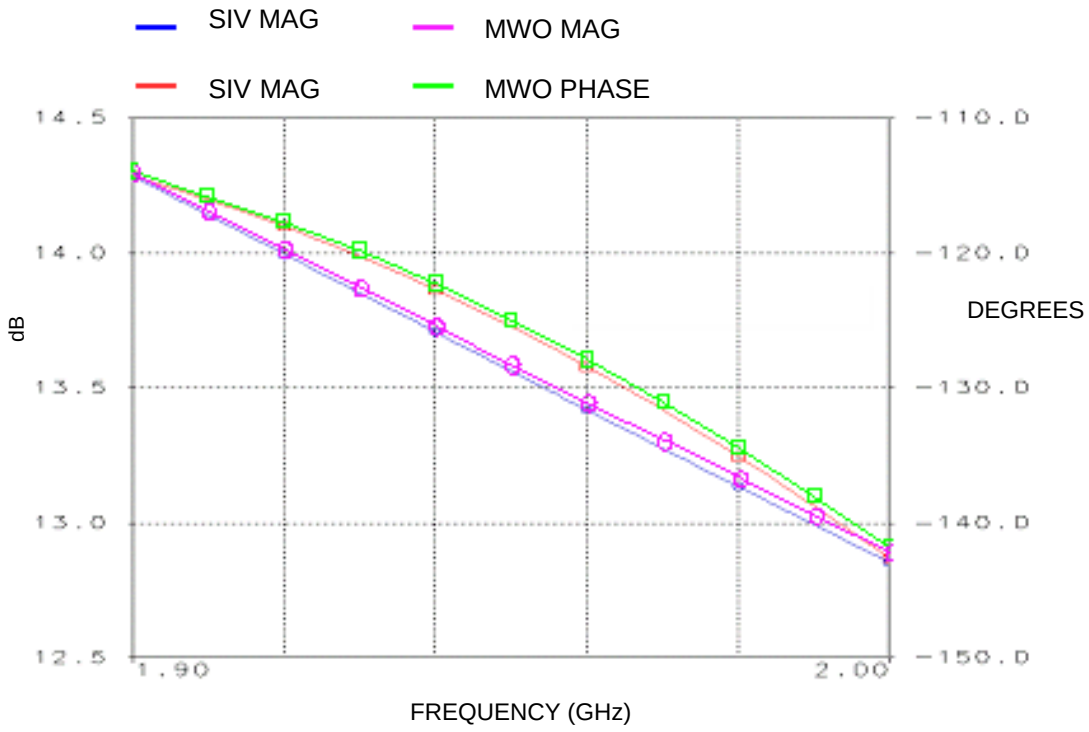

Figure 46. Power amplifier small-signal gain (S_{21}).

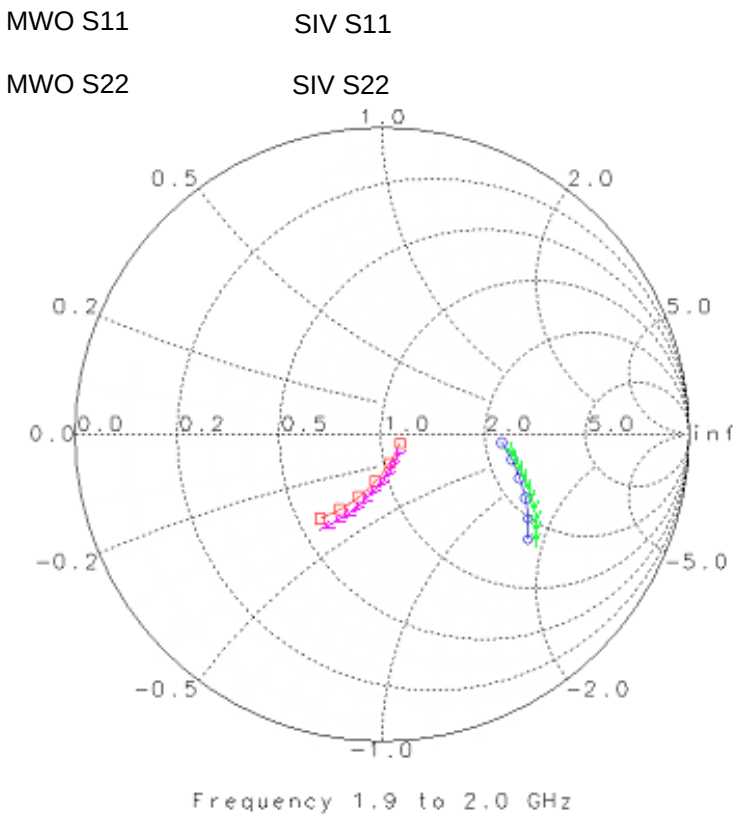

Figure 47. Power amplifier small-signal, S_{11} and S_{22}, plotted on a Smith Chart.

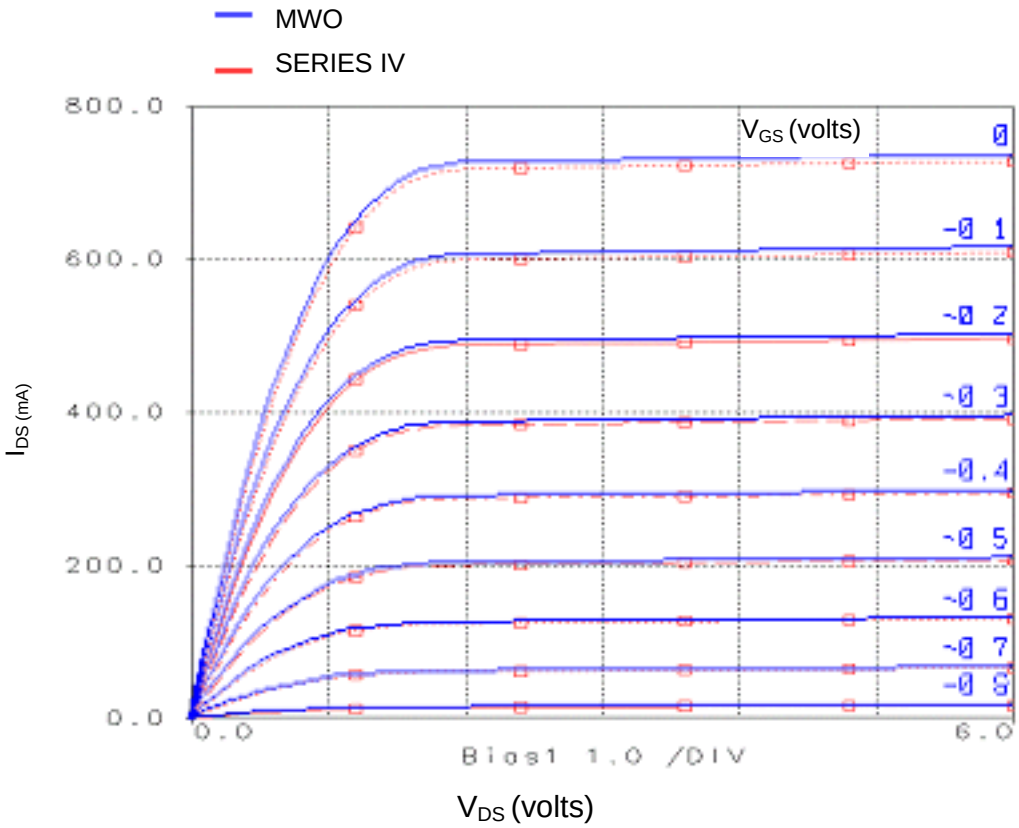

Figure 48. Power amplifier I-V curves.

Large-signal parameters such as the I-V curves, AM-AM, AM-PM distortion, and power-added efficiency were simulated and had fairly good agreements until the circuit went into the deep compression region. Figure 48 shows the I-V curves from this simulation. These curves show the relationship between the drain-source current, drain-source voltage, and gate-source voltage of the transistor device within the amplifier. These curves show the intrinsic characteristics of the transistor, not the amplifier properties. Series IV and MWO predictions are identical for all curves.

The design engineer characterizes and simulates the distortion created by the power amplifier. Two distortion parameters were considered: amplitude and phase. Real amplifiers have a maximum output power (saturation level) and an input-output power relationship that will depart from a straight line as the output power approaches the saturation level; this is called AM/AM distortion. Similarly, a phase shift depending on the power level will also occur, generating AM/PM distortion. Figure 49 shows the AM-AM and AM-PM distortion predicted by both codes. This figure shows that the predicted AM-AM distortion increases as power increases, starting at 14 dB with a 0-dBm input that increases steadily as power is increased. At greater than 14-dBm input power, the codes deviate slightly. MWO predicts an AM-AM distortion of 27 dB at 20-dBm input power while Series IV predicts 25.8 dB at 20-dBm input power, the deep compression zone of the circuit. The AM-PM distortion also shifts as power is increased from –128 degrees at 0.0 dBm to –107 degrees at 20 dBm. However, the two codes slightly disagree in the deep compression zone above 14 dBm. MWO predicts a shift of –107 degrees at 20 dBm while Series IV predicts –112 degrees. While these codes have some small disagreements in the data, overall, they correlate very well. The curves all follow the same profile and the discrepancies are only limited to a few degrees.

Large-signal gain is also an important parameter that the M&S software must accurately model. Figure 49 shows the predicted large-signal gain, S21, from MWO and Series IV. Gain is highest at lower powers, 14 dB at 0 dBm, decreasing as input power is increased. Again, these predictions agree with the theory behind transistors and their response to increases in input power. The curves from MWO and Series IV agree over the entire simulated power sweep.

A power amplifier's power-added efficiency defines how well the power amplifier converts the dc power applied to the circuit to the ac power delivered to the load, another important parameter that defines the overall performance of a power amplifier. Power-added efficiency is the difference between the output in input power magnitudes divided by the dc power magnitude. Figure 50 shows the power-added efficiency curve for this circuit as input power increases. The graph shows that the power-added efficiency is low at low-input powers at about 2.2 percent at 0 dBm. Power-added efficiency increases as input power increases, which is typical for these types of devices. MWO predicts that the efficiency will be about 44.3 percent at 20-dBm input power. However, the two codes disagree in the deep compression zone at above 14 dBm, which demonstrates Microwave Office's greater ability to characterize high-power, high-frequency simulations by accounting for the parasitic effects.

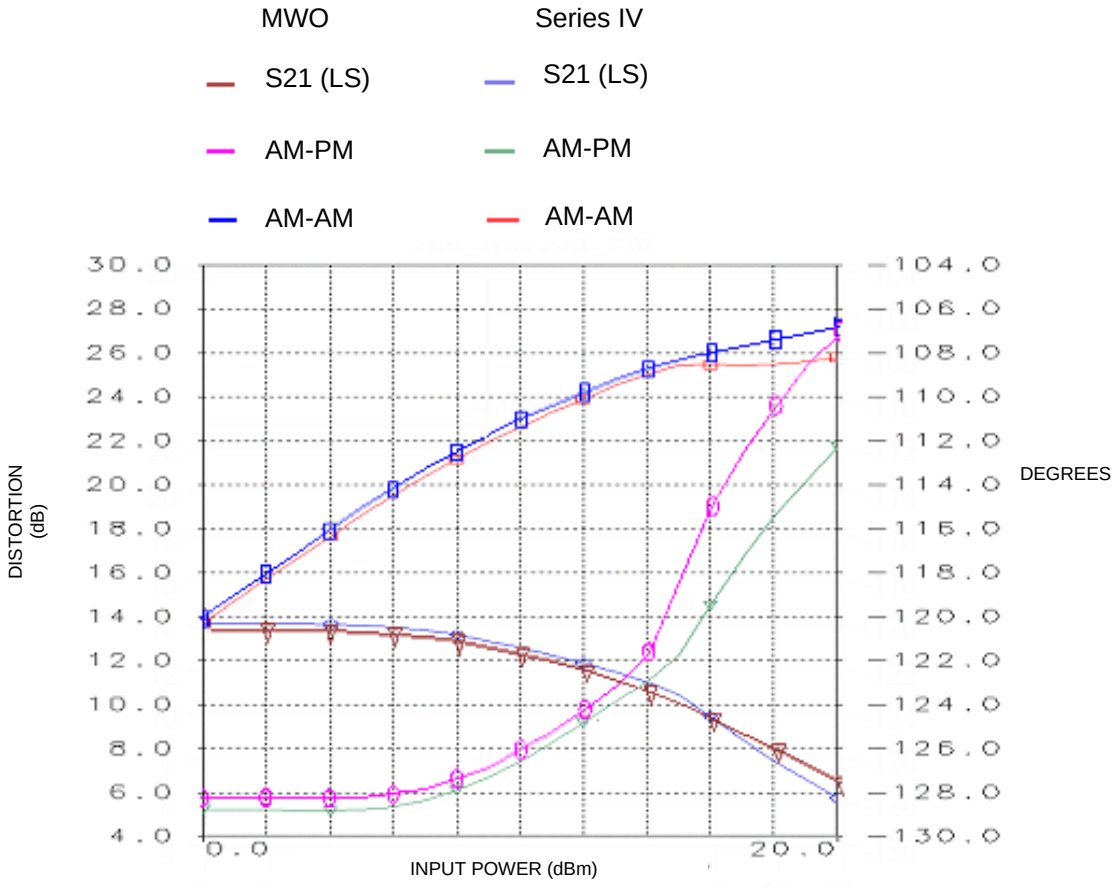

Figure 49. Power amplifier large-signal gain and distortion conversion.

$$\frac{|P_{Out}|-|P_{In}|}{P_{dc}} \times 100\%$$

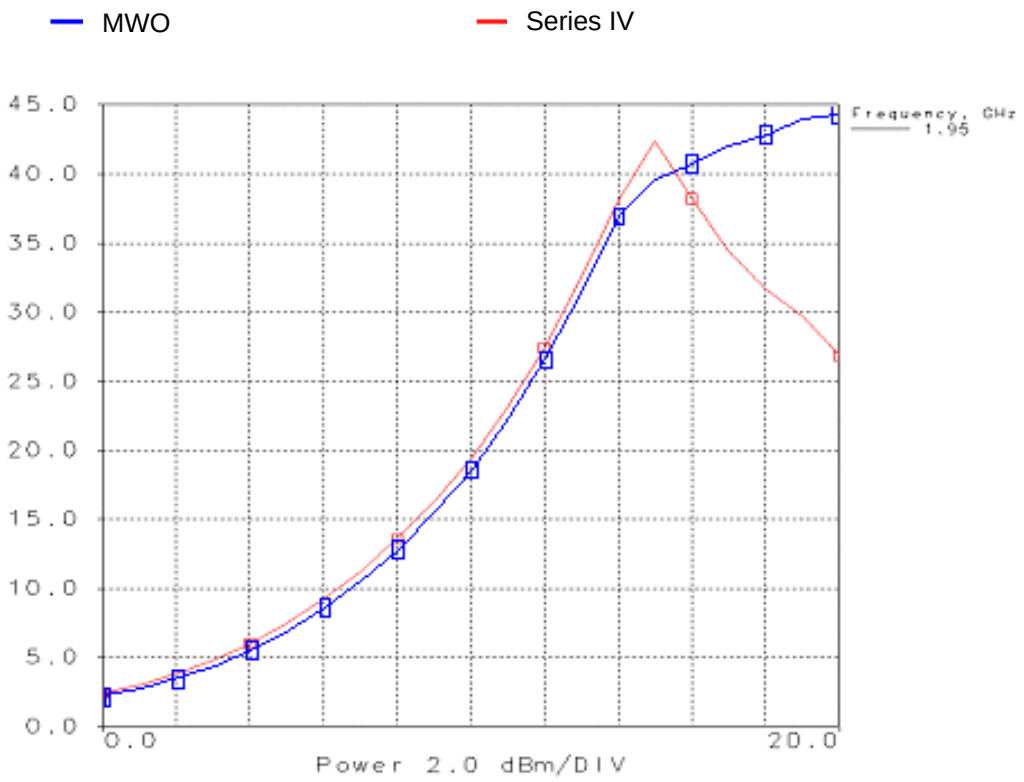

Figure 50. Power amplifier power-added efficiency.

The nonlinear characteristics of this device also produce harmonic distortion. Harmonic distortion is a form of processing error that creates signals at frequencies that are not necessarily present in the input and occur at integer products of the fundamental signal. Figure 51 shows that the single-tone power spectra from the two codes agree. This graph shows that the power at the fundamental frequency of 1.9 GHz is 23.1 dBm. Harmonic distortions appear at 3.8 and 5.7 GHz, but both are better than 35 dBc. These results indicate fidelity in the gain compression and second and third harmonic power levels.

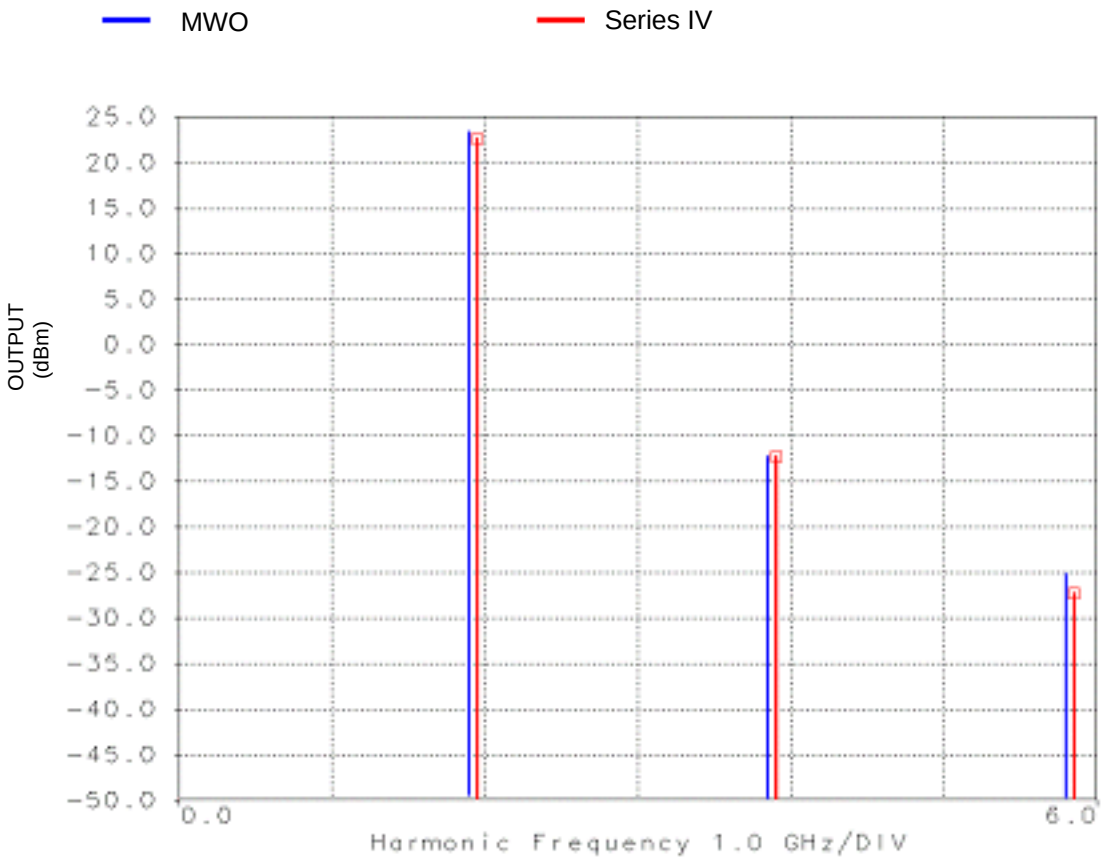

Figure 51. Power amplifier single-tone power spectrum.

3.4.3 Active Mixer Using an FET Device

Mixers are mostly used to translate signals up or down in frequency while minimizing distortions. In practice, they can downconvert RF to an intermediate frequency (IF) for further processing. A mixer combines a low-level RF signal and an RF local oscillator (LO) to produce this IF. Combining the RF signal with the LO produces two resulting frequencies. One is the IF, which is the difference between the RF and LO signals, and the second is the sum of the two signals, which occurs at higher frequencies. This frequency can be filtered out. The main shortcomings of real mixers are that they generate outputs at other than the wanted sum and difference frequencies and they produce nonlinear distortion on the signals passing through them.

The circuit under test consists of a combination of lumped elements and transmission lines for the matching and biasing networks. A conformal gate-mixer configuration is chosen in the simulation. The mixer device is a GaAs MESFET NE76038A. Its nonlinear TOM model was implemented in MWO and Series IV for comparison. Figure 52 shows the circuit configuration. The circuit is designed so that it can provide high-conversion gain at an 8-GHz center frequency. A common source mixer configuration will be used to downconvert an RF input signal to an IF output signal. RF and LO signals are injected at ports 1 and 2, and the IF output exits at port 10. The RF center frequency is 8.0 GHz with a 2-GHz span and was carefully analyzed by comparing the results from Series IV.

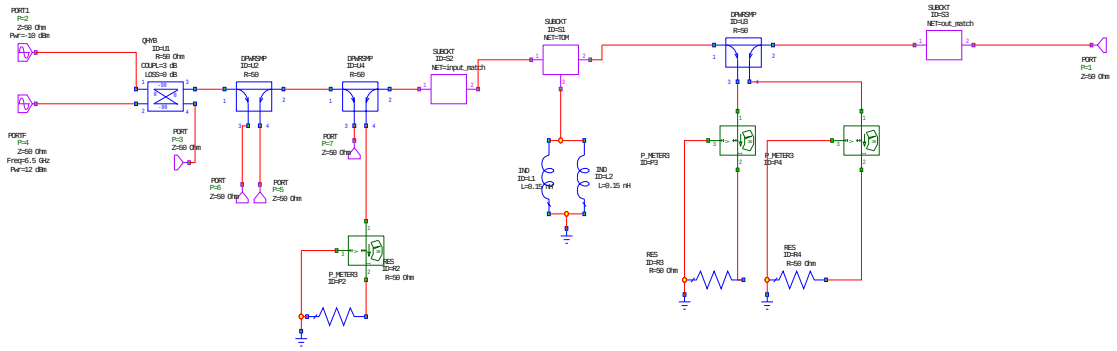

LO port

RF port
Hybrid coupler

1-pF capacitor for dc block
Open stub transmission line – Impedance:
50 Ω; electrical phase length: 57.4° at 8 GHz

Transmission line – Impedance: 50 Ω; electrical phase length: 44.5° at 8 GHz
NE76038A Field-Effect Transistor
Transmission line – Impedance 50 Ω: Electrical phase length: 70.9° at 8 GHz
Low-pass filter
IF port

Figure 52. Active mixer schematic.

Mixer conversion was predicted as a function of the RF input frequency (Figure 53). MWO and Series IV gave very similar results, with both programs showing the center frequency as 8 GHz, which agrees with theory because the circuit configuration was designed to provide high-conversion gain at 8 GHz. The peak power level simulated was about –2.0 dBm.

Mixers use nonlinear devices to frequency-convert an input signal. This nonlinearity causes outputs to appear that are not the sum and difference frequencies. For this test case, the previous circuit was retuned to a 6.5-GHz operating frequency. Both M&S codes were used to simulate the mixer power spectrum. Figure 54 shows the result comparison over the 0- to 20-GHz frequency range. The strongest signal is about 9.8 dBm at 6.5 GHz, as intended. The mixer output power spectrum shows reasonable correlation between the two codes, with the simulations of the main signal within 1 dB.

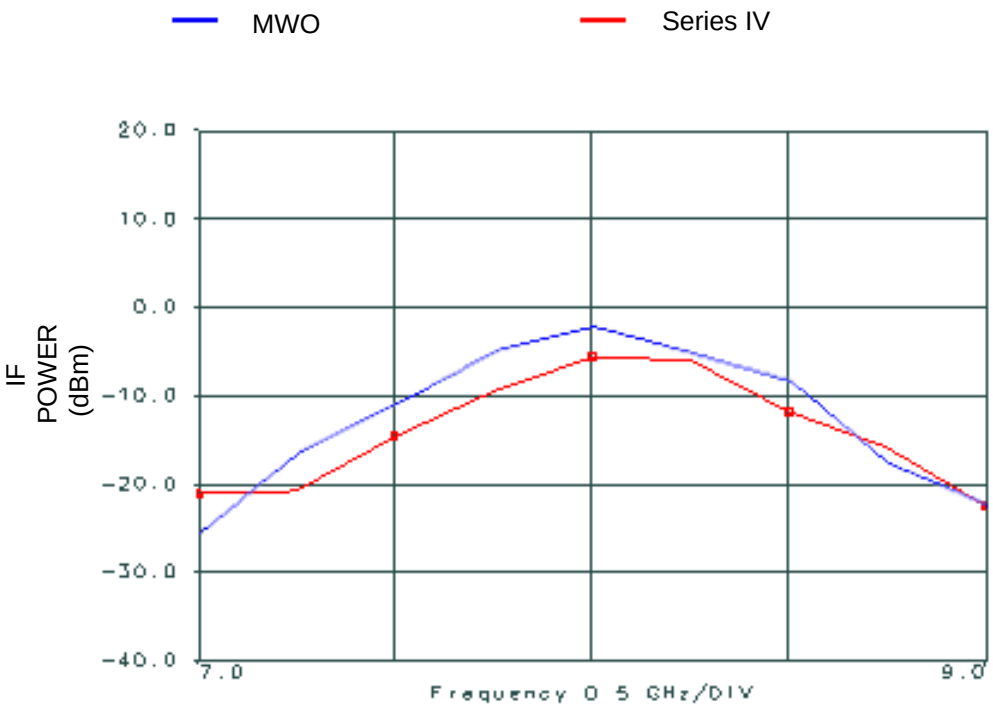

Figure 53. Active mixer IF power versus RF frequency.

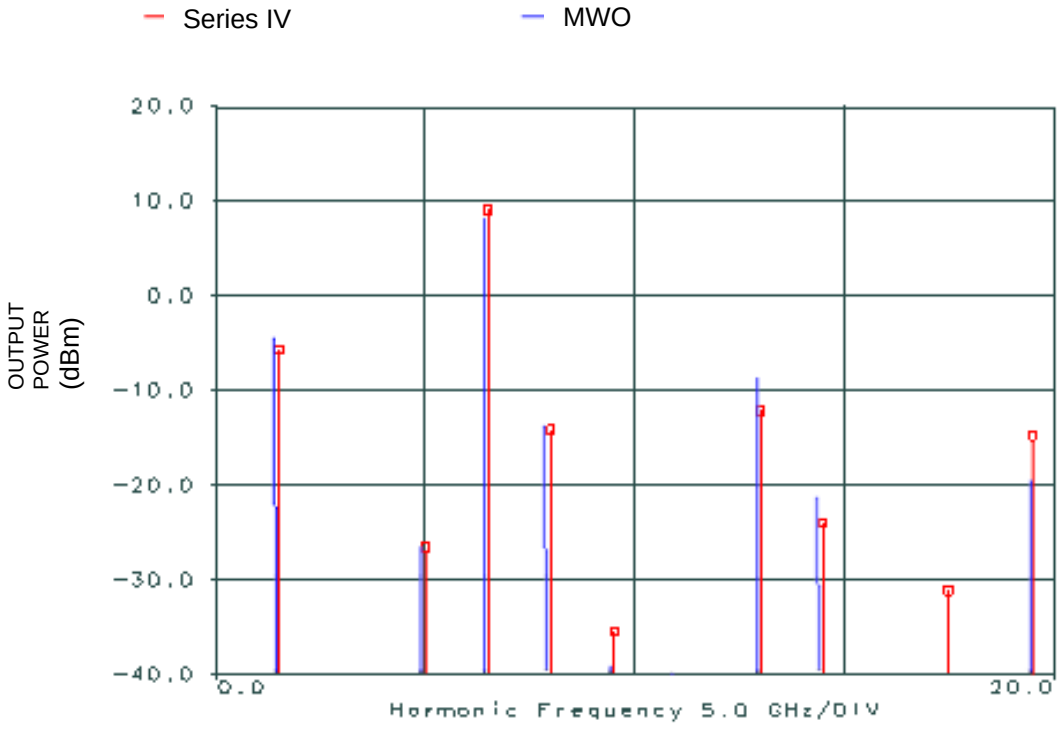

Figure 54. Active mixer output power spectrum.

3.4.4 Microwave FET Oscillator

A microwave oscillator converts dc power to RF power, so it is one of the most basic and essential components in a microwave system. A solid-state oscillator uses an active nonlinear device such as a diode or transistor with a passive circuit to produce a sinusoidal steady-state RF signal. At startup, however, transients or noise trigger oscillation, after which, a properly designed oscillator reaches a stable oscillation state. Modeling and simulation of oscillators is difficult, but necessary, in microwave system design. One common application for oscillators is to provide LO input to mixers.

This test case was a 6-GHz oscillator circuit realized in Low-Temperature, Co-fired Ceramic (LTCC) substrate. A cavity resonator is realized in LTCC by flat plates and walls, and is modeled by an equivalent circuit (Figure 55). In MWO and ADS®, we adjusted the excitation level at port 1 until oscillation conditions were met between ports 1 and 2 to determine the oscillator's frequency and output power. When these conditions were met, the output power and spectrum were those of the free-running oscillator, which was done manually in MWO but automatically in ADS®. The oscillator device used was a TOM nonlinear FET model NE72218.

Figure 56 shows the oscillator simulation results for MWO and Series IV. Since an oscillator is a nonlinear device, spurious frequencies besides the primary frequency are generated. The graph shows that the oscillator is operating at 6 GHz because that frequency has the largest signal, 19.5 dBm. Harmonics exist at 12 GHz and 18 GHz, but both signals are below –18.5 dBm. These results show very good agreement between MWO and ADS®.

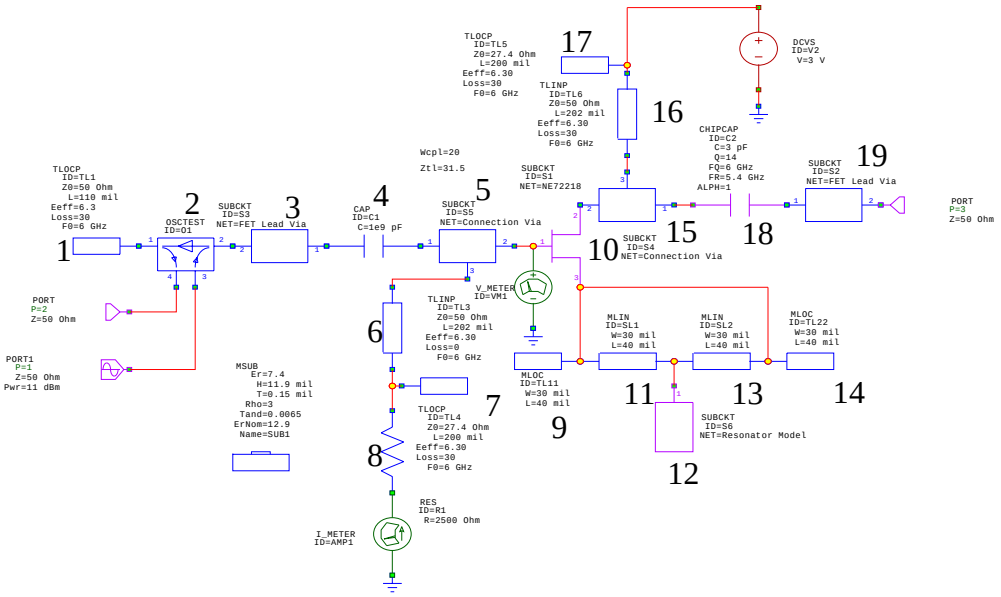

Transmission line – Length: 110 mil; Impedance: 50 Ω at 6 GHz
OSCTEST Block
Lead via
Capacitor 1 pF
Connection: via
Transmission line – Length: 202 mil; Impedance 50 at 6 GHz
Transmission line – Length: 200 mil; Impedance: 27.4 at 6 GHz
Resistance: 2500
Transmission line – Length: 40 mil; Width: 30 mil
NEC bipolar transistor: NE72218
Transmission line – Length: 40 mil; Width: 30 mil
Cavity resonator circuit model
Transmission line – length: 40 mil; Width: 30 mil
Transmission line – Length: 40 mil; Width: 30 mil
Connection: via
Length: 202 mil: Impedance: 50 Ω
Length: 200 mil, Impedance: 27.4 Ω
Capacitor: 3 pF
FET lead

Figure 55. Tunable FET oscillator schematic.

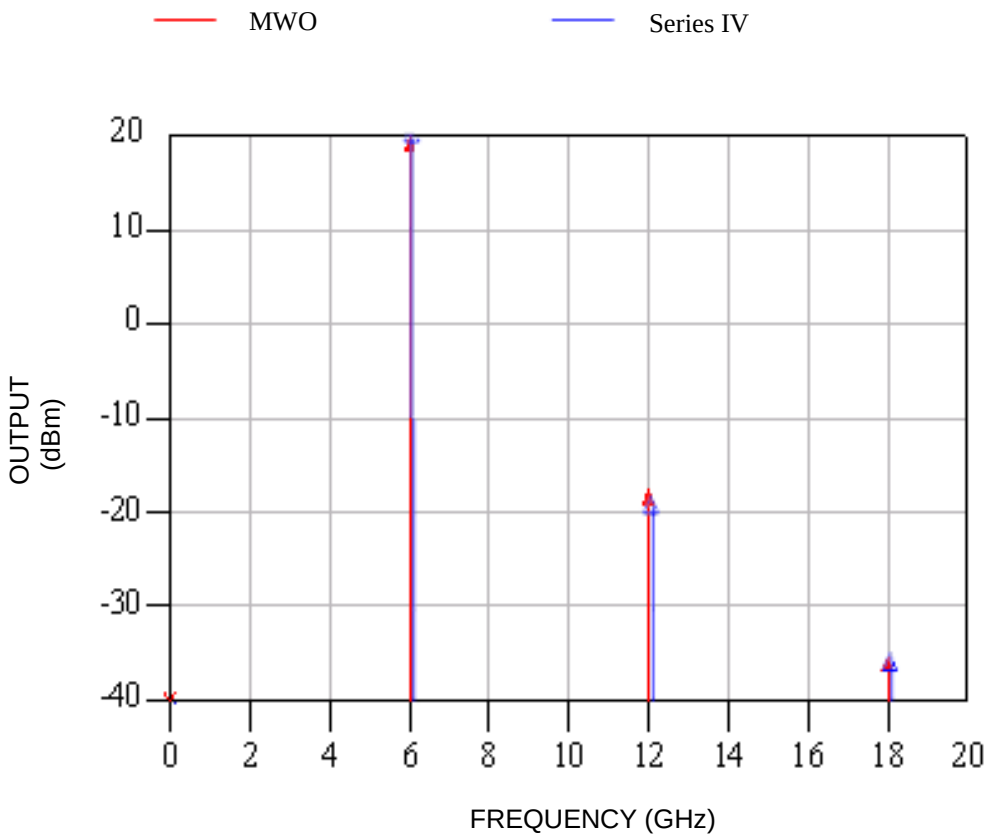

Figure 56. LTCC oscillator output spectrum.

3.5 SYSTEM-LEVEL ANALYSIS

Purpose

The M&S software can also perform system-level analysis. In the final five test cases, we investigated the fidelity of this feature. System designers are faced with the challenge of combining the numerous available devices and circuits to perform a desired system function. Often, the system engineer does not possess detailed component-level descriptions of the available devices and must rely on system performance metrics such as gain, the 1-dB compression point, the third-order intermodulation product intercept point, etc. M&S software provides system block element performance that can be specified as system metrics.

Assumptions

Performance of the system devices used in the M&S software depends on the operating frequency. Except for the system cascade case, the following experiments used multi-tone excitations. The performance of devices used in the experiments was characterized over the full range of excitation frequencies.

Procedure

The general method for validating the system analysis feature was to compare the M&S predictions to measured data. System parameters of actual devices were measured in the laboratory and input into the M&S software. Typical microwave systems were constructed in the M&S design environment and the electronics laboratory. M&S prediction results and experimental measurements were then compared. Comparison between experiment and simulation consisted primarily of spectral data analysis. From the data, power levels in the fundamental and intermodulation product tones can

be retrieved and used. In the system cascade experiment, data comparisons were similar to the linear active component test cases reported previously. M&S system device parameters were also measured within the simulation itself. This test determines the consistency of the software and provides an additional check on the validity of the model.

3.5.1 System LNA (Five-Tone)

3.5.1.1 Introduction

An LNA operating at UHF frequencies was driven at five distinct fundamental frequencies. Three sets of power levels for the fundamentals were used with a range from the linear mode to well into saturation mode. We used a spectrum analyzer to record amplifier frequency-domain input and output signal levels. From these measurements, we determined the gain in the fundamental frequencies and power levels for the nonlinear products.

We compared the experiment results to system model predictions from Microwave Office™. The purpose of this example was to determine the accuracy with which the MWO SYSTEM AMP component represents the performance of an actual device. Four system parameters characterize the SYSTEM AMP: gain, a 1-dB compression point, a second harmonic intercept point, and a third-order intermodulation product intercept point. We entered these quantities into the model. Product manufacturers often supply this information, but we measured these figures experimentally (Section 3.5.1.3).

MWO provides nonlinear harmonic balance analysis that allows up to three independent tones. Independent tones are primary signal tones that cannot be produced by any combination of the harmonics and intermodulation products of existing signals. Selection of frequencies in the simulation are pursued by properly choosing the fundamental tones and only allowing the significant harmonic components to be computed. This procedure was used to perform the five-tone excitation in this example. A convenient method that is used to include multiple tones in the MWO project is through a modulated port input. This harmonic balance signal source was developed to perform analysis on input signals with finite pulse widths. The modulated port simulation used two-tone analysis to reproduce the pulse shape. The fundamental frequencies, f1 and f2, were separated by an amount, df = f2 – f1. By including the appropriate number of harmonics and intermodulation products of these two fundamentals, the entire frequency range of the pulse was spanned. Amplitude and phase of each discrete frequency in the pulse could be chosen independently and were listed in a user-defined signal file. Five-tone excitation was created by specifying finite amplitudes at the desired frequencies and turning off the amplitudes of all other frequencies.

3.5.1.2 Experimental Setup

Five signal generators were used to drive a MITEQ® LNA block. Since the amplifier has only a single input port, we used two 3:1 power dividers to combine the signals from the signal generators. The power level was adjusted accordingly. Figure 57 shows a schematic diagram of the setup. We used the first power combiner (PC) to couple the signals from the first three sources into one transmission line. This line was then combined with signals from the fourth and fifth sources in the second power combiner. Therefore, the output of PC II contained five continuous wave (CW) carrier signals with power levels and frequencies that could be independently adjusted. The output transmission line from PC II was connected to the input port of the block for measurement of output and input spectra respectively. The LNA output port was connected to the spectrum analyzer through a 0- to 60-dB variable attenuator with 10-dB increment adjustments. The attenuator was necessary to protect the spectrum analyzer from excess power levels.

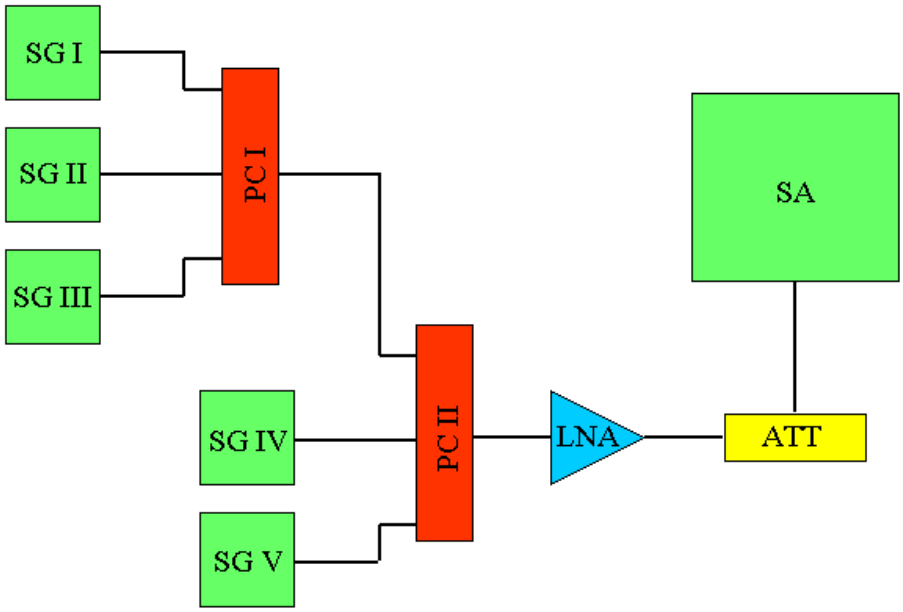

Figure 57. System five-tone LNA schematic.

Table 1 lists equipment used in this experiment. Manufacturer model numbers and serial numbers are listed. Connectors and cables used are not listed; however, a brief description follows. The signal generators, attenuator, and spectrum analyzer are equipped with male N-type connecting ports. The LNA and power combiners use male SMA connectors. The entire circuit was constructed with N-type to SMA converters and 2-foot coaxial transmission lines.

Table 1. System LNA equipment list.

Equipment	Model Number	Serial Number
SG I	HP 8648A	PB47749
SG II	HP 8648A	PB47750
SG III	HP 8648 A	PB17129
SG IV	HP 8662A	PA90466
SG V	HP 8780A	PA93893
PC I	MC 15542	ZA3PD-4 (9517 03)
PC II	MC 15542	ZA3PD-2 (9523 04)
LNA	MITEQ® AU-3A-0150	478491
ATT	HP 354A	01449
SA	HP 8566B	PB97532
DC supply	Topward 6306D	983452

Figure 58 shows the experimental setup. The five signal generators are arranged in a vertical column on the left. A personal computer was used to obtain digital data from the spectrum analyzer via the General Purpose Interface Bus. An in-house software tool was used to read the data from the spectrum analyzer, display the trace on the monitor, and write the information to a file on the hard drive. A 15-Vdc supply (shown on the right) powered the LNA. Two power combiners, an attenuator, and an LNA are shown from left to right in the foreground.

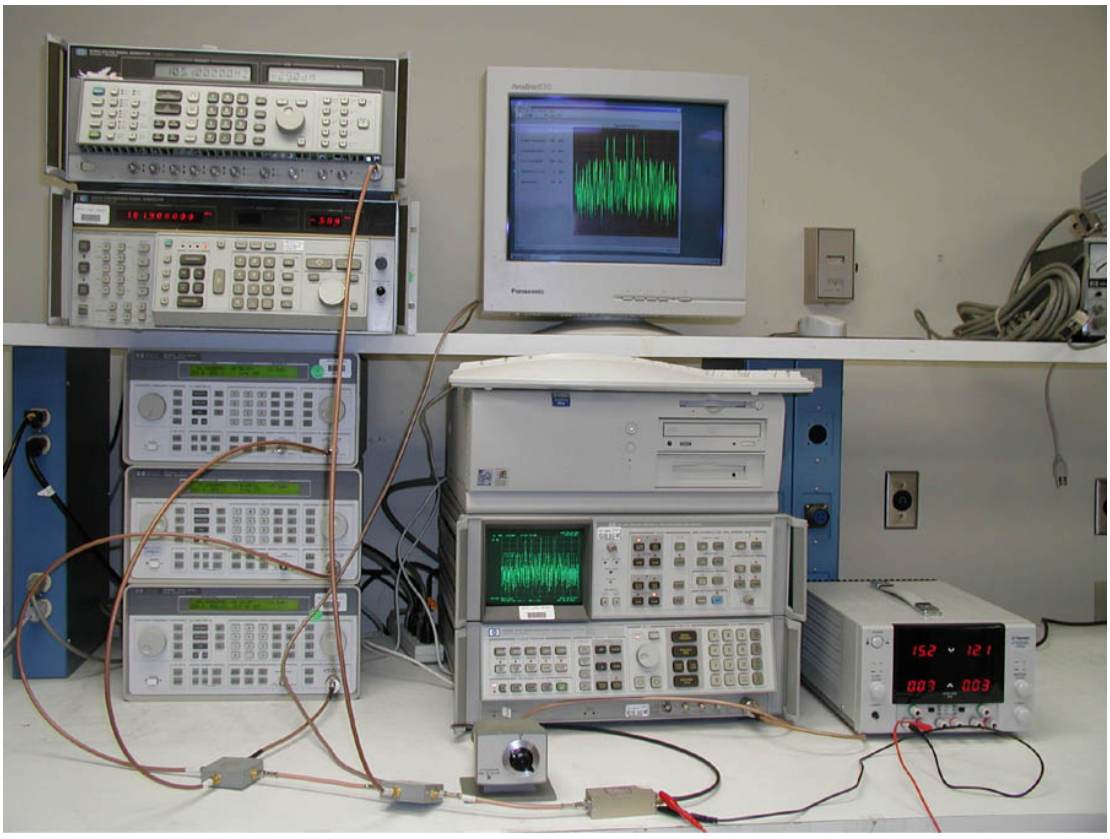

Figure 58. System five-tone LNA experiment.

3.5.1.3 System Model Parameters

This section describes the method used to determine the system parameters for the amplifier under test. Stated values agree well with values listed by the manufacturer. Determining the nonlinear performance of the amplifier requires two measurement sets. System amplifier models in MWO depend on the operating frequency. Therefore, we must obtain system parameters near the frequencies of its intended use.

We obtain the gain, second harmonic intercept point, and 1-dB compression point from input and output levels for a single-signal power sweep. The sweep must include a substantial portion of the linear operating region and extend into the saturation region. A 100-MHz signal was injected into the amplifier and the power level was varied from –66 dBm to –30 dBm at 1-dB increments. We recorded output power at the fundamental (100 MHz) and nearest harmonic (200 MHz). The red and blue dotted curves of Figure 59 represent these data. Note that an attenuator was used to protect the spectrum analyzer from the large output power from the amplifier. This loss was added to the readings from the spectrum analyzer to obtain the actual output power level at the amplifier output port. The attenuator was independently characterized at low power levels. We assumed that the loss remains constant as the input power is increased. Furthermore, we made input and output measurements with the fewest number of cable losses to eliminate the possibility of errors that might be caused by cable losses. We measured output power levels with the amplifier in the circuit and the attenuator set to the appropriate loss. We removed the amplifier and set the attenuator loss to 0 dB to measure the input power levels.

Additional measurements were required to determine the third-order intercept point. We fed two input signals of slightly differing frequencies and equal power levels into the amplifier. In this case, the frequencies were f1 = 100 and f2 = 105 MHz. Power levels of the two signals were swept simultaneously over a large range as in the previous test setup. We recorded output power levels at the nearest third-order intermodulation product for each power level setting in the sweep. Third-order products nearest the fundamental were 95 MHz (2f1 to f2) and 110 MHz (2f2 to f1). Since f1 and f2 have equal power, these two third-levels will be the same in the absence of frequency-dependent effects. We used the data from the 110-MHz intermodulation product to determine the intercept point. Figure 59 shows the measured data as a green dotted curve.

From the plots of the measured data in Figure 59, we could determine the system-level parameters for the amplifier. The linear operating region is easily identified at input power levels below –37 dBm. In this region, all the data portray a linear relationship between the input and output power levels. The amplifier gain is the slope of the line that interpolates the data in the linear region of the data for the fundamental signal. In this case, we found a 46.9-dB gain. A straight line through these data is extended into the nonlinear operating region. The 1-dB compression point is the output power level at which the gain was reduced by 1 dB because of saturation. For this amplifier, the 1-dB compression point power level is 11.5 dBm. The second harmonic intercept point, IP2, is the output power level at which the extrapolated linear data from the fundamental and nearest harmonic intersect. Likewise, the third-order intermodulation intercept point, IP3, is the output power level at which the extrapolated linear data from the fundamental and the third-order product intersect.

Specification of the four parameters determines the complete nonlinear behavior of the system amplifier device model (see Table 2). For simplification to occur, MWO must make an assumption concerning the functional description of the amplifier gain curves. The shapes of these gain curves are fixed for the system amplifier device. The system parameters determine their slopes and relative positions. A numerical experiment identical to the measurements described above can test the validity of the MWO gain curve assumptions. We constructed a model of our experiment within

MWO, used the system parameters that were measured experimentally, and produced the gain curves for the fundamental, nearest harmonic, and nearest third-order intermodulation product. By comparing the measured and predicted gain curves, we validated the underlying assumption of the model.

The solid curves in Figure 59 represent the gain curves predicted from the simulation. The fundamental and third-order intermodulation product curves agree well with the measurements in the linear and nonlinear regions. However, the second-harmonic gain curves agree only in the linear operation region. Above the 1-dB compression point, the simulation predicts harmonic power levels well below the actual values. This discrepancy does not affect the intercept point because it is solely determined from the data in the linear regime.

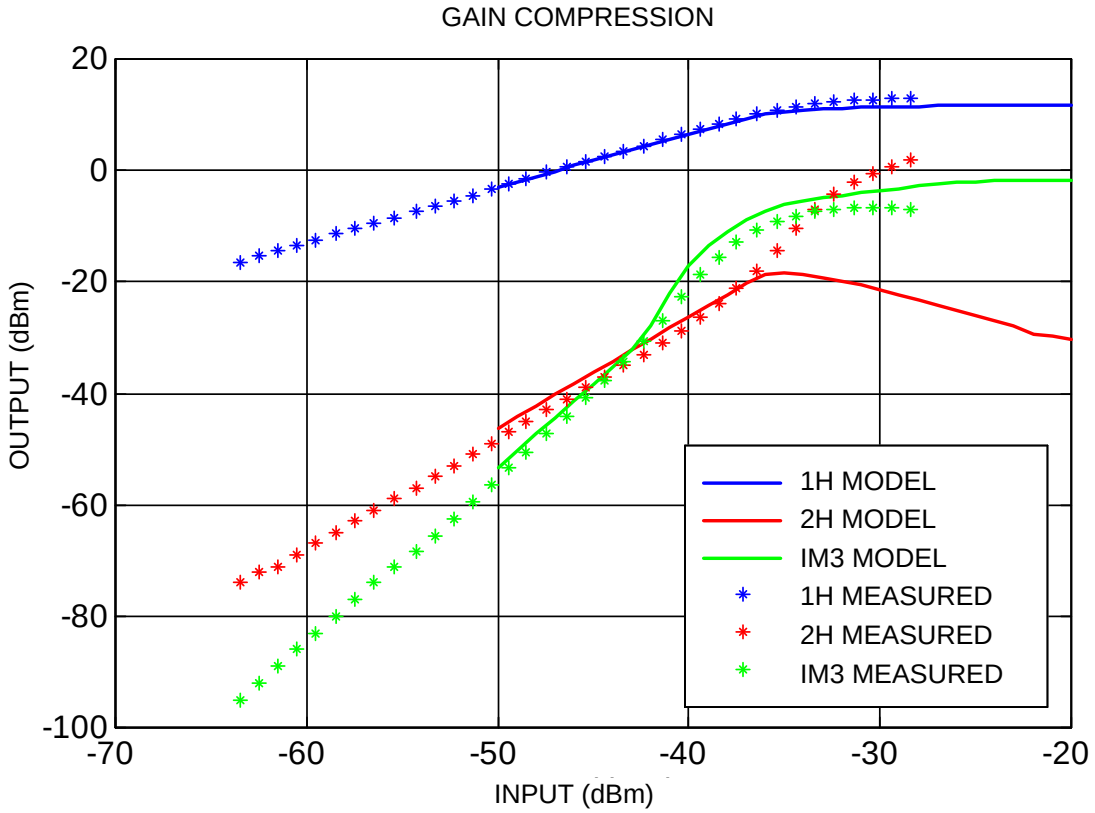

Figure 59. Power sweep data.

Table 2. LNA measured system parameters.

Parameter	Measurement	Frequency (MHz)
Gain	46.9 dB	100
1-dB compression point	11.5 dBm	100
2H intercept point	40 dBm	200
IM3 intercept point	22 dBm	110

3.5.1.4 Results

This section presents results that represent comparisons between predicted and measured power spectra for the LNA block excited at five frequencies near 100 MHz. We examined three different cases in which the power levels of the input signals were varied from linear operation to operation near the 1-dB compression point and into the saturation region. The number of harmonic components kept in the simulation was increased repeatedly until further increases produced no noticeable changes on the outcome. Figures 60 through 62 show the input and output spectra. Measured input spectra include spurious signals between –80 and –100 dBm. The noise floor for the input spectra of the simulation was set at the theoretical minimum.

Case 1—Low Input Level: Amplifier was driven within its linear operation region.

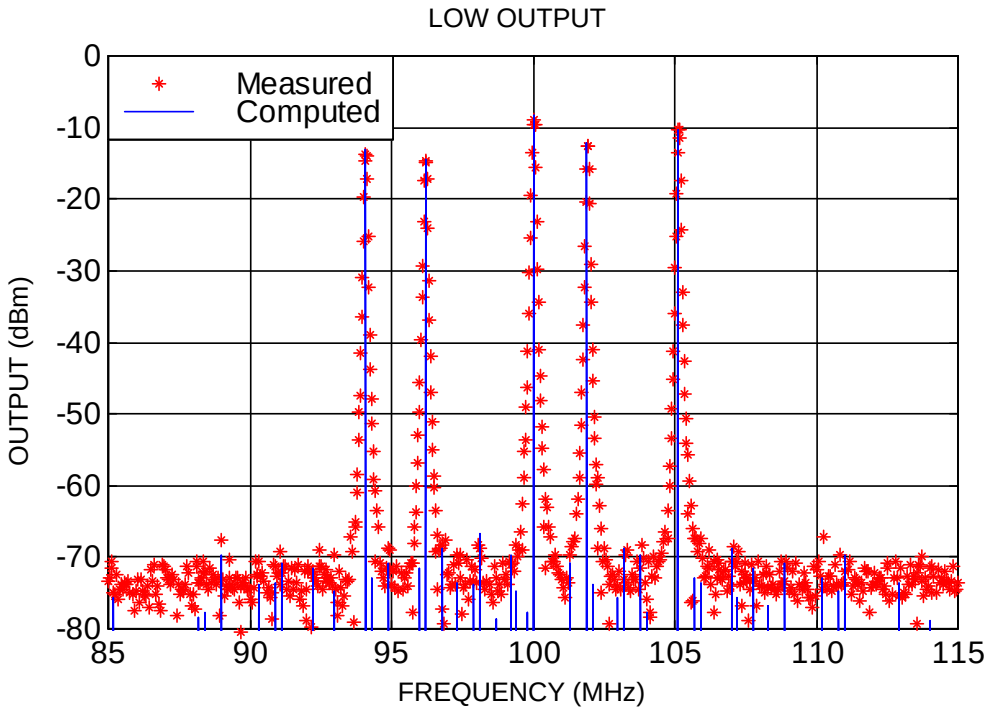

Figure 60. LNA output spectrum low drive.

Case 2—Middle Input Level: Amplifier was driven near its 1-dB compression point.

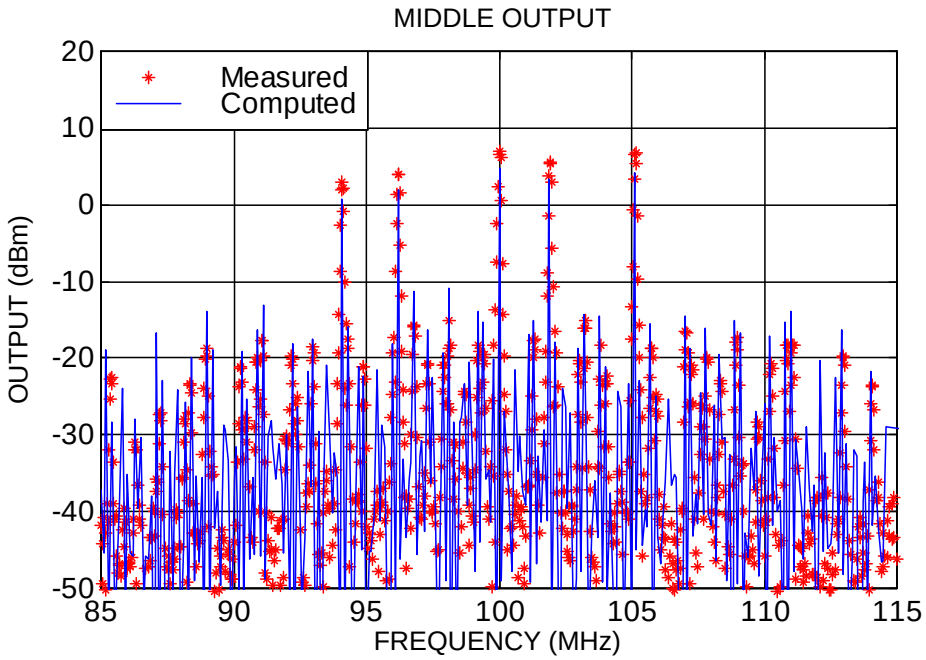

Figure 61. LNA output spectrum middle drive.

Case 3—High Input Level: Amplifier was driven well into saturation

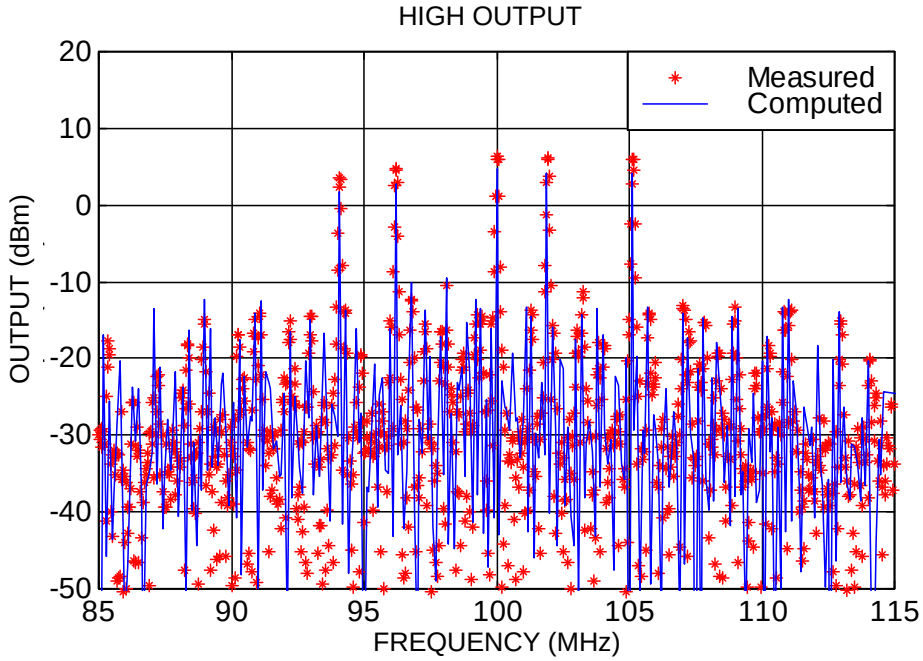

Figure 62. LNA output spectrum high drive.

Predictions of the MWO simulations agree reasonably well with the measured values. In the linear region, the agreement was almost exact. Agreement was not surprising because gain determines the linear performance. The only possibly source of error for the linear performance predictions would be a frequency-dependent gain variation in the physical device. Lack of any significant discrepancy in the data comparison suggests that the amplifier gain is constant from 94 to 105 MHz.

Middle and high drive simulation results are quite similar and are analyzed together. Predicted output power levels for the fundamental tones are several decibels below the measured values. Results are consistent with the trend observed in the gain curve discrepancy between the amplifier model and the actual device in Figure 59. Saturation of the physical device is not as severe as the theoretical model predicted.

Model predictions for the frequencies of intermodulation products are quite accurate. This simulation used 0.1-MHz increments for the frequency spectrum, a result that is consistent with that amount of resolution. Power levels predicted for the most significant intermodulation products differ from the measured quantities within 4 dB for the middle level drive and up to 7 dB for the high-level drive. These results are again consistent with Figure 59, where the predicted gain curve for the third-order intermodulation products are several decibels above the measured value.

3.5.2 System Cascade

3.5.2.1 Introduction

A useful tool for system designers is the S-parameter cascade calculation. In this approach, an S-parameter file specifies the frequency response of each component. Since the simulation is linear, the analysis remains valid only if each component is operating in its linear region. If a nonlinear device is used, its S-parameter file representation must be obtained at actual operating power levels. Harmonics and intermodulation products cannot be calculated. This technique does provide the magnitude and phase of the signals that transverse through each segment of the system as a function of frequency. It is not restricted to using only measured data for component definitions. Any combination of measured and model components can be constructed. The software provides a large library of device models. Alternatively, we could create a component with an arbitrary or formal base frequency response for insertion in our system. Once the correct response is found to complete the system, component designers can fabricate a physical device to match the needed response. MWO can be used to perform this type of analysis.

In this example, we used only measured S-parameters obtained for each individual component to synthesize the response of a network. A network consisted of three components: a low-pass filter, an attenuator/LNA, and a power amplifier/attenuator. We used a network analyzer over a 100- to 500-MHz frequency range to obtain the complex S-parameters (magnitude and phase) of each component. The components were then connected in series and the S-parameters of the entire system were measured. S-parameter data measured with the network analyzer were written to disk and converted to a standard format. We used individually measured component S-parameters to compare measured system performance to the MWO prediction.

The following procedure was used to obtain the predicted system performance. Measured S-parameter files for the components were imported into Microwave Office™ in the standard Touchstone® format, s2p files. Each data file loaded into the simulator was represented schematically as a subcircuit. A MWO schematic was created and a series cascade circuit was constructed from the three individually measured subcircuit files (see Figure 63). Behavioral response of this circuit was computed over a 100- to 500-MHz frequency range. The results of this calculation were then compared to the measured system S-parameters (Section 3.5.2.4).

3.5.2.2 Experimental Setup

The three components used in this experiment included all the cables and connectors necessary to complete the system circuit. The network analyzer (NA) was calibrated with a male SMA connector at port 1 and a female connector at port 2. Each component used in the experiments had a female SMA connector at the input port and a male SMA connector at the output port. This configuration was necessary to avoid introducing any new cables or connectors that would not be represented in the component measurements into the system measurement.

Components were chosen to represent typical electronics in an RF network. A low-pass filter (LPF) provided a strong frequency-dependent response to the system. Amplifiers represent active devices. To reduce the overall power (PWR) in the network, attenuators (ATTs) were placed at the output ports of the amplifiers. ATT I protected the low-noise amplifier (LNA) and ATT II protected the network analyzer.

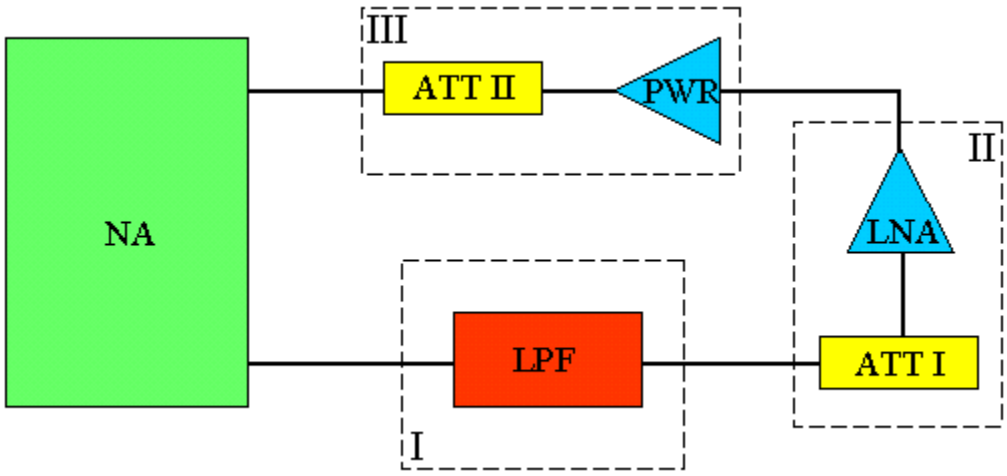

Figure 63. UHF system cascade schematic.

A dc power supply provided 24 Vdc to the power amplifier and 15 Vdc to the LNA. Table 3 lists the model and serial numbers for the devices used in the measurements.

Table 3. UHF system cascade equipment list.

Device	Model Number	Serial Number
NA	HP 8510C	PB47749
LPF	CD 2150	08-00924-001
ATT I	HP 354A at 50dB	01449
ATT II	HP 355D at 30 dB	
LNA	MITEQ® AU-3A-0150	478491
PWR	MC ZHL-1-2W-N	D101397-14

We connected the three functional blocks in series to construct the complete UHF system. Figure 63 shows a schematic of this system circuit. The entire cascading system was connected to the network analyzer and the S-parameters were measured and used in the simulation. We calibrated the network analyzer before the measurements and the maintained the calibration settings for all three functional blocks and the system measurement. Figure 64 shows a layout of the system measurement experiment.

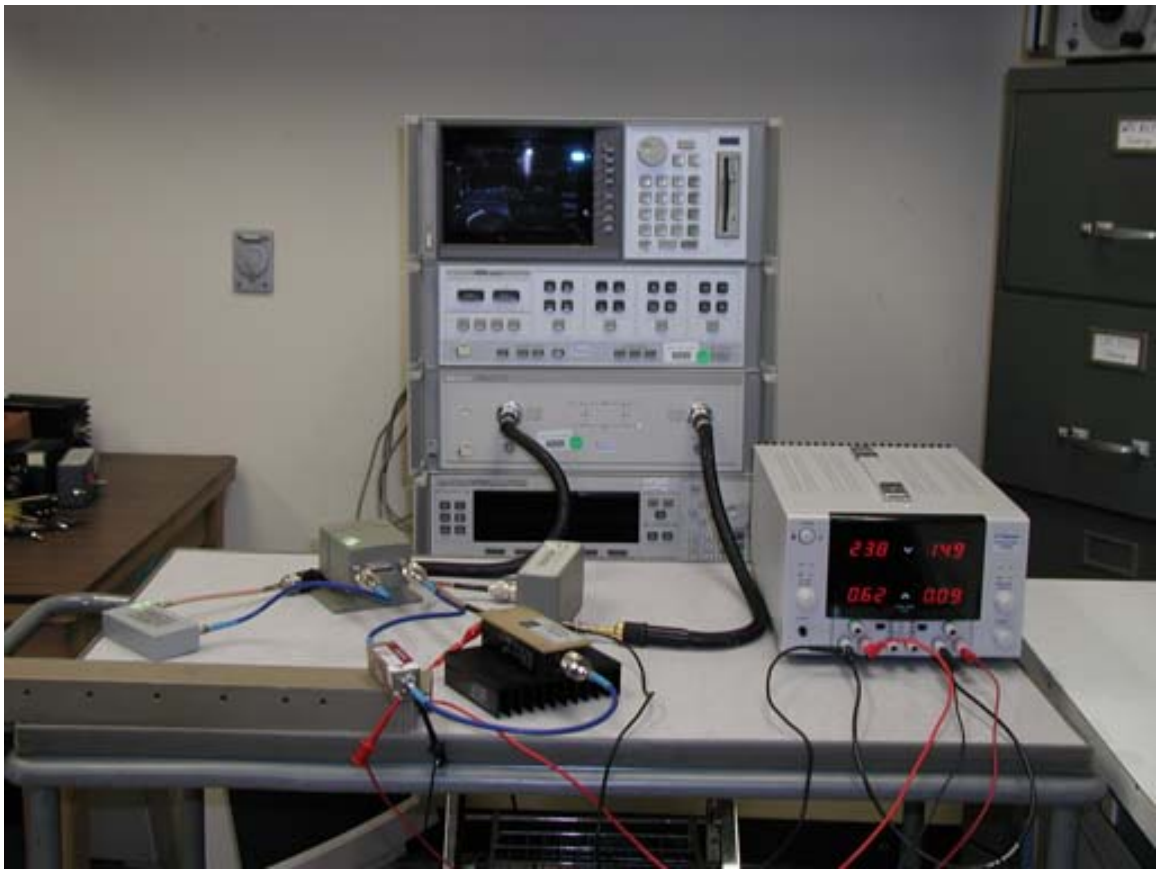

Figure 64. UHF system cascade experiment.

3.5.2.3 System Model Parameters

Since we used experimentally measured data to create all the components in this test case, system model parameters in the simulation could not be adjusted. The S-parameters characterized individual components for this experiment. Figures 65 through 67 show each complete component.

S-parameters for each component were measured on the network analyzer and used in the simulation. S-parameter data for each component were then imported into MWO as a subcircuit to define the performance model of each component.

Figure 65. Functional Block I: low-pass filter.

Figure 66. Functional Block II: LNA/attenuator.

Figure 67. Functional Block III: Power amplifier/attenuator.

3.5.2.4 Results

We plotted the predicted S-parameter performance from MWO with the measured S-parameter data (Figures 68 through 70). Predicted performance of the UHF Cascade System correlated extremely well with the measured results. Measured data and input and output return losses all agreed extremely well with the calculations. The input and output return losses were very low at the lower frequencies and deteriorated at the higher end. The data show reasonably good impedance matching at the input and output ports below 400 MHz. Gain was constant across most of the passband before dropping off. System isolation is not shown because of the limited dynamic range of the network analyzer. The lowest measurable isolation that can be obtained from the network analyzer is about –50 dB. Since each amplifier provides at least 50 dB of isolation, the actual S_{12} for the system was well below the detectable level of the network analyzer.

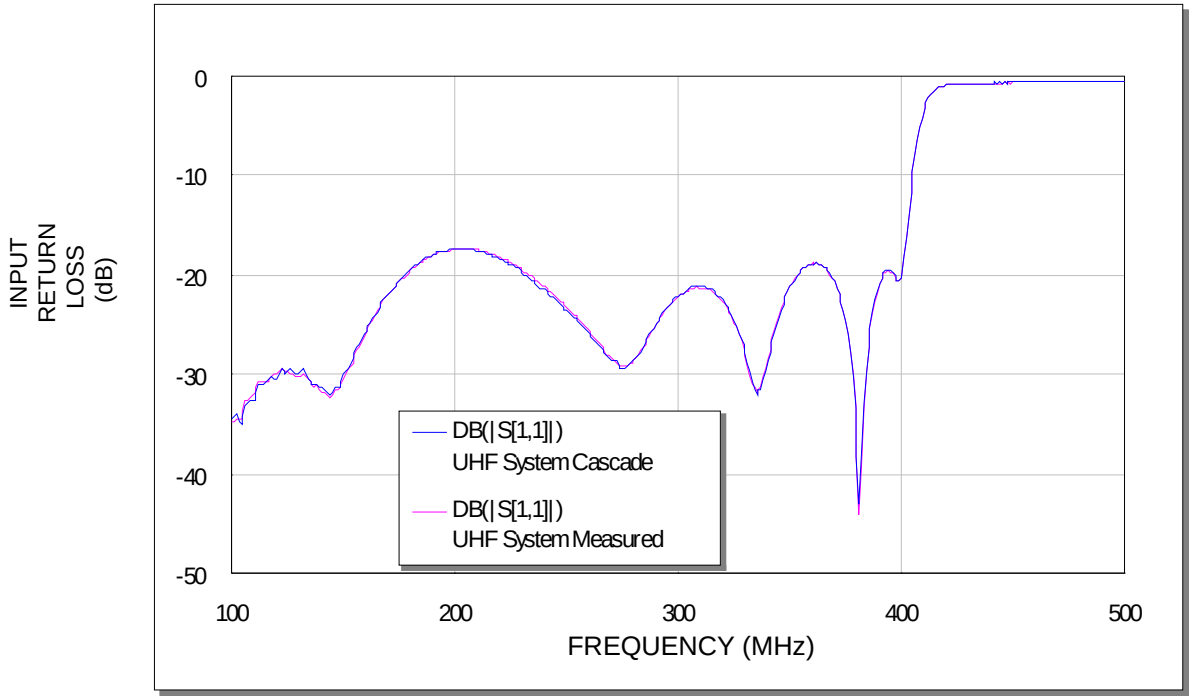

Figure 68. UHF system input return loss magnitude comparison.

Figures 71 through 73 show the S-parameter measurement phases. Again, the results agree quite well in regions where the magnitudes of the signals are in the –50-dB dynamic range. The maximum error in these regions is ±2°. Phase information was very reliable above the minimum detection level of the network analyzer described above.

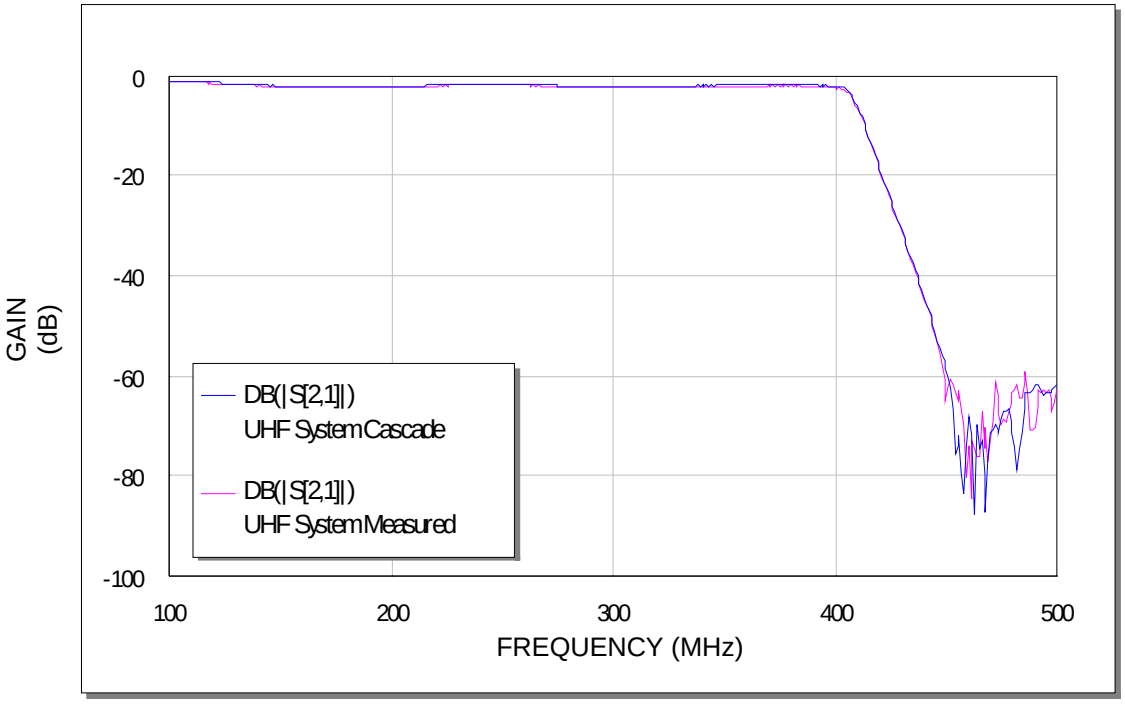

Figure 69. UHF system gain magnitude comparison.

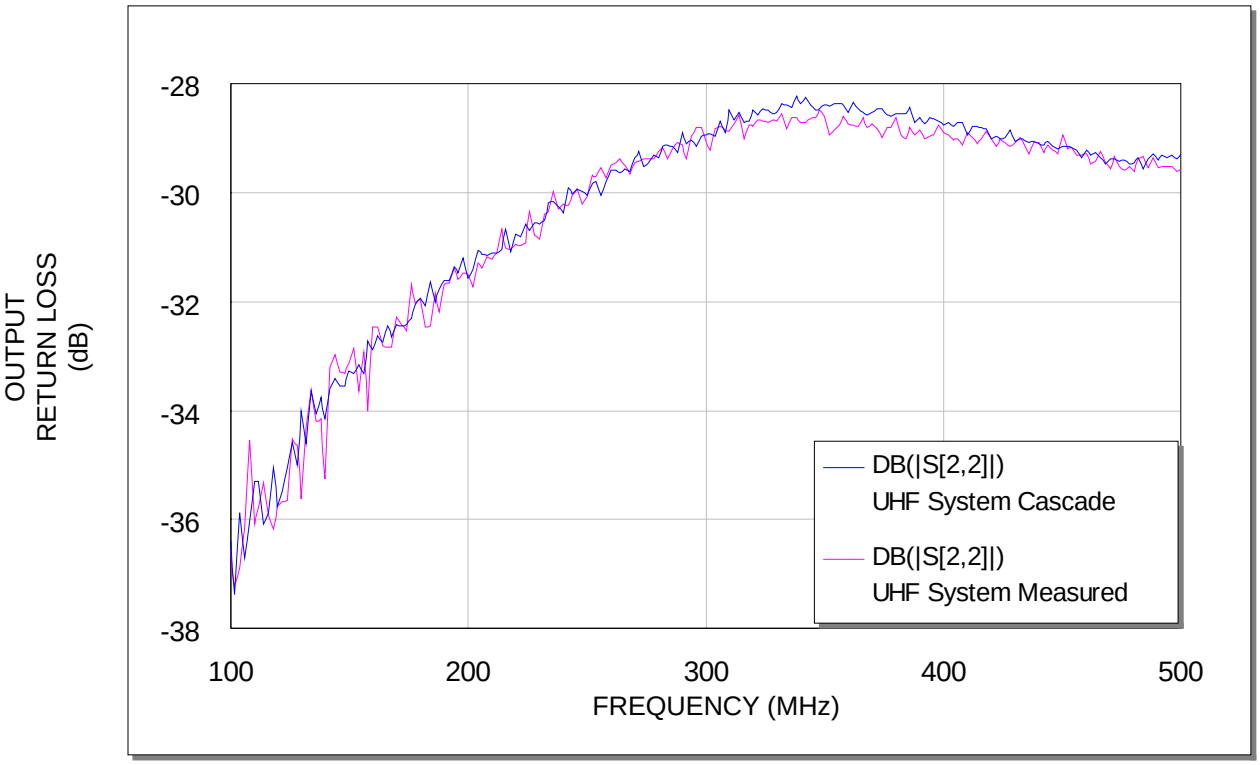

Figure 70. UHF system output return loss magnitude comparison.

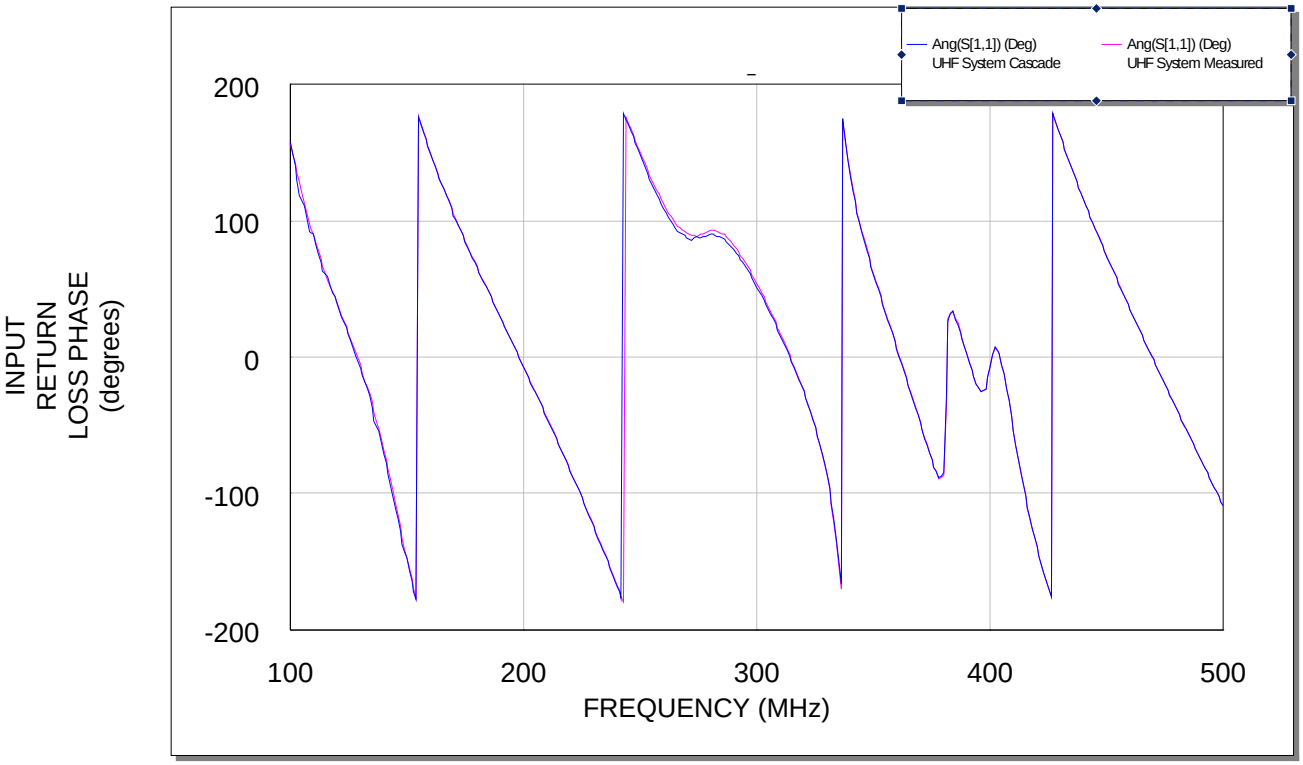

Figure 71. UHF system input return loss phase comparison.

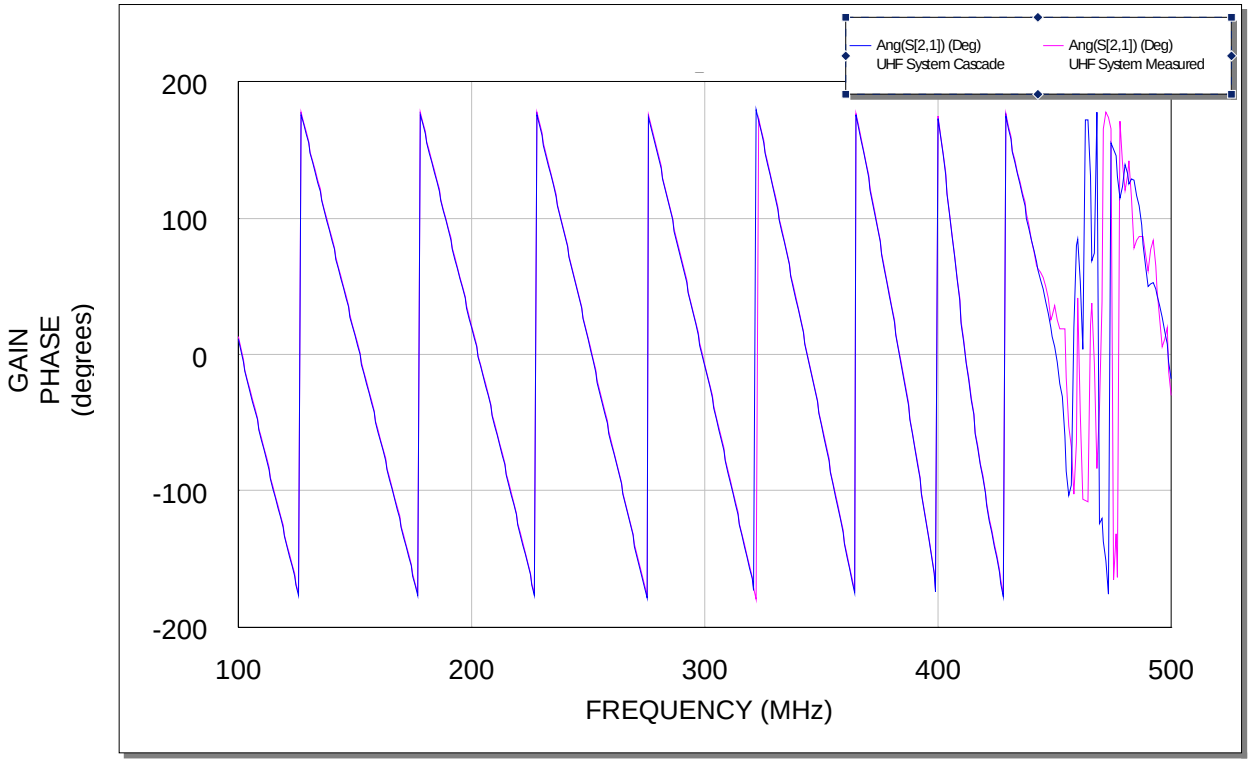

Figure 72. UHF system gain phase comparison.

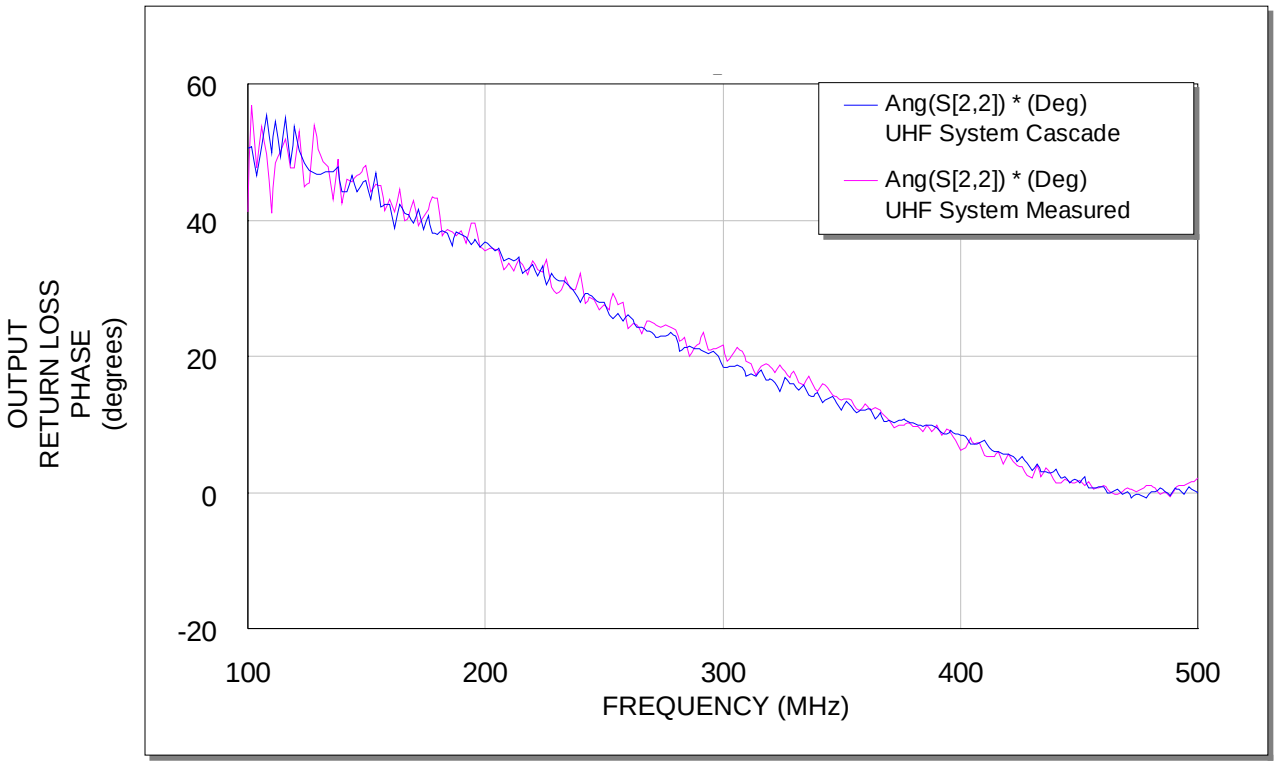

Figure 73. UHF system output return loss phase comparison.

The UHF system cascade experiment verified the ability of MWO to predict the system S-parameter response when using experimentally measured data for the components. This capability is important for system designers because they often deal with measured or manufacturer-provided S-parameter data and cannot create component-level models of manufacturer's devices. The MWO simulation provides extremely accurate analysis of systems involving S-parameter cascaded functional blocks.

3.5.3 System Power Amplifier (Three-Tone)

3.5.3.1 Introduction

Three distinct fundamental frequencies drive a power amplifier operating at UHF frequencies. The amplifier output spectrum was measured and simulated in linear, weakly nonlinear, and saturation regimes. We used a spectrum analyzer to record frequency-domain input and output signal levels from the experiment. From these measurements, we could determine the gain in the fundamental frequencies and power levels for the nonlinear products of the fundamentals.

We compared the experiment results to Microwave Office™ system model predictions. The purpose of this example was to determine the accuracy with which the SYSTEM AMP component in MWO represents the performance of a commercial 2-watt UHF amplifier. SYSTEM AMP has four system parameters: gain, a 1-dB compression point, a second harmonic intercept point, and a third-order order intercept point. We measured these quantities and entered them into the model. Product manufacturers often supply this information, but we measured these figures experimentally for verification (Section 3.5.3.3).

MWO provides nonlinear harmonic balance analysis for up to three independent tones. In the previous LNA example, a novel technique was used to create and analyze a five-tone

excitation. In this example, we used the built-in three-tone system model in MWO and a two-tone analysis where the third tone was specified as a harmonic product of the first two to perform a three-tone analysis. From the comparison of these calculations, one can determine whether the multitone technique is valid in the three-tone limit. In the independent tone analysis, three separate harmonic balance sources were coupled together through a 3:1 power combiner and fed into the SYSTEM AMP element. The three frequencies were chosen from frequency values close to the actual operating frequencies. The number of harmonic components was increased until no noticeable changes occurred in the output spectra over the 80- to 120-MHz frequency range. In the multitone calculation, a PORTMOD source provided all three frequencies in a similar fashion to the previous LNA example.

3.5.3.2 Experimental Setup

A Mini-Circuits® 2-watt amplifier was injected with three signal generators (SGs). Since the amplifier has only a single input port, the signals from the signal generators were combined using a 3:1 power divider. Figure 74 shows a schematic diagram of the setup. We used the power combiner (PC) to couple the signals from the three sources into one transmission line. PC output contained three unmodulated carrier signals with power levels and frequencies that could be independently adjusted. The output transmission line from the PC was connected to the amplifier input port. The power amplifier output port was connected to the spectrum analyzer (SA) through a series of three attenuators (ATTs). The first two attenuators were set for a total of –20 dB. The third attenuator was variable, 0 to 60 dB with 10-dB increments. Attenuators were necessary to protect the spectrum analyzer from excess power levels.

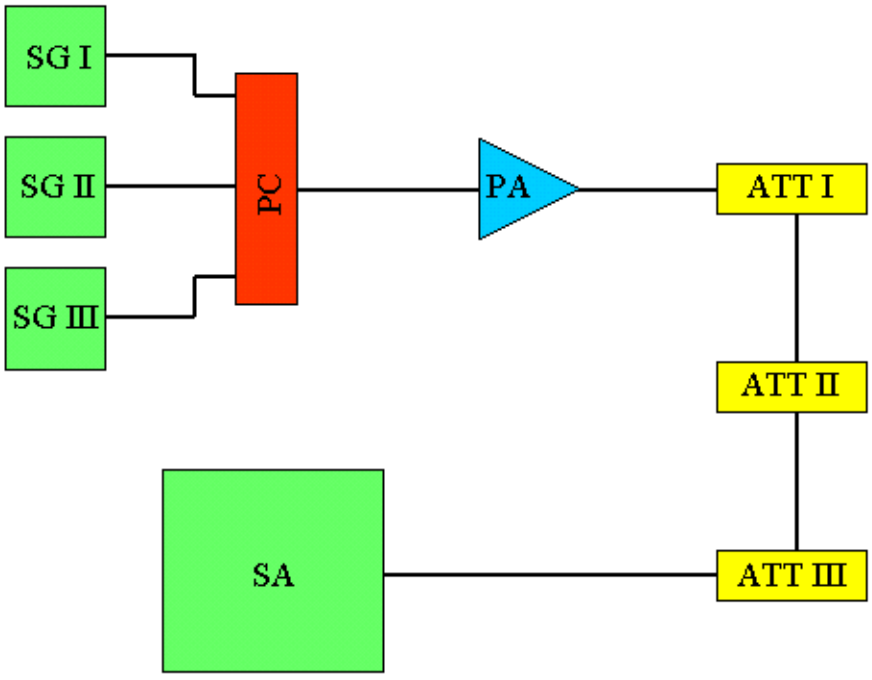

Figure 74. System power amplifier schematic.

Table 4 lists the equipment used in this experiment. The signal generators, attenuators, spectrum analyzer, and amplifier are equipped with N-type connecting ports. The power combiner has SMA connectors. The entire circuit was constructed with N-type to SMA converters and 2-foot coaxial transmission lines. Figure 75 shows the physical layout of the experimental setup. Figure 76 shows the Mini-Circuits® power amplifier used in this experiment.

Table 4. System power amplifier equipment list.

Equipment	Model Number	Serial Number
SG I	HP 8648A	PB47749
SG II	HP 8648A	PB47750
SSG III	HP 8648A	PB17129
PC	MC 15542	ZA3PD-4 (9517 03)
PA	MC ZHL-1-2W-N	D101397-14
ATT I	PE7021-10	2 (100 Watt at 10 dB)
ATT II	PE7021-10	3 (100 Watt at 10 dB)
ATT III	HP 354A	01449
SA	HP 8566B	PB97532

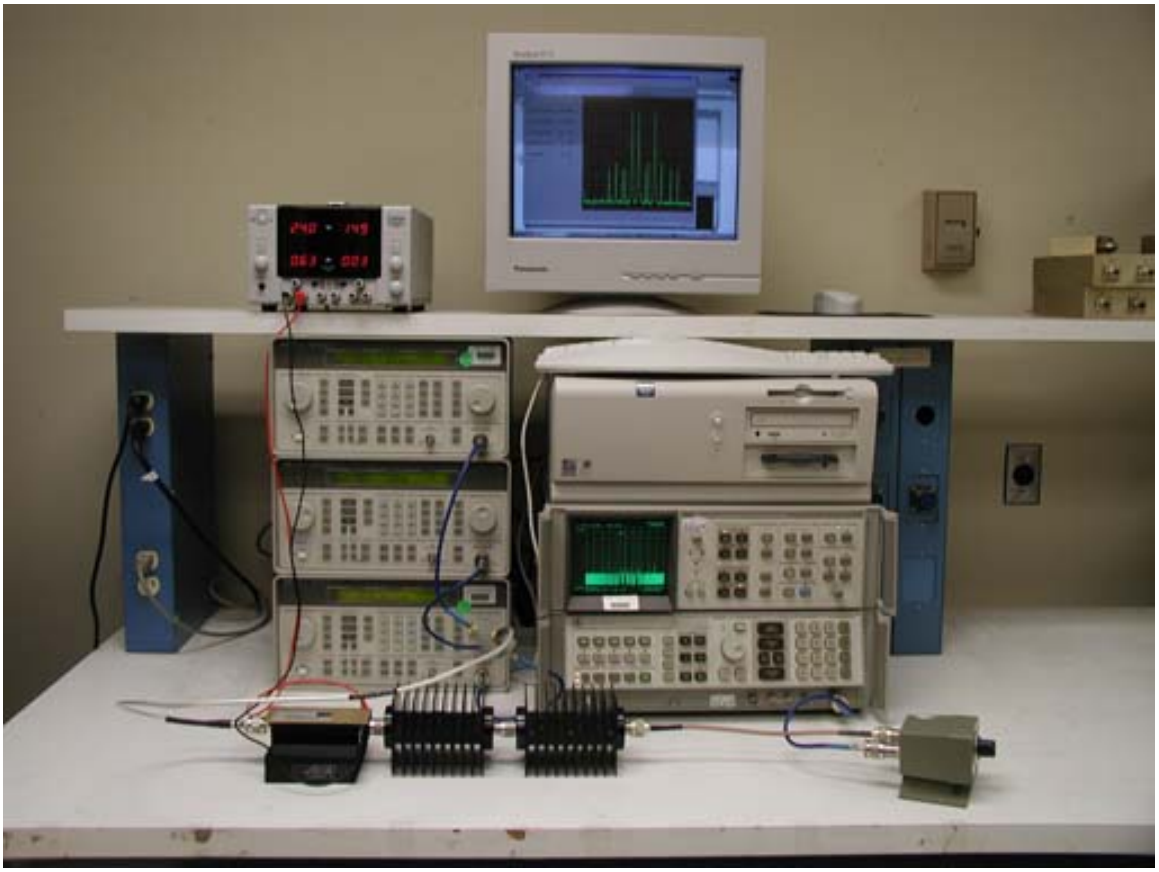

Figure 75. System power amplifier experiment.

Figure 76. Mini-Circuits® power amplifier.

3.5.3.3 System Model Parameters

This section describes the method used to determine the system parameters for this amplifier unit. The parameters of interest were gain, a second harmonic intercept point, a 1-dB compression point, and a third-order order intercept point. Since the system amplifier model in MWO is frequency-dependent, the system parameters must be obtained near the frequencies of intended applications.

The gain, second harmonic intercept point, and 1-dB compression point were again obtained from input and output power levels for each signal power sweep. Using a 100-MHz signal input to the amplifier and varying the power level from –30 dBm to 5 dBm in 1-dB steps, we recorded the output power at the fundamental (100 MHz) and nearest harmonic (200 MHz). Figure 77 shows these data as the red-dotted and blue-dotted curves. To account for the additional loss of the three attenuators used to protect the spectrum analyzer, we added attenuator loss values to the spectrum analyzer readings to obtain the actual output power level at the amplifier output port.

An additional measurement was required to determine the third-order intercept point. We fed two input signals of slightly differing frequencies and equal power levels into the amplifier, f1 = 100 and f2 = 105 MHz, to determine the third-order intercept point. The power levels were swept simultaneously over a large range and the output power levels at the nearest third-order intermodulation product were recorded for each power level setting in the sweep. The third-order products nearest the fundamental were 95 MHz and 110 MHz, and because they had equal power, their levels will be the same in the absence of frequency-dependent effects. We used the data from the 110-MHz intermodulation product to determine the intercept point (green-dotted curve in Figure 77).

We determined the system-level parameters for the amplifier from the measured data plots in Figure 77. The linear operating region is identified at input power levels below –5 dBm. The amplifier gain is the slope of the line that interpolates the data in the linear regime of the data for the fundamental signal and was 34.1 dB. The 1-dB compression point was 34.4 dBm. The second harmonic intercept point was 59 dBm, with the third-order intermodulation intercept point at 45 dBm. Table 5 shows these measured system parameters for this amplifier and they agree well with the manufacturer values.

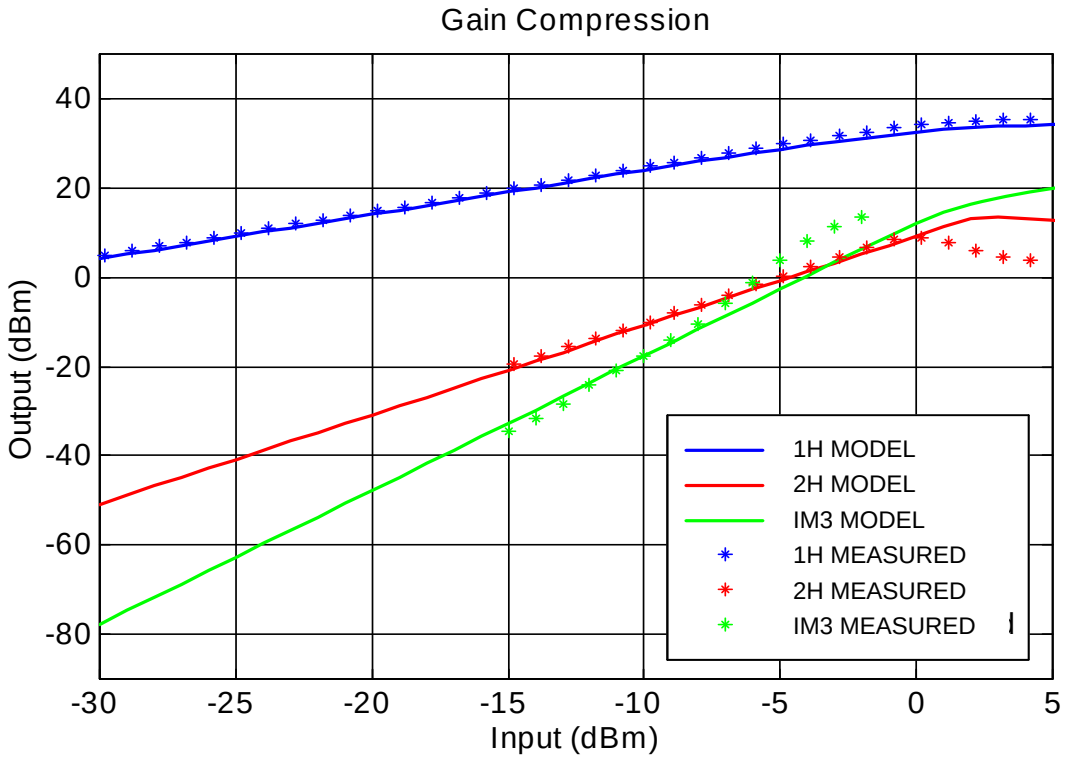

Figure 77. Power amplifier gain curves.

Table 5. Measured system parameters for power amplifier.

Parameter	Measurement	Frequency
Gain	34.1 dB	100 MHz
1-dB compression point	34.3 dBm	100 MHz
2H intercept point	59 dBm	200 MHz
IM3 intercept point	45 dBm	110 MHz

The specification of the four parameters determines the complete nonlinear behavior of the system amplifier device model. For this simplification to occur, MWO must make an assumption concerning the functional description of the gain curves for the amplifier. The device model contained within MWO determines the output power levels of the fundamental, harmonics, and intermodulation products at all input power levels. Since the user specifies only a few scalar quantities to represent the entire performance of the unit, the simulation software must assume some functional form for the gain compression curves (i.e., output power versus input power at the fundamental, second harmonic, and third-order intermodulation product frequencies). The shapes of these gain curves are fixed for the system amplifier device. The system parameters determine their slopes and relative positions. We performed a numerical experiment that was identical to the measurement described above to test the validity of the MWO gain curve assumptions. In other words, we constructed a model of the experiment within MWO, used the system parameters measured experimentally, and produced the gain curves for the fundamental, nearest harmonic, and nearest third-order intermodulation product. By comparing the measured and predicted gain curves, we could validate the underlying assumption of the model.

3.5.3.4 Results

This section presents the results of comparisons between predicted and measured power spectra for the power amplifier excited at the three frequencies: 97.5, 100, and 106 MHz. Three different drive levels are investigated: linear, weakly nonlinear, and fully saturated. The number of harmonic components kept in the simulation was increased repeatedly until further increases produced no noticeable changes on the outcome in the 80- to 120-MHz frequency range. The output spectra in Figures 78 through 80 represent measured data and the results from the independent tone and port mod simulations. The blue line plots indicate measured data. The agreement between measured data and the simulations is excellent for the fundamental tones and the significant intermodulation products at the middle and high drive levels. For the low drive situation, the predicted power levels for the harmonic products are typically 4 dB higher than the measured values, whereas the power in the fundamentals agrees within a tenth of a decibel.

The comparison between the independent tone and port mod analysis suggest that the multitone technique is valid. The two calculations have excellent agreement for the fundamentals and lower order harmonic components. Some noticeable discrepancies exist at high-order components, but these discrepancies are mainly attributable to the slight frequency offset used to avoid overlapping tones in the tone analysis. The main difference in the two results is that the tone analysis produces several closely spaced harmonic components at lower levels than the port mod calculation, which combines these components into a single high-level signal.

The MWO simulation predictions agree quite well with the measured quantities. In the linear regime, predictions for the gain in the fundamental tones are within a tenth of a decibel. Middle and high drive simulation results are quite similar and agree well with the measured data. The predicted output power levels for the fundamental tones agree with measured values to within a decibel. Furthermore, the port mod and independent tone analyses coincide exactly with one another, suggesting equivalence in the two techniques for predicting multiple-signal gain levels.

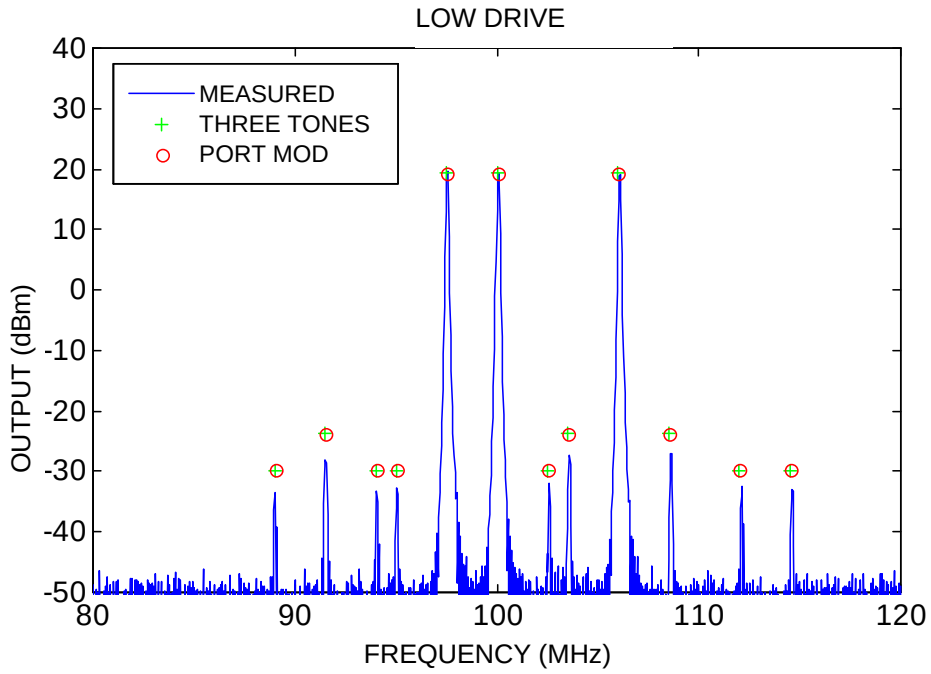

Figure 78. Power amplifier output spectrum low drive.

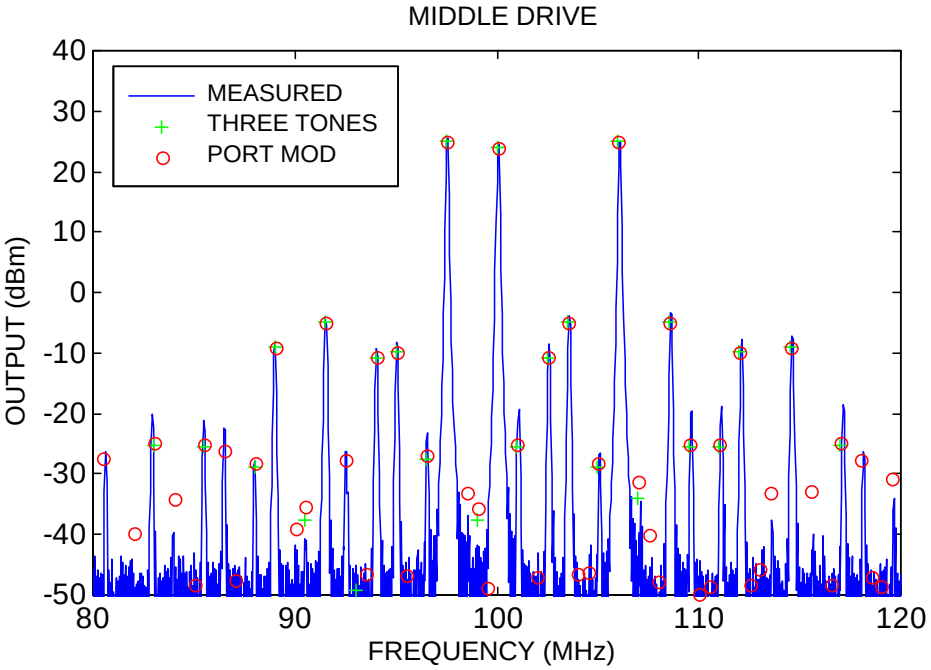

Figure 79. Power amplifier output spectrum middle drive.

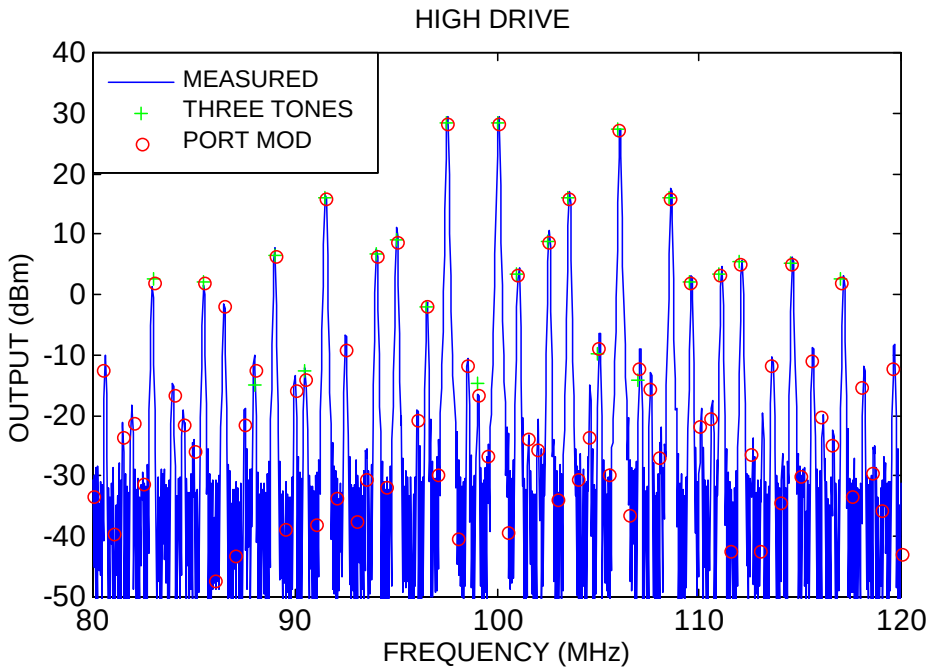

Figure 80. Power amplifier output spectrum high drive.

The model predictions for the frequencies of significant intermodulation products are also quite accurate. The two types of simulations agree with experimental data for the lower order, higher level intermodulation products. For high-order products, port mod analysis agrees better with the measurements because finite bandwidth averaging in the spectrum analyzer lumps closely spaced frequencies together into a single large peak. The independent tone analysis represents the limit of purely sinusoidal signals, where the spectrum is composed of delta function spikes and the bandwidth resolution is ideal.

3.5.4 System Mixer (Three-Tone)

3.5.4.1 Introduction

In this case, we tested the prediction capabilities of the system mixer. RF mixers typically upconvert IF signals to the RF frequency band for transmission or alternatively downconvert incoming RF signals to the IF frequency for signal processing. Here, the mixer downconverted two independent signals at 325 and 330 MHz via a local oscillator at 300 MHz. The power levels for the three signals were fixed within the operating region of this mixer device.

The mixer in this experiment was a three-port (RF, LO, IF) passive device that uses the nonlinearity of a diode for frequency conversion. Under normal downconversion operating conditions, a modulated RF signal is input to the RF port and a pure sinusoidal signal at a different frequency is injected at the LO port. The IF signal at the output port is the difference between the RF carrier and the local oscillator. Under ideal conditions, the RF and LO signals are completely isolated from the IF port. In practice, there will be some leakage. In this experiment, two RF signals were downconverted simultaneously in the same mixer. The RF signals were unmodulated and only the power spectrum data were analyzed.

We used the SYSTEM MIXER component to compare the measured output spectra to predictions from a MWO simulation. Four parameters characterized the performance of the SYSTEM MIXER model: conversion gain, local oscillator to IF isolation, RF to IF isolation, and third-order intermodulation product intercept point. We determined these quantities experimentally through independent measurements and they compare favorably with the manufacturer. The details concerning the values and techniques used to measure the system parameters are in Section 3.5.4.3. The output spectra from measurements and the simulation are compared in Section 3.5.4.4. This simulation is effectively a three-tone calculation and can be performed directly by using the three-tone harmonic balance analysis in the MWO computational engine. The three frequencies used as independent fundamentals may not be commensurate with the specified harmonic order of the simulation.

3.5.4.2 Experimental Setup

Two unmodulated signals drive the mixer at the RF input port. SG I and SG II power was combined with a power combiner. A third SG III signal was injected at the mixer LO port. The signal output from the IF port was fed into the spectrum analyzer. Figure 81 shows a schematic diagram of this setup.

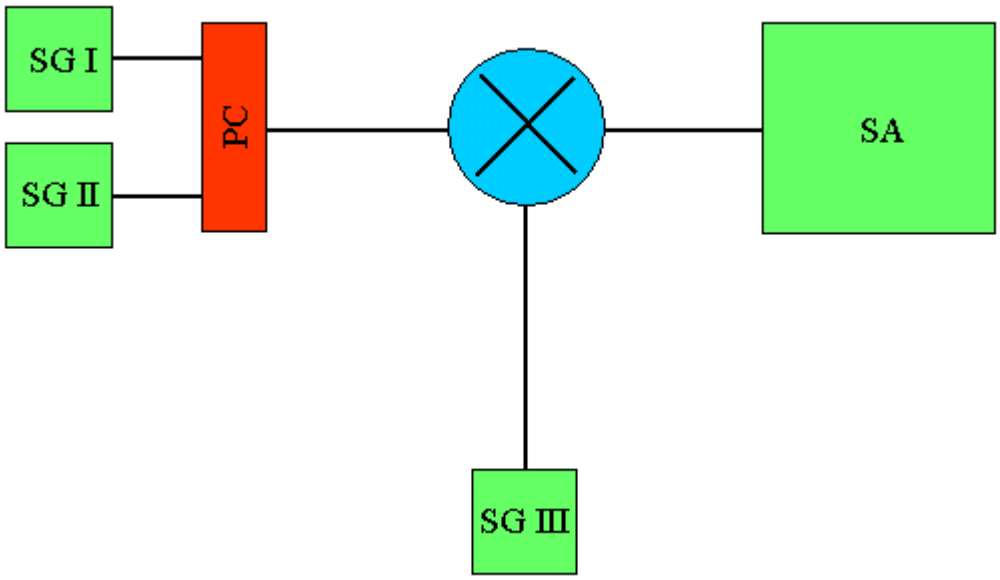

Figure 81. System mixer schematic.

Table 6 lists the equipment used in this experiment, including manufacturer model numbers and serial numbers. The signal generators, attenuator, and spectrum analyzer are equipped with male N-type connecting ports. The mixer and power combiner have BNC connectors. The entire circuit was constructed with N-type to SMA and SMA to BNC converters, and 2-foot coaxial transmission lines.

Table 6. System mixer equipment list.

Equipment	Model Number	Serial Number
SG I	HP 8648A	S/N PB47749
SG II	HP 8648A	S/N PB47750
SG III	HP 8648A	S/N PB 17129
PC	BNC Type	
X	HP 10514A	
SA	HP 8566B	S/N PB97532

The experimental setup is similar to the setup for previous experiments (Figure 82). The setup uses three signal generators arranged in a vertical column on the left. A personal computer connected to the spectrum analyzer gathers and stores the data. Figure 83 shows the mixer unit used in this experiment.

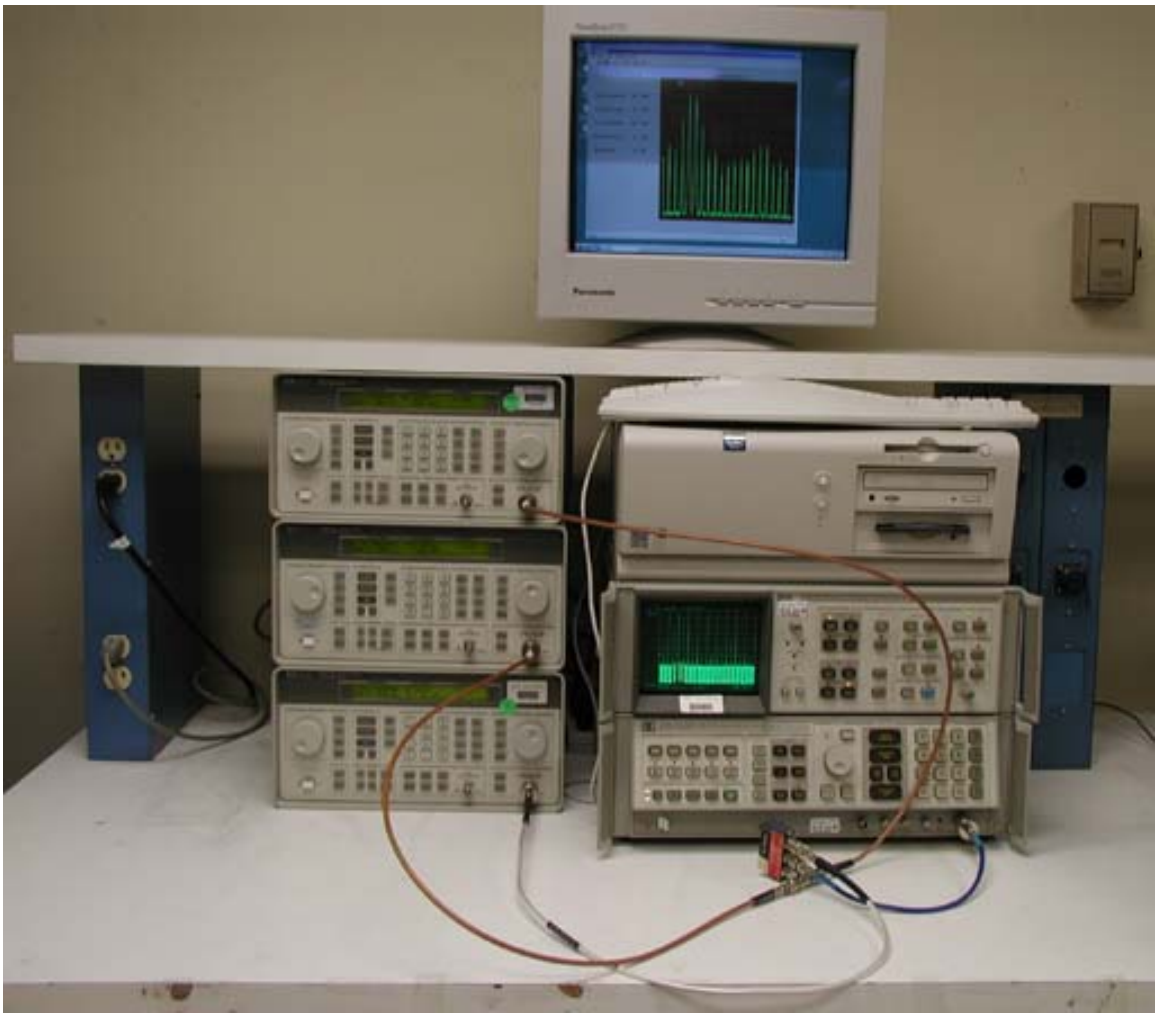

Figure 82. System mixer experiment.

Figure 83. HP 10514A mixer device.

3.5.4.3 System Model Parameters

The system parameters for the mixer must be found experimentally, and this section describes the method used for finding these parameters. The quantities found agree well with the manufacturer values. The system mixer model in MWO is frequency-dependent; therefore, we must specify the system parameters close to the operating frequencies. The LO was operated at 300 MHz, and the RF inputs were operated at 325 and 330 MHz. Therefore, IF fundamentals were produced at 25 and 30 MHz.

We measured isolation at a 0-dBm input power level. Since the isolation is a power-independent parameter in the model, one measurement near the intended operation point was sufficient. To obtain the isolation, the mixer was in normal operation, with 7 dBm at 300 MHz at the LO port, 0 dBm at 325 MHz at the RF port, and the spectrum analyzer loaded the IF port. The power levels in the IF spectrum at 300 and 325 MHz were then used to calculate the LO2IF and RF2IF isolation parameters respectively. We obtained the conversion gain and 1-dB compression points from an input RF power sweep, –20 to 6 dBm at 325 MHz. The conversion gain was –7.9 ±0.1 dB over a range of –20 to 2 dBm and represents the ratio of input RF power at 325 MHz to output IF power at 25 MHz. To determine the third-order intermodulation products, two RF signals were combined and injected into the RF port. For the system mixer, the definition of IM3 is slightly different than for the amplifiers. The third-order intermodulation products are referenced to the downconverted IF signals rather than the RF inputs. For instance, with RF inputs of 325 and 330 MHz, as well as an LO at 300 MHz, the fundamental IF tones are produced at 25 and 30 MHz. Third-order products of these IF signals will appear at 2 x 25 – 30 = 20 and 2 x 30 – 25 = 35 MHz. The IP3 system parameter refers

to the production of these products. The power levels at the 20-MHz intermod were used to determine IP3. The two RF inputs had the same power level for the power sweep used to obtain the data. Table 7 shows all the system model parameters for the mixer. All parameters agree well with manufacturer values.

Table 7. Measured system parameters for mixer.

Parameter	Measurement	Frequency (MHz)
Gain	–7.9 dB	25
1-dB compression point	4 dBm	25
IP3 intercept point	10 dBm	20
RF to IF isolation	–31.8 dB	325 to 25
LO to IF isolation	–37.3 dB	300 to 25
LO lower level	7 dBm	300

3.5.4.4 Results

The initial results of the spectral data comparison for the system mixer element contained some discrepancies. Several intermodulation products were observed in the IF band of the experimentally measured data that were absent from the calculation. Upon further investigation, we determined that the large signal levels used to saturate the mixer and obtain the nonlinear distortion had important consequences in the signal generators themselves. Since the signal generators were not isolated from one another, the RF tones were mixed in the signal generators themselves, which produced an effective four-tone RF input for the mixer. Therefore, the RF input spectrum to the mixer actually contained additional RF tones at 320 and 335 MHz that were about –50 dBm. Once this fact was realized, we used the proper input signal to redo the simulation, with the results agreeing favorably with the measurements. Figure 84 shows the measured data and simulation data in the IF range. The main IF signals are at 25 and 30 MHz and show that the simulation is extremely accurate in predicting the desired products. The high driving amplitudes make the remaining signals spurious products. Although not shown in Figure 84, the RF to IF and LO to IF isolation parameters were also correctly represented in the simulation. These parameters agree with the measurements to within 0.5 dB.

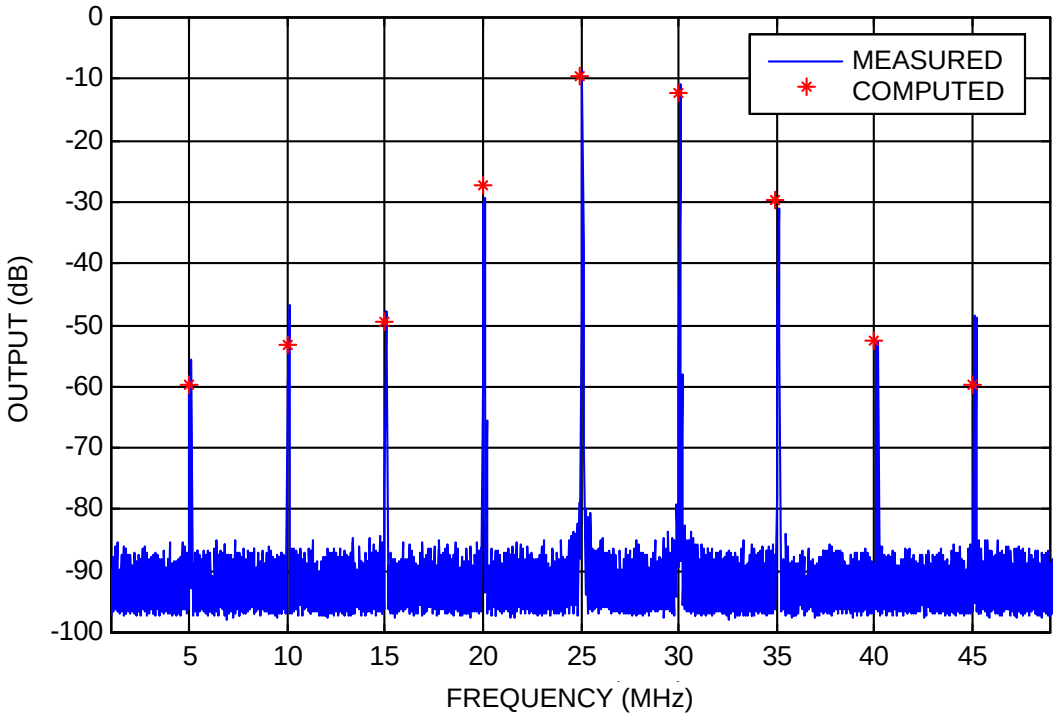

Figure 84. Mixer output spectrum IF range.

3.5.5 System Super High Frequency (SHF) Amplifier (Three-Tone)

3.5.5.1 Introduction

Three distinct fundamental frequencies drive an amplifier operating at super high frequency (SHF). The amplifier was operated in the linear and nonlinear region. We used a spectrum analyzer to record the frequency-domain input and output signal levels to the amplifier. This example is similar to the other amplifier cases, differing only in the operating frequency.

The experiment results were compared to system model predictions from Microwave Office™. The purpose of this example was to determine the accuracy with which the SYSTEM AMP component in MWO represents the performance of an amplifier operating near 10 GHz. As before, we specified the performance of the SYSTEM AMP model by four system parameters: gain, 1-dB compression point, second harmonic intercept point, and third-order intermodulation product intercept point. These quantities were calculated from gain curve measurements of the fundamental and harmonic products. MWO provides nonlinear harmonic balance analysis for up to three independent tones. This simulation used the independent tone analysis described above.

3.5.5.2 Experimental Setup

Three signal generators drive the MITEQ® SHF amplifier. We used a 3:1 power divider to combine the signals from the source. Figure 85 shows a schematic diagram of the setup. The power combiner coupled the signals from the three sources into one transmission line. Power combiner output contains three CW carrier signals with power levels and frequencies that can be independently adjusted. Transmission line output from the power combiner was connected to the SHF amplifier input port or an SMA thru for measurement of output and input spectra respectively. We connected the amplifier output port to the spectrum analyzer through a 0 to 60-dB variable attenuator with 10-dB increments.

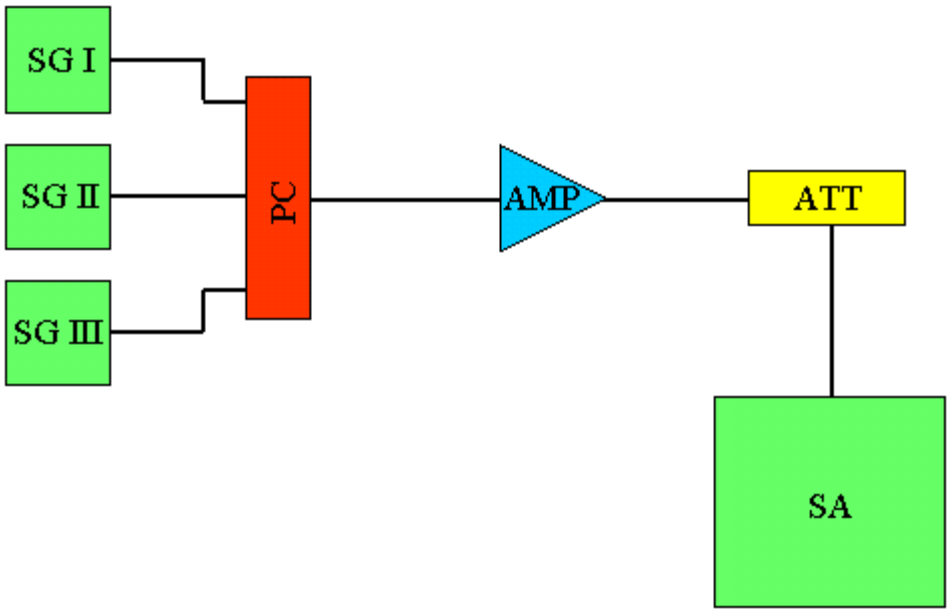

Figure 85. System SHF amplifier schematic.

Table 8 lists the equipment used in this experiment, including manufacturer model and serial number. The signal generators, attenuator, and spectrum analyzer are equipped with male N-type connecting ports. The SHF amplifier and power combiners use male SMA connectors. The entire circuit was constructed with N-type to SMA converters and 2-foot coaxial transmission lines.

Table 8. System SHF amplifier equipment list.

Equipment	Model Number	Serial Number
SG I	HP 8341B	2819A01803
SG II	HP 8673E	3146A00700
SG III	HP 8340A	2520A01268
PC	OS 2090-6309-00	
AMP	MITEQ® AMF-6B-080120-30-27P	404736
SA	HP 8566B	PB97532

Figure 86 shows the experimental setup. This setup uses the same three signal generators as used in previous experiments. A personal computer was again used to obtain and record digital data from the spectrum analyzer. The SHF amplifier was powered with a 15-Vdc power supply (lower center, Figure 86). The power combiner, attenuator, and SHF amplifier are shown from left to right in the foreground. The amplifier is bolted to a rectangular metallic base that acts as a heat sink. Figure 87 shows the SHF amplifier and Omni-Spectra power combiner used in this experiment.

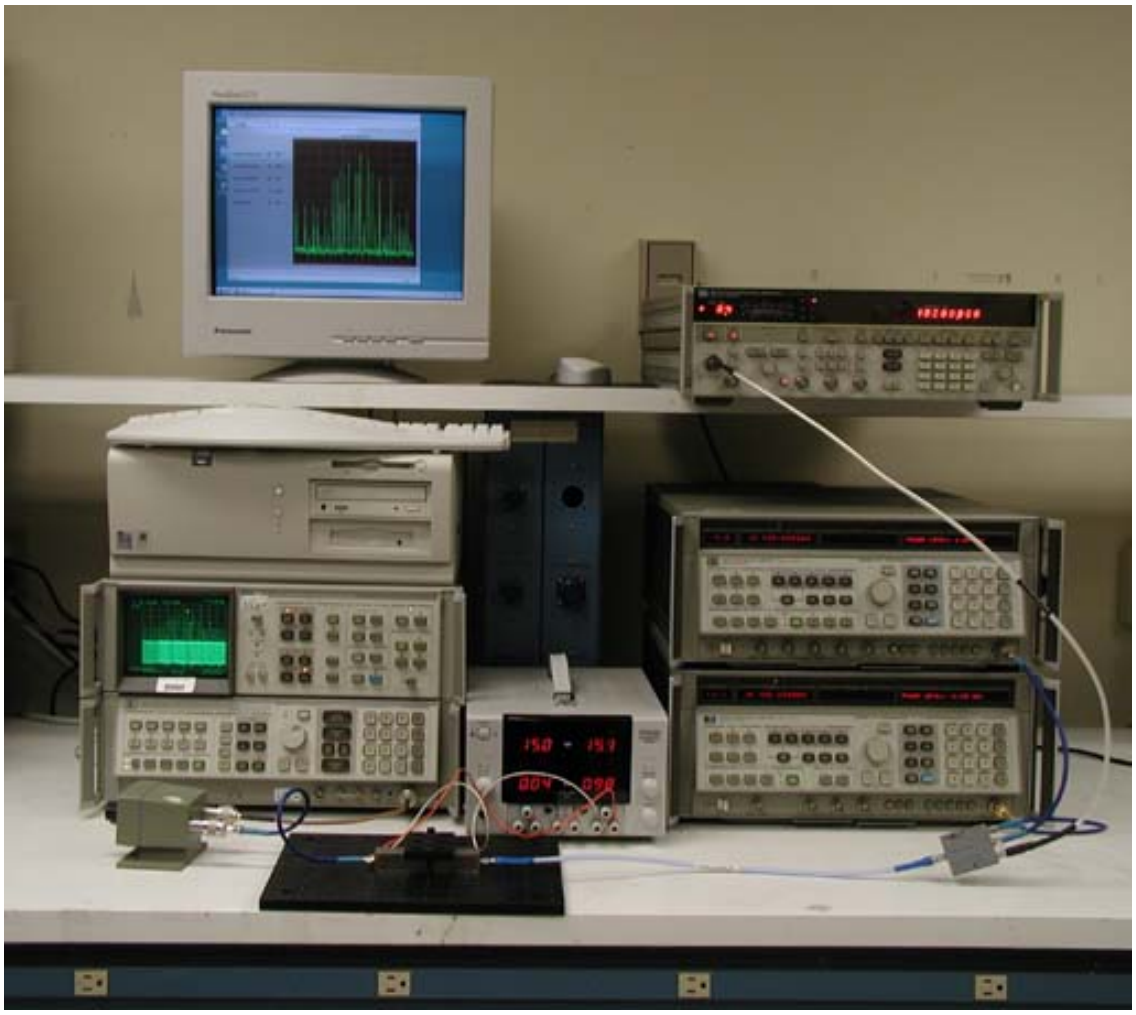

Figure 86. System SHF amplifier experiment.

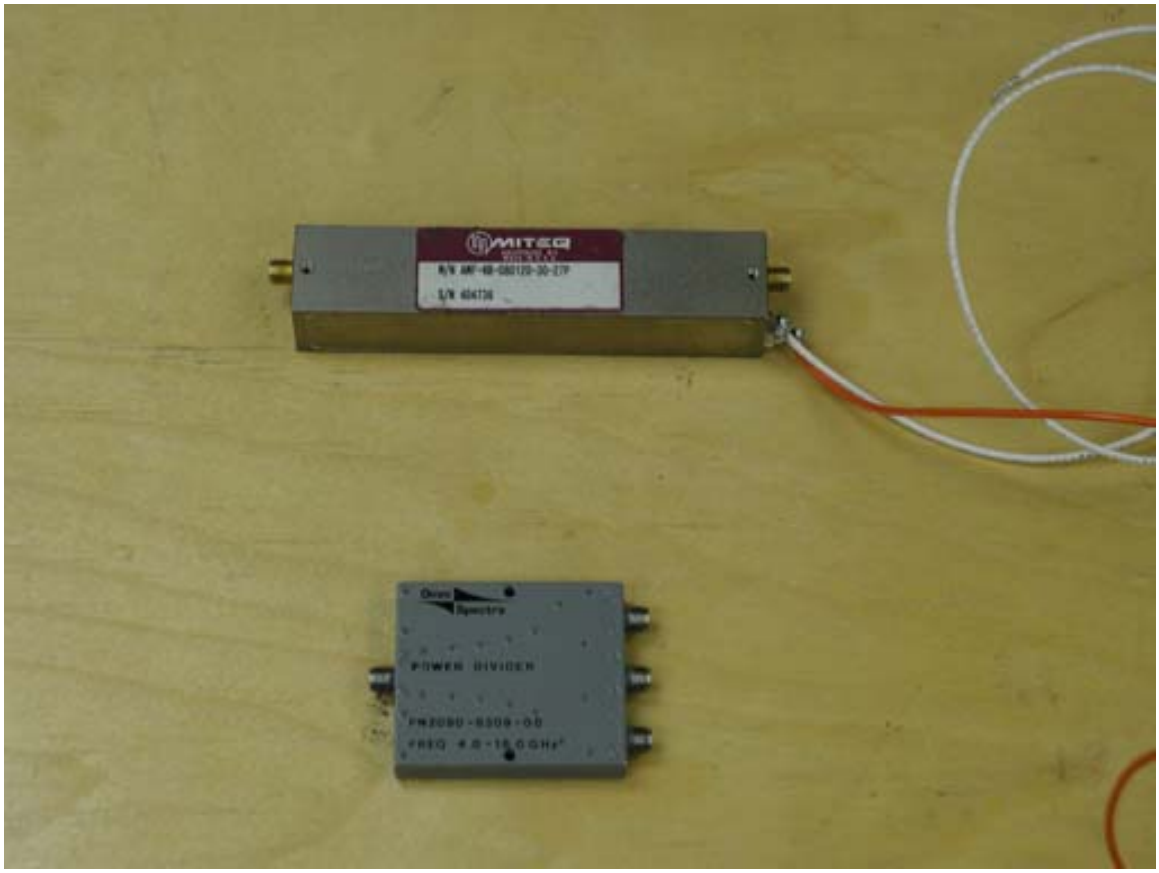

Figure 87. MITEQ® SHF amplifier and Omni-Spectra power combiner.

3.5.5.3 System Model Parameters

Once again, the system parameters for the amplifier element had to be found experimentally. Two sets of measurements were required to determine the nonlinear performance of the amplifier, including the gain, second harmonic intercept point, 1-dB compression point, and third-order intercept point.

The gain, second harmonic intercept point, and 1-dB compression point were obtained from input and output levels for a single-signal power sweep. We input a 10-GHz signal to the amplifier and varied the power level from –40 dBm to –17 dBm in 1-dB increments. The red and blue dotted curves in Figure 88 indicate the output power at the fundamental (10 GHz) and nearest harmonic (20 GHz).

The third-order intercept point was determined as it was in previous experiments. We fed two input signals of slightly differing frequencies and equal power levels into the amplifier and swept them simultaneously over a large range. Output power levels at the nearest third-order intermodulation product were recorded for each power level setting in the sweep and the resulting nearest fundamentals were 9.5 and 11 GHz. Since they have equal power and are the same in the absence of frequency-dependent effects, the data from the 11-GHz intermodulation products were used to determine the intercept point. Figure 88 shows these data as a green dotted curve.

We can determine amplifier system-level parameters from the measured data plots in Figure 88. The linear operating region is easily identified at input power levels below –22 dBm. Amplifier gain is the slope of the line that interpolates the data in the linear regime of the data for the fundamental

signal and was 44.3 dB. The 1-dB compression point is the output power level at which the gain has been reduced 1 dB because of saturation and is 21 dBm. The second harmonic intercept point is 66 dBm, while the third-order intermodulation intercept point is 35 dBm. Table 9 lists the measured system parameters for the SHF amplifier. The parameters agree well with the manufacturer values.

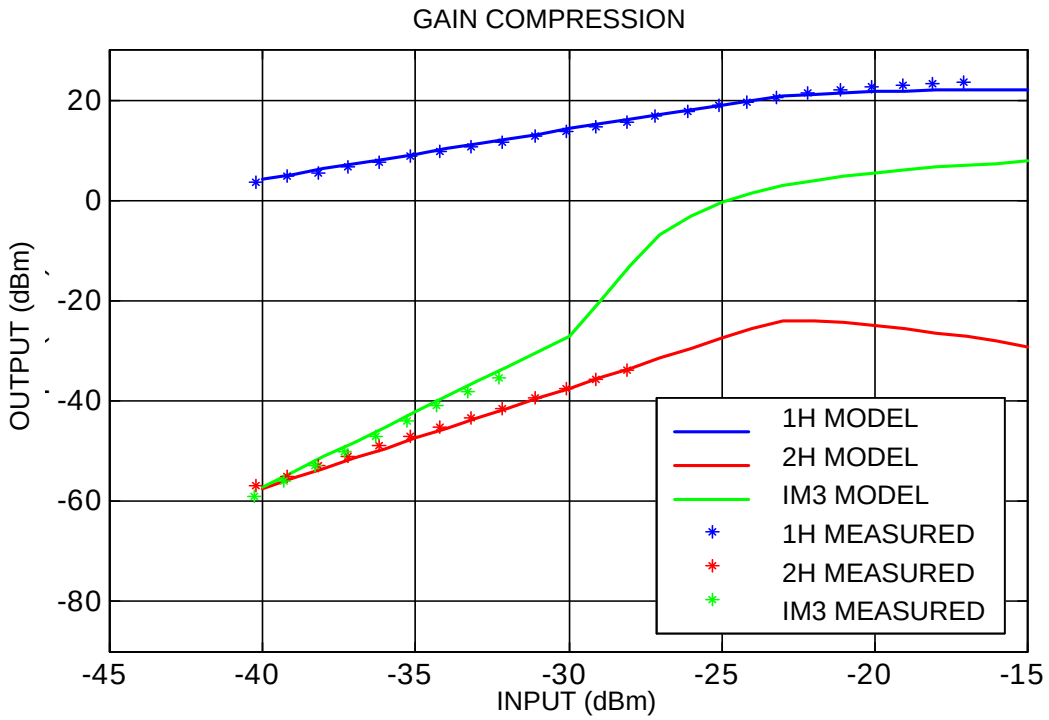

Figure 88. SHF amplifier gain curves.

Table 9. Measured system parameters for SHF amplifier.

Equipment	Measurement	Frequency (GHz)
Gain	44.3 dB	10
1-dB compression point	21 dBm	10
2H intercept point	66 dBm	20
IM3 intercept point	35 dBm	11

The specification of four parameters determines the complete nonlinear behavior of the system amplifier model. For this simplification to occur, MWO must make an assumption concerning the functional description of the amplifier gain curves. The shapes of these gain curves are fixed for the system amplifier. The system parameters determine their slopes and relative positions. We can perform a numerical experiment identical to measurements described above to test the validity of the MWO gain curve assumptions. We constructed a model of our experiment within MWO, used the system parameters that were measured experimentally, and produced the gain curves for the fundamental, nearest harmonic, and nearest third-order intermodulation product. By comparing the measured and predicted gain curves, we could validate the underlying assumption of the model.

3.5.5.4 Results

This section presents the results that compare the predicted and measured power spectra for the SHF amplifier excited at three frequencies near 10 GHz. Two different cases are examined in which the power levels of the input signals are in the linear operating and nonlinear regions. We increased the number of harmonic components kept in the simulation repeatedly until further increases produced no noticeable changes on the outcome. Figures 89 and 90 show the output spectra from each drive level.

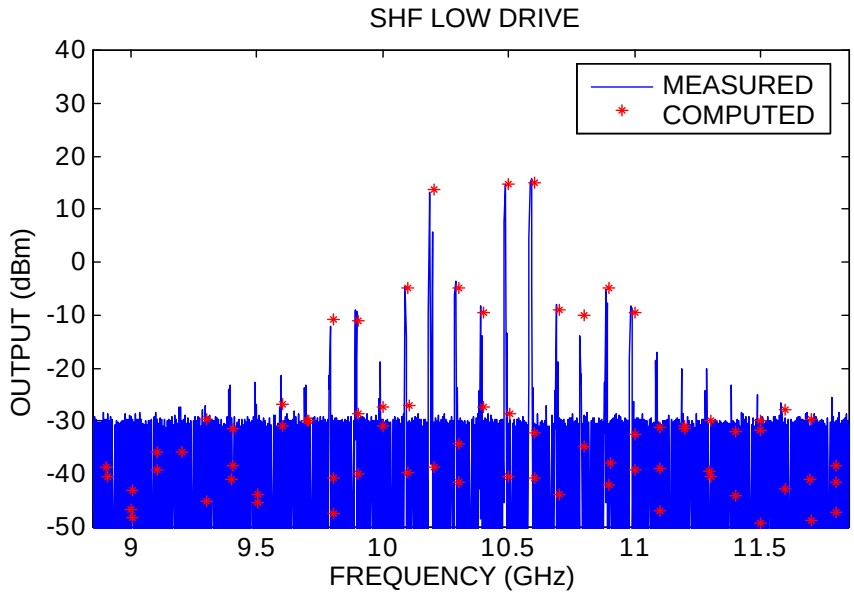

Figure 89. SHF output spectrum low drive.

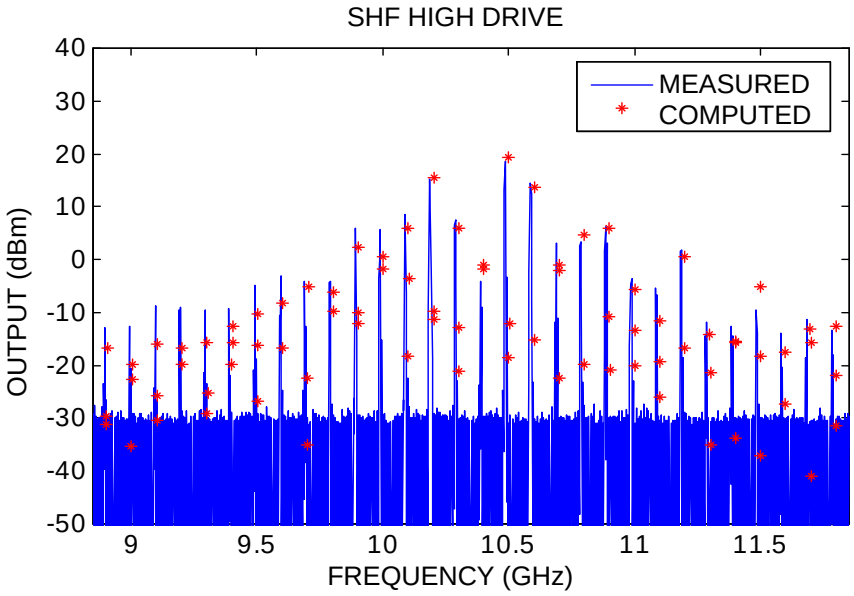

Figure 90. SHF output spectrum high drive.

The MWO predictions simulations agreed well with the measured quantities. In the linear and nonlinear regimes, the discrepancies between measurement and simulation were, at most, on the order of a few decibels. Results for the fundamental signal levels were in excellent agreement. Predicted harmonic product levels were slightly higher than the measured levels in the linear regime and slightly lower than measured levels in the nonlinear regime. The frequencies of the harmonic products agreed to within the error of observation.

3.6 COMPUTER RUNTIME

An important consideration for the DD(X) design teams when using any M&S tool is the time required to generate a model and run a simulation. For the design teams to successfully use MWO throughout many design iterations, the computing runtime must be sufficiently fast to quickly simulate design concepts. During this V&V effort, some ITD problems were timed while the simulation was running. Table 10 shows the computing runtime for these test problems. All these problems were timed on a Pentium III 933-MHz computer with 512-MB RAM and a 40-GB hard drive.

Table 10. Computing runtime.

Problem	Runtime
Distributed amplifiers	1 sec
Single-ended power amplifier	20 sec
VHF lumped element	1 sec
X-band distributed element	2 sec
RF cascade network	1 sec
Downconverter	4 min
Three-tone VHF amplifier	4 min
Three-tone SHF amplifier	6 min
Five-tone RF Rx front-end	10 min

The computing runtimes for the problems shown in Table 10 would provide a sufficiently fast simulation. The longest runtime was for the five-tone RF Rx front-end problem, which took only 10 minutes. Therefore, the time required to run a simulation on a design concept is not so inordinately long as to make the M&S software a burden to the design teams.

4. CONCLUSIONS

To address the shortfall in adequate M&S software that can model a wide range of electromagnetic problems, PEO-DD(X)/PMS 500 commissioned the development of a plan for delivery of a Validated, Integrated, Physics-based Electromagnetic Radiation (VIPER) tool set. Microwave Office™ was identified as one of the most promising microwave electronics simulation codes and was selected for further development and verification and validation. This report shows a wide range of EM test cases in which Microwave Office™ simulations included linear passive components, linear active components, nonlinear components, and system-level circuits.

Linear passive components are basic building blocks to most EM circuits, and thus are important for any EM M&S tool to accurately predict their performance. Microwave Office™ was used to simulate various linear passive components, including microstrip step, cross, and tee elements, a VHF bandpass filter, a parallel-coupled line filter, and an 8:1 power combiner. The results compared favorably with ADS®, a commercial electronics design simulation package that is widely accepted in industry. Microwave Office™ properly characterized the performance of each component and was better at accounting for parasitic effects at higher frequencies than ADS®. This ability shows that Microwave Office™ can accurately predict the performance of linear passive components.

Linear active components are also very important devices because they enable amplifier circuits that are used extensively in RF transmitters and receivers. All the linear active test cases involve a transistor. Microwave Office™ was used to model and simulate various configurations, including a transistor circuit, an FET circuit, a UHF bipolar transistor amplifier, a Microwave FET amplifier, a feedback amplifier, a balanced amplifier using feedback, an LNA, and a distributed amplifier. The results compared favorably to Touchstone®, another commercial electronics design simulation package widely accepted in industry. The low-noise and distributed amplifier test cases compared favorably with ADS®. Each test case result showed that Microwave Office™ agreed very well with comparison codes in predicting the performance of these circuits, validating the program's ability to accurately predict the performance of linear active components.

In electronic circuit design, not all circuits and components operate in the linear regime. Components such as mixers and oscillators are inherently nonlinear, and high-powered amplifiers can be driven to saturation or into their nonlinear operation mode. Since these components are widely used, it is important to accurately predict their performance with any M&S package. Microwave Office™ was used to run many test cases, including an X-Band amplifier, a large-signal-band power amplifier, an active mixer, and a microwave oscillator. The results from Microwave Office™ agreed quite well with ADS® and Series IV, which were used as comparison codes for these examples. Microwave Office™ correctly and accurately characterized the performance of these circuits, including such nonlinear effects as gain compression, harmonic generation, and intermodulation distortion. Microwave Office™ demonstrated a greater ability than the comparison codes to characterize high-power, high-frequency simulation by accounting for parasitic effects. These results validate the program's ability to accurately predict the performance of nonlinear components and circuits.

The ability of an electromagnetic M&S package to accurately predict the performance of individual components and small circuits is important; however, it also must accurately predict the performance of full system-level designs. System-level analysis was performed by using Microwave Office™ during the V&V effort, which included a system low-noise amplifier, a system cascade, a system power amplifier, a system mixer, and a system SHF amplifier. Each system simulated with Microwave Office™ was then assembled and tested in the laboratory to characterize the real

performance of these systems and was compared with the simulated results from Microwave Office™. The Microwave Office™ results compared favorably to the measured data for each experiment. Microwave Office™ validated the ability to characterize the system parameters and performance accurately, including linear and nonlinear regimes.

The verification and validation of Microwave Office™ conducted under this study was a major success. Each test case designed for this V&V effort was chosen to verify Microwave Office™ performance in a specific area of user need or to validate the underlying theoretical framework of the M&S package. Microwave Office™ has demonstrated its ability to accurately predict the performance of a wide range of electromagnetic problems. Microwave Office™ was verified and validated as a capable modeling and simulation tool for electronic systems to be used on the DD(X) program.

5. REFERENCE

R. B. Hallgren and P. H. Litzenberg. 1999. TOM3 “Capacitance Model: Linking Large-and Small-signal MESFET Models in SPICE,” *IEEE Transactions on Microwave Theory Techniques*, vol. 47, no. 5 (May), p. 556.

REPORT DOCUMENTATION PAGE

Form Approved
OMB No. 0704-01-0188

PLEASE DO NOT RETURN YOUR FORM TO THE ABOVE ADDRESS.

1. REPORT DATE *(DD-MM-YYYY)*	2. REPORT TYPE	3. DATES COVERED *(From - To)*
08–2005	Final	

4. TITLE AND SUBTITLE

VERIFICATION AND VALIDATION REPORT: MICROWAVE OFFICE™ 2002 MODELING AND SIMULATION FOR ELECTRONIC SYSTEMS

5a. CONTRACT NUMBER

5b. GRANT NUMBER

5c. PROGRAM ELEMENT NUMBER

6. AUTHORS

T. Ho, T. Hilsabeck, C. Hewett — **SSC San Diego**
D. Zolnick, M. Kragalott, D. Taylor — **NRL**
M. Baugher — **NSWC, Dahlgren Div.**
T. Itoh — **UCLA**
A. Agrawal — **Johns Hopkins Univ. APL**

5d. PROJECT NUMBER

5e. TASK NUMBER

5f. WORK UNIT NUMBER

7. PERFORMING ORGANIZATION NAME(S) AND ADDRESS(ES)

SSC San Diego
San Diego, CA 92152–5001

8. PERFORMING ORGANIZATION REPORT NUMBER

TR 1928

9. SPONSORING/MONITORING AGENCY NAME(S) AND ADDRESS(ES)

Naval Sea Systems Command (PMS 500)
1333 Isaac Hull Avenue S. E.
Washington Navy Yard, D.C. 20376

10. SPONSOR/MONITOR'S ACRONYM(S)

NAVSEA

11. SPONSOR/MONITOR'S REPORT NUMBER(S)

12. DISTRIBUTION/AVAILABILITY STATEMENT

Approved for public release; distribution is unlimited.

13. SUPPLEMENTARY NOTES

14. ABSTRACT

To address the shortfall in adequate M&S software that can model a wide range of electromagnetic problems, PEO-DD(X)/ PMS 500 commissioned the development of a plan for delivery of a Validated, Integrated, Physics-based Electromagnetic Radiation (VIPER) tool set. Microwave Office™ was identified as one of the most promising microwave electronics simulation codes and was selected for further development and verification and validation. This report shows a wide range of EM test cases in which Microwave Office™ simulations included linear passive components, linear active components, nonlinear components, and system-level circuits.

15. SUBJECT TERMS

Mission Area: Communications
modeling and simulation software, electromagnetics, verification, validation, linear passive components, linear active components, nonlinear components, system-level circuits

16. SECURITY CLASSIFICATION OF:			17. LIMITATION OF ABSTRACT	18. NUMBER OF PAGES	19a. NAME OF RESPONSIBLE PERSON
a. REPORT	b. ABSTRACT	c. THIS PAGE			Thinh Q. Ho
U	U	U	UU	105	19B. TELEPHONE NUMBER *(Include area code)* (619) 553–3783

INITIAL DISTRIBUTION

20012	Patent Counsel	(1)
21511	L. Mc Daniel	(1)
21512	Library	(2)
21513	Archive/Stock	(3)
2825	T. Ho	(15)

Defense Technical Information Center
Fort Belvoir, VA 22060–6218 (1)

SSC San Diego Liaison Office
C/O PEO-SCS
Arlington, VA 22202–4804 (1)

Center for Naval Analyses
Alexandria, VA 22311–1850 (1)

Government-Industry Data Exchange
Program Operations Center
Corona, CA 91718–8000 (1)